Pipeline Variable Uncertainties And Their Effects on Leak Detectability

A Report Prepared for the American Petroleum Institute

API PUBLICATION 1149
NOVEMBER 1993

American Petroleum Institute
1220 L Street, Northwest
Washington, D.C. 20005

Pipeline Variable Uncertainties And Their Effects on Leak Detectability

By Dr. Jim C. P. Liou, P.E.
Department of Civil Engineering
University of Idaho
Moscow, Idaho 83843

Manufacturing, Distribution and Marketing Department

API PUBLICATION 1149
NOVEMBER 1993

American
Petroleum
Institute

FOREWORD

This report was prepared for the American Petroleum Institute by Dr. Jim C. P. Liou, P.E., Department of Civil Engineering, University of Idaho.

API publications necessarily address problems of a general nature. With respect to particular circumstances, local, state, and federal laws and regulations should be reviewed.

API is not undertaking to meet duties of employers, manufacturers or suppliers to warn and properly train and equip their employees, and others exposed, concerning health and safety risks and precautions, nor undertaking their obligations under local, state, or federal laws.

Nothing contained in any API publication is to be construed as granting any right, by implication or otherwise, for the manufacture, sale, or use of any method, apparatus, or product covered by letters patent. Neither should anything contained in the publication be construed as insuring anyone against liability for infringement of letters patent.

This report may be used by anyone desiring to do so. Every effort has been made by the American Petroleum Institute to assure the accuracy and reliability of the material contained in it at the time in which it was written; however, the Institute makes no representation, warranty, or guarantee in connection with the publication of this guideline and thereby expressly disclaims any liability or responsibility for loss or damage resulting from its use or for the violation of any Federal, State or Municipal regulation with which this guideline may conflict, nor does the Institute undertake any duty to ensure its continued accuracy.

ACKNOWLEDGEMENT

This study was funded by the American Petroleum Institute(API). The author sincerely thanks members of the Pipeline Leak Detection Task Force of the Transportation Department of API, who provided assistance throughout this study.

CONTENTS

4. LINEFILL AND ITS UNCERTAINTY

5. LEAK DETECTABILITY FOR STEADY-STATE FLOW BASED ON THE PRINCIPLE OF MASS CONSERVATION

6. FIELD TRIALS - STEADY-STATE FLOW

7. RANKING OF VARIABLES - LEAK DETECTION BY MASS BALANCE

EXECUTIVE SUMMARY

Software-based leak detection systems are playing an increasingly important role in pipeline risk management. These systems give notification of an accidental release of liquids in a timely manner, thus minimizing emission. For any given pipeline, it is useful to know the leak detectability, that is: how small and how quickly a leak can be detected, and the sensitivity of leak detectability with respect to the variables involved.

Software-based methods use a supervisory control and data acquisition (SCADA) system to obtain field data. The data is then analyzed by mathematical algorithms to detect the onset of a leak in real-time. These algorithms are based on mass balance, mass balance with linefill correction, and transient flow analyses, which includes simulations, pattern recognition, and pressure change monitoring. Fluid properties, pipeline parameters, instrumentation performance, SCADA characteristics, and states of flow are the variables used in the algorithms. The magnitude of and the uncertainty in these variables determine the leak detectability.

The liquids considered in this study are crude oils and refined products. A single pipeline segment with pressure, temperature, and flow rate measurements at both ends is considered. Fluid batches and pipeline discontinuities such as diameter changes are allowed. The rationale, the variables involved, the uncertainty estimations, and the sensitivity of leak detectability are discussed.

For steady-state flow and using volumetric mass balance, a leak becomes detectable when the volume of the leak in a given time period, called response time, exceeds the volume uncertainties due to flow measurements and linefill change. A step-by-step procedure and a data base for calculating leak detectability, together with an application example and field trial results are provided in Chapters 5 and 6.

When a short response time is used, and when the pipeline dry volume is large and throughput small, a reasonable leak detectability can be established based on temperature uncertainty alone. When a long response time is used and when the pipeline dry volume is large and throughput small, a reasonable leak detectability can be established based on flowrate uncertainties alone. Pressure uncertainty becomes important only when the response time is short and temperature uncertainty small, and the pipeline has a large dry volume but with a small throughput. A procedure to establish the sensitivity of leak detectability and an application example are given in

Chapter 7.

Changes of pressure and/or flow at pipe ends are necessary to move from one state of flow to the next. Transients occur during the period of transition and are likely to persist after the desired changes at the pipe ends have been implemented. Transients introduce additional linefill uncertainty in the volumetric mass balance. Besides the transition period being a variable itself, there are infinitely many ways that these changes can take place over the transition period. Consequently, it becomes impossible to establish a universal data base for evaluating transient-induced linefill uncertainty. However, it is possible to estimate the transient-induced linefill uncertainty according to a dimensionless parameter R and the severity of the transients.

The parameter R characterizes a pipeline. It is a dimensionless combination of five pipeline variables: friction factor, length, diameter, velocity, and wave speed. A single R value encompasses infinitely many sets of the five variables as along as these five variables yield the same R. The usage of R simplifies variable analysis and makes the results more general.

The transient-induced linefill uncertainty downgrades leak detectability by the volumetric mass balance method. This uncertainty can be minimized by correcting linefill changes according to pressure changes. Additional pressure measurements along the pipeline may be used for this purpose. Alternatively, a transient flow model may be used to compute the linefill changes. An example demonstrates the estimation of transient severity, the transient-induced linefill uncertainty, the degradation of leak detectability, and the subsequent improvement using additional pressure data.

In leak detection by transient flow analysis, discrepancies between measurements and calculations appear whenever a leak occurs. Specific patterns of discrepancies emerge as a result of the propagation nature of transient flow. The onset of a leak is declared once a discrepancy pattern associated with a leak is recognized. The response time of this approach is the time needed for a wave to travel from the leak site to the farthest pressure or flow sensor adjacent to the site. The response time is independent of the leak size and is generally much shorter than the response time of the volumetric mass balance approach.

The leak detectability based on transient flow analysis is a function of R, uncertainty in R, type of transient flow (flow increasing or decreasing), leak location, and data noise. The leak detectability is greater (i.e., the size of the minimum detectable leak is smaller) for smaller R and for flow decreasing transients. When R is large and/or when the transients cause flow to increase, leak signals suffer greater attenuation and smearing, resulting in a degradation of leak detectability.

The leak detectability is tolerant of the uncertainties in the five pipeline variables that form the parameter *R*. The leak detectability decreases almost linearly with increasing uncertainty in *R*. The rate of decrease is the greatest for flow increasing transients, and the smallest for steady-state flow. Very large uncertainty in *R* (greater that 30 percent) can be tolerated without appreciable degradation in leak detectability for steady flow.

Data noise adversely and strongly impacts leak detectability. It also adversely affects the reliability of leak detectability. With the presence of noise, methods based on transient flow analysis can detect large leaks (approximately 15 percent of throughput and larger) with certainty. However, smaller leaks (approximately 1 percent of throughput) become difficult to detect. Longer time intervals to gather more data and different leak analysis algorithms are required.

Chapter 1

INTRODUCTION

1.1 RATIONALE

The Pipeline Transportation Cybernetics Committee of the American Petroleum Institute (API) formed a Pipeline Leak Detection Task force in 1989 to investigate software-based leak detection systems. The Task Force recognized the importance of pipeline variable uncertainties and retained the University of Idaho to study the effects of variable uncertainties on leak detectability, and to establish procedures to evaluate leak detectability. The findings of this study are provided in this report.

Advances in Supervisory Control and Data Acquisition (SCADA) technologies are moving pipeline leak detection from periodic inspections to software-based systems. These systems are implemented using field instrumentation, SCADA, and computers. Software-based leak detection systems have three components: (1) mathematical algorithms, (2) pipeline variables, and (3) operator experience. The mathematical algorithms are based on physics and abide by the conservation principles of mass, momentum, and energy. Pipeline variables are the parameters pertaining to SCADA systems, instrumentation, fluid properties, physical attributes of pipelines, pressure, temperature, and rate of flow. Because the mathematical algorithms are approximations of reality, and because the pipeline variables are never known with certainty, the first two components do not make a perfect detector. Operator experience is needed to deal with the consequence of uncertainties.

Leak detection is vital to pipeline companies (Mears (1993))*. An understanding of the effect of pipeline variables and their uncertainties on leak detectability helps interested parties to appreciate the capabilities and limitations of the technology. A procedure to evaluate leak detectability will be useful in the planning, design, upgrading, and operation of leak detection systems.

According to a survey conducted by the API Pipeline Leak Detection Task Force (Oppenheim Research (1991)), the majority of the responding companies expressed interest in having a method to perform variable impact studies on software-based leak detection systems. This study was commissioned to satisfy this need.

* References are cited by author's name and the year of publication. A complete list of references can be found at the end of the report.

1.2 LEAK DETECTION POTENTIAL

The leak detection potential of a pipeline quantifies how small and how quickly a leak can be detected, given the instrumentation and SCADA capabilities. The detectable leak size can be expressed as a function of response time.

Besides instrumentation and SCADA capabilities, leak detection potential depends on the state of flow and the physical configuration of the pipeline. For a given pipeline and with a specified response time, the detectable leak size is smaller for steady flows than for transient flows.

1.3 OBJECTIVES

This study quantifies the effects of variables on leak detection using common software-based leak detection methods. This study provides a data base and a step-by-step methodology to evaluate leak detection potential of a given pipeline with specified instrumentation and SCADA capabilities. Incremental improvement of leak detectability resulting from upgrading individual variables can also be determined.

The utility of the results from this study is to enable users (i.e., pipeline companies) to determine the achievable level of leak detection for a specific pipeline with a specified set of instrumentation and SCADA system. The results also help users to understand the sensitivity of leak detectability with respect to the variables involved. This information is useful in several ways: investigating the feasibility of leak detection systems, justifying and prioritizing changes to instrumentation and SCADA systems, configuring pipeline and measurement stations, and aiding leak detection operations.

1.4 SCOPE

Three general types of software-based leak detection methods are addressed in this study: (1) mass balance, (2) mass balance with linefill correction, and (3) transient flow analysis. The leak detection potential of these methods will be discussed based on hydraulics to the extent possible. Specific implementations of software-based methods will be avoided.

The liquids considered are crude oils and refined petroleum products such as gasoline, jet fuel, and fuel oil.

The pipeline configuration considered is a pipe segment with pressure, temperature, and volumetric flow measurements at each end. During steady-state flow, this configuration applies to pipelines with booster pumping stations where rates of flow are measured only at the inlet and the outlet of the entire system.

All variables affecting leak detection will be listed. General relationships between the variable uncertainties and leak detection potential will be analyzed. The methodology will be described and verified with field tests. The variables will be ranked according to their importance to leak detectability. A step-by-step method and a data base will be established to enable simple hand calculations for establishing leak detectability based on mass balance. The method and the data base will be verified with field data. The rationale and the procedure to establish leak detectability using mass balance with line pack correction and transient flow simulations will be given and illustrated with examples and field trial results.

1.5 REPORT FORMAT AND OUTLINE

This report is organized into eleven chapters and a list of references.

Chapter 2 addresses the physical basis for leak detection by outlining the principle of mass conservation and Newton's second law of motion. Relevant properties of fluids and pipelines are pointed out.

Chapter 3 reviews the density-pressure-temperature relationships for crude oils and refined products. It then discusses variables pertaining to pipelines, process measurements, and SCADA systems. Ranges of variables and levels of uncertainties are listed. Methods of estimating overall uncertainty for compound processes are described.

Chapter 4 studies linefill and its uncertainty. It shows how to compute linefill and demonstrates the sensivity of linefill with respect to the independent variables. Changes in linefill over time as a result of uncertainties in the process variables are discussed.

Chapter 5 establishes a procedure and associated data bases for leak detection by volumetric mass balance. For a given pipe size and length, the size of the minimum detectable leak, expressed as a fraction of a reference flow rate, is viewed as a function of response time. The rationale for the procedure is explained in detail. The data bases for the rates of change of linefill with temperature and pressure are developed for both refined products and crude oils. A step-by-step method to establish leak detectability is described, followed by an application example and an accuracy assessment.

Chapter 6 presents results of field trials on the volumetric mass balance method and the associated data bases. Nonrepeatability in measurements due to instrumentation and fluctuations in pressure and flow are discussed.

Chapter 7 generalizes the expression for leak detectability using the ratio of the response time over a residence time. This generalization allows the size and length of pipelines to enter the leak detectability formulation. Variables are then ranked according to their importance to leak detectability.

Chapter 8 introduces transients. The equations that govern transient flows are discussed. A similitude parameter R is established to characterize pipeline systems from the viewpoint of transient flow, and to simplify variable uncertainty analysis. This chapter ends with a procedure for estimating a mass imbalance error when waterhammer equations are used to compute linefill changes in leak detection applications.

Chapter 9 addresses the uncertainty in linefill change induced by transient flow. A method to characterize the severity of transients is suggested. When transients-induced linefill changes are regarded as uncertainties, the leak detectability based on volumetric mass balance must be downgraded. One approach is illustrated with an example.

Chapter 10 establishes a method of leak detection by transient flow simulations. The effects of uncertainties in pipeline parameters are expressed in terms of the similitude parameter R. The effect of the type of transients (i.e., flow increase or flow decrease), the location of the leak, and noise in the measured data are also discussed.

Chapter 11 presents field trial results for the leak detection method by transient flow simulations. The high R value and the noise in the measured data necessitated a modification to the method described in Chapter 10. The influence of data noise on leak detectability and the tolerance for uncertainty in R by this method are demonstrated.

Chapter 2

PHYSICAL BASIS FOR LEAK DETECTION

2.1 CONSERVATION OF MASS

The principle of mass conservation as applied to liquid flow in pipelines states that the time rate of mass inflow to a pipe segment minus the time rate of mass outflow equals the time rate of mass increase (decrease is considered as a negative increase) in the pipe segment. The rate of mass outflow includes any leaks that may exist in the pipe segment.

Quantitative expression of the principle of conservation of mass depends on the state of flow. For steady flow where there is no mass inventory change in the pipe segment, conservation of mass demands that the rate of mass inflow be identical to the rate of mass outflow.

Unsteady flow or transient flow is a general state of flow of which steady flow is a special case. In unsteady flow, pressure changes cause changes in mass inventory in the pipeline. This change takes place simultaneously in two main forms: liquid compression and density change, and pipe cross-sectional area change. The relative importance of the two depends on the compressibility of the liquid and the diameter to wall thickness ratio of the pipe. Therefore, besides the rates of mass inflow and outflow, stress-deformation characteristics of the liquid and the pipe are needed in stating the principle of mass conservation.

2.2 CONSERVATION OF ENERGY

The first law of thermodynamics states that the energy increase in a body of mass over a time period equals the difference between the heat transferred to the mass and the work done by the mass during the same period. For flow in pipes, the energy can be separated into a mechanical part and a thermal part. During the flow process, some of the mechanical energy is converted through viscous stress into thermal energy. Consequently, there is a loss of mechanical energy. This loss of energy for a unit weight of the fluid under consideration is called head loss.

The head loss is related to the square of the average velocity in the pipe through the Darcy-Weisbach friction factor, which depends on the Reynolds number of the flow and the relative roughness of the pipe wall.

2.3 NEWTON'S SECOND LAW OF MOTION

This law states that the net force imparted to a body of mass equals the time rate of change in the momentum of the body. Since the time rate of change in momentum equals the product of mass and acceleration, this principle can be stated alternatively as the net force equals mass times acceleration.

For transient flow, pressure and flow interact to maintain a dynamic equilibrium describable by Newton's second Law of Motion. For steady flow, there is no acceleration and consequently no net force, and this principle has no further utility.

The conservation principles of mass and energy and the Newton's second law of motion enable us to describe the pressure and flow in a pipe segment as a function of space and time.

2.4 FLUID AND PIPE PROPERTIES

From the viewpoint of leak detection, mass density is one of the most important fluid properties. To a large extent, a reference density at the standard condition of 15°C and 1 atmosphere (or degree API at 60°F in customary English units) will identify the type of product. Each product (gasoline, gasoline-jet fuel transition, jet fuel, and fuel oil) encompasses a standard mass density range, and has a unique relationship between the standard mass density, pressure, and temperature. Such relationships, also viewed as equations of state, are standardized and published by the petroleum industry.

Although the usual units used for mass are kg, pound mass, or slugs, an alternative unit of barrels is used in the industry. Strictly speaking, barrel is a unit for volume not mass. However, barrel can be used as a measure of mass if the following definition is adopted: Barrel refers to the mass contained in one barrel (42 gallons) at the standard condition of 15°C and 1 atmosphere. One barrel of a lighter product contains less mass. As will become evident later in this report, barrel, used in conjunction with a reference mass density, is a convenience unit in leak detection.

An attribute of line pipe pertaining to leak detection is the enclosed volume as a function of pressure and temperature. For an operating pipeline with through flow, the pressure and temperature are independent of each other as liquids are freely accumulated or depleted in the pipeline as temperature or pressure changes. Consequently, changes in the enclosed volume due to pressure and temperature can be considered separately, and the results are additive.

Knowing the pressure and temperature as a function of distance and time, changes in mass inventory due to all causes at any instant can be calculated.

2.5 BASIS FOR LEAK DETECTION

In principle, if the rate of mass flow at the pipe outlet is smaller than that at the inlet, <u>and</u> if the mass inventory change has been accounted for properly, then a leak or leaks must exist. In practice, allowances must be made for uncertainties in the rates of mass flow and in the estimation of the mass inventory change. Consequently, a deterministic prediction with certainty of leak occurrence is not possible.

Chapter 3

VARIABLES AND UNCERTAINTY LEVELS

3.1 FLUID PROPERTIES

Mass density and bulk modulus (reciprocal of compressibility) of the fluid are the properties of primary importance to leak detection. Established procedures in the form of various standards can be used to compute these properties and their variations with pressure and temperature. These procedures are reviewed here.

Oils are mixtures of pure substances. The properties of mixtures depend on their composition and density range. According to ASTM (1980), oils are categorized into statistically different groups: crude oil, gasoline, gasoline-jet fuel transition, jet fuels, and fuel oils. The latter four are regarded as products. To a large extent, a reference density at 15 °C and 1 atm, ρ_0, can be used to identify the products as shown in Table 3.1. Note that the reference density between crude oils and products overlap. As a result, separate representations of properties for crude oils and products are necessary. Both the fluid type (crude oils or refined products) and the reference density are needed to identify the properties of the fluid.

Table 3.1 Petroleum fluids and their reference density range.

Fluids	Reference Density Range, kg/m^3
Crude Oil	$610.0 \leq \rho_0 < 1075.0$
Gasoline	$653.0 \leq \rho_0 < 770.5$
Gasoline-Jets	$770.5 \leq \rho_0 < 787.5$
Jet fuels	$787.5 \leq \rho_0 < 839.0$
Fuel oils	$839.0 \leq \rho_0 < 1075.0$

The mass density of fluids at non-reference conditions can be calculated by applying volume correction factors for temperature C_T and for pressure C_P to ρ_0

$$\rho = C_P C_T \rho_0 \tag{3.1}$$

The volume correction factor for temperature is expressed as (ASTM (1980))

$$C_T = e^{-\alpha_T \Delta T(1 + 0.8\alpha_T \Delta T)} \tag{3.2}$$

where

$$\alpha_T = \frac{K_0 + K_1 \rho_0^{\beta}}{\rho_0^2} \tag{3.3}$$

and ΔT = temperature departure in Centigrade from 15°C. The constants K_0, K_1, and β for the fluid groups are shown in Table 3.2. In computing C_T, ρ_0 is rounded to the nearest 0.5 kg/m^3 and temperature to the nearest 0.05°C, in accordance with the ASTM D 1250-80 Standard.

Table 3.2 Coefficients for the volume correction factor for temperature.

Products	K_0	K_1	β
Crude Oil	613.9723	0	1
Gasoline	346.4228	0.4388	1
Gas-Jets	2680.3206	-0.003363	2
Jet fuels	594.5418	0	1
Fuel oils	186.9696	0.4862	1

The above constants were established through correlations. The predicted precision for C_T at the 95 percent confidence level varies from ±0.05 percent at 38°C (100°F) to ±0.35 percent at 121°C (250°F).

The volume correction factor for pressure is a function of the compressibility factor F of the fluid. API (1984) uses the following relationship for F in kPa^{-1}:

$$F = \frac{e^{\left(A + BT + \frac{C}{\rho_0^2} + \frac{DT}{\rho_0^2}\right)}}{1000000} \tag{3.4}$$

where A = -1.6208, B = 0.00021592, C = 0.87096, D = 0.0042092, ρ_0 = density at the reference state in g/cm^3, T = temperature in °C and P = gauge pressure in kPa. The constants A, B, C, and D were established from correlations of experimental data. The ranges of the data are: 681 kg/m^3 $\leq \rho_0 \leq$ 934 kg/m^3, 0°C $\leq T \leq$ 150°C, and 0 kPa $\leq$ $P \leq$ 4902 kPa. Within these ranges, the maximum uncertainty in the compressibility factor is ±6.5 percent. In computing F, ρ_0 is rounded to the nearest 2 kg/m^3 and temperature to the nearest 0.25°C according to the Manual of Petroleum Measurement Standards, Chapter 11.2.1M.

Jessup (1930) suggested that mean compressibility could possibly decrease by about 0.00073 percent per kPa pressure increase. At what pressure this effect becomes significant is not definitely known. In the volume uncertainty analysis, API (1984) assumed that the pressure effect starts to take place at 0 kPa gauge. This assumption is used in this study. Consequently,

$$F = \frac{e^{\left(A + BT + \frac{C}{\rho_0^2} + \frac{DT}{\rho_0^2}\right)}}{1000000}(1 - 0.0000073P) \tag{3.5}$$

The bulk modulus of the oils K is the inverse of the compressibility factor

$$K = F^{-1} \tag{3.6}$$

Following the definition for C_P in API (1984) but assuming the bubble point of the oils to be atmospheric, it can be shown that

$$C_P = (1 - FP)^{-1} \tag{3.7}$$

Knowing the mass density at the reference condition and the correction factors C_P and C_T , the mass density of the oils at pipeline conditions can be computed from Eq. (3.1).

The wave speed a, assuming the pipe to be rigid, is

$$a = \sqrt{\frac{K}{\rho}} \tag{3.8}$$

The variations in mass density, bulk modulus, and rigid-pipe wave speed with pressure and temperature are quantified in Fig. 3.1. The left column of this figure has a fixed temperature of 15°C. The right column has a fixed pressure of 3500 kPa. It is seen that variations of the properties with reference density, temperature, and pressure are significant. Similar curves for crude oil can be generated using the data presented in this section.

3.2 PIPELINE SYSTEM PARAMETERS

This category of parameters includes geometric properties, material properties, and a pipe-fluid property. The geometric properties are: diameter, length, pipe wall thickness, and pipeline elevation profile. The material properties are Young's modulus of elasticity and the thermal expansion coefficient of the pipe material. The pipe-fluid property is the Darcy-Weisbach friction factor, which is a function of the roughness of the pipe inside wall, the viscosity of the fluid, and the Reynolds number of the flow.

The pipe diameter and wall thickness and the associated tolerances can be found in standard references on manufactured pipe. The length and elevation profile of the pipeline may be obtained from construction specifications as as-built values. The actual values may vary, especially for older lines that have gone through changes. The Young's modulus and the thermal expansion coefficient are found from standard references once the type of pipe steel is known. As will be shown later, these two parameters have only marginal influence on leak detection potential. The Darcy-Weisbach friction factor can be determined from the pressure, elevation and flowrate data. This parameter is usually considered a "tuning" parameter as one seldom predicts the friction factor from pipe roughness and fluid's viscosity. For this reason, fluid viscosity is not explicitly considered as a fluid property for leak detection.

3.3 PROCESS VARIABLES

The main process variables of leak detection are flowrate, pressure, temperature and reference mass density (or degree API at 60°F). Usually the flowrate, pressure and temperature at the ends of a pipe segment are sampled periodically by a SCADA system.

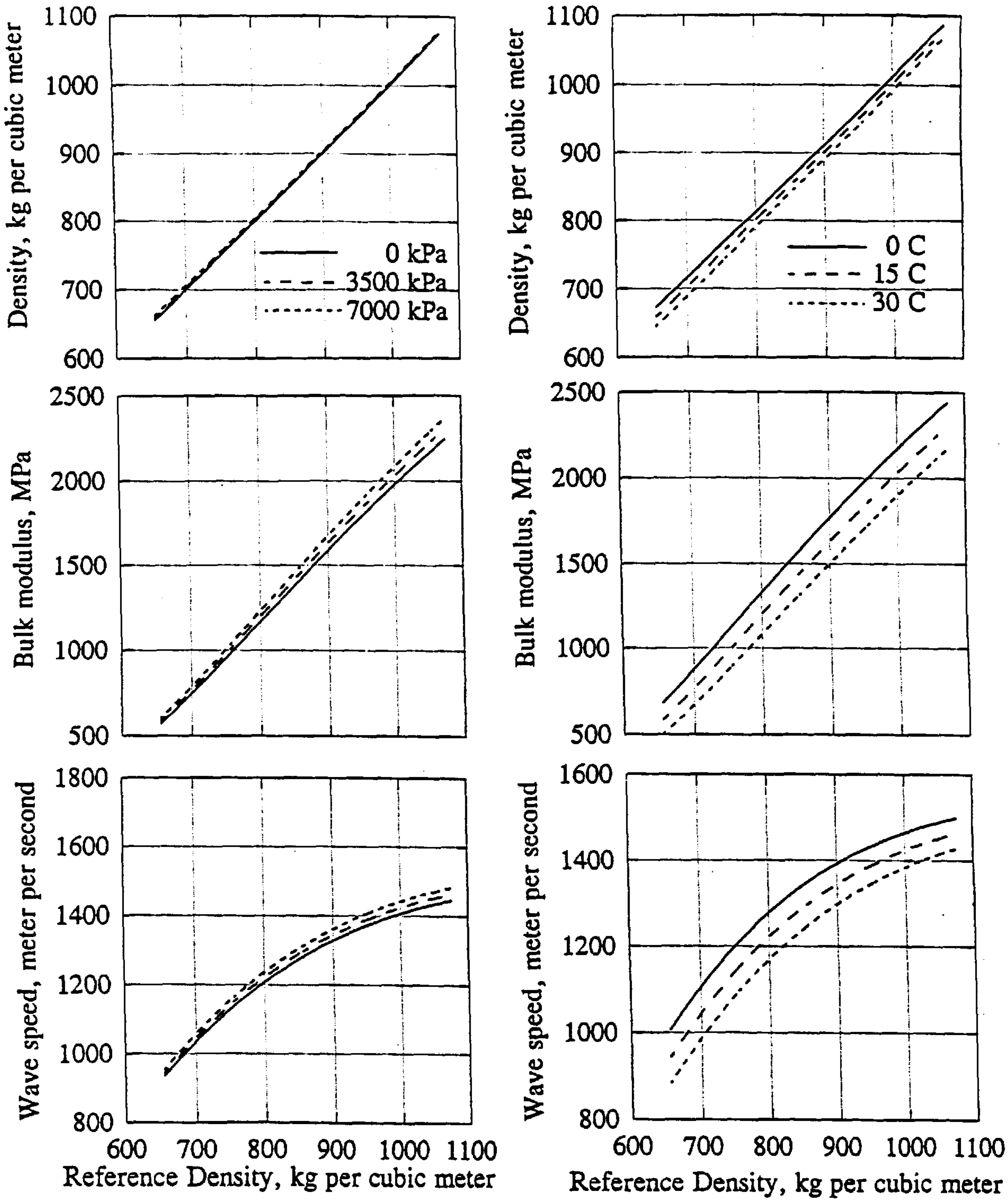

Fig. 3.1
Mass density, bulk modulus, and rigid pipe wave speed for generalized petroleum products. Left: fixed temperature of 15°C. Right: fixed pressure of 3500 psig

Two additional process variables need to be considered. They are the representative reference mass density of each product batch, and the position of batch interfaces, if present. The reference mass density for a product batch may be inferred from the type of the product. A more representative value for a batch can be obtained by sampling the product at a fixed time interval as the product passes a fixed point. After the batch leaves the pipe segment, the reference density of the composite of all the samples is determined and is taken as the reference mass density of the batch. The batch interface may be inferred by a batch-tracking algorithm or a stream tape, and may be confirmed by densitometers at fixed locations.

3.4 SCADA VARIABLES

The SCADA variables of importance in leak detection are polling time and time skew. They pertain to scheduling the reading of multiple sensors. Normally, the SCADA system reads each sensor, processes the data, pauses, and loops back to the first sensor to repeat the cycle. Polling time is the period between two consecutive cycles. Time skew is the time difference between two readings within a polling cycle. Time skew exists unless the SCADA system is designed to obtain simultaneous snapshots of all relevant sensors.

When the flow is at steady-state, the polling time and time skew are immaterial as nothing changes with time. However, they become significant for transient flows.

3.5 VARIABLE RANGE AND LEVEL OF UNCERTAINTIES

Table 3.3 shows the range and the uncertainties applicable to this variable analysis study.

Table 3.3 Range of Variables and Their Uncertainties
(data prepared by API Pipeline Leak Detection Task Force)

Range of Physical Pipeline Variables

pipe	minimum		maximum
diameter	4 inch		48 inches
wall thickness	0.125 inches		1 inch
length of a single pipe segment	5 miles		500 miles
wall roughness	0.0009 inches		0.0025 inches
pipe material Young's modulus	29,000,000 psi		29,000,000 psi
Poisson's ration	0.25		0.35

Range of Liquid Property Variables

petroleum	minimum		maximum
bulk modulus	26,000 psi		300,000 psi
viscosity	0.1 centistokes		2000 centistokes
density	81.0° API		25.0° API
celerity			

Table 3.3 continued

Range of Instrumentation Variables

pressure	minimum		maximum
uncertainty	0		+/- 1.0% span
max span	0 psig		1500 psig
spacing	5 miles		60 miles

temperature	minimum		maximum
uncertainty	0°F		5°F
max span	0.0°F		120.0°F
spacing	5 miles		120 miles

density	minimum		maximum
uncertainty	0.0° API		20.0° API
max span	81.0° API		25.0° API
spacing	5 miles		500 miles

flow rate	minimum		maximum
uncertainty	0		+/- 5.0% span
max span	turbulent flow		7.0 ft./sec.
spacing	10 miles		250 miles

Table 3.3 continued

Range of SCADA Variables

	minimum		maximum
poll time of data	2 seconds		60 seconds
time skew of data	0 seconds		60 seconds

Range of Piping System Variables

	minimum		maximum
pipeline elevation at pressure measurement locations on one pipeline segment	0 feet		1500 feet
product batch position location error	0 barrels		50% of linefill volume

3.6 OVERALL UNCERTAINTY ESTIMATIONS

The final outcome of a process is often determined by a number of independent and direct measurements, each of which has its own uncertainty. If the individual uncertainties are known, what is the overall uncertainty of the process?

Let Q be a quantity that continuously depends on directly measured quantities q_1, q_2, ... q_n.

$$Q = f(q_1, q_2, \dots q_n) \tag{3.9}$$

Denote incremental changes in q_1, q_2, ... q_n by dq_1, dq_2, ... dq_n. Then

$$dQ = \frac{\partial f}{\partial q_1} dq_1 + \frac{\partial f}{\partial q_2} dq_2 + \dots + \frac{\partial f}{\partial q_n} dq_n \tag{3.10}$$

If dq_1, dq_2, ... dq_n are taken as upper bounds of the individual errors, then the maximum possible error in Q is

$$dQ_{abs} = \left|\frac{\partial f}{\partial q_1} dq_1\right| + \left|\frac{\partial f}{\partial q_2} dq_2\right| + \dots + \left|\frac{\partial f}{\partial q_n} dq_n\right| \tag{3.11}$$

The absolute-value signs are used because the partial derivatives, called sensitivity coefficients, can be either positive or negative. Without using the absolute-value signs, a negative sensitivity coefficient combined with a positive dq would reduce the overall error estimation.

Note that so far the dq's are viewed as upper bounds or absolute limits on the individual errors. When dq's are considered as uncertainties, then the overall uncertainty should be computed from the following Root-Sum-Square (RSS) process instead of from Eq. (3.11) (Doebelin (1983), Scarborough (1962))

$$dQ_{RSS} = \sqrt{\left(\frac{\partial f}{\partial q_1} dq_1\right)^2 + \left(\frac{\partial f}{\partial q_2} dq_2\right)^2 + \dots + \left(\frac{\partial f}{\partial q_n} dq_n\right)^2} \tag{3.12}$$

The interpretation for dQ_{RSS} is the same as those for dq's. If the dq's follow the normal distribution and are set to ±2 standard deviations of individual direct measurements, then dQ_{RSS} also follows the normal distribution and represents ± 2 standard deviations of Q. That is, 95.46 percent of the values of Q are expected to fall within the mean of $Q \pm dQ_{RSS}$.

For the same dq's, the error bound estimation from Eq. (3.11) always exceeds the RSS uncertainty from Eq. (3.12). Both estimates are useful. For a given process, one may regard the overall uncertainty to be possibly as large as dQ_{abs}, but probably not larger than dQ_{RSS}. dQ_{RSS} is preferred in this study as it is more realistic and less conservative that dQ_{abs}.

Chapter 4

LINEFILL AND ITS UNCERTAINTY

4.1 LINEFILL AND ITS UNCERTAINTY IN A UNIFORM PIPE SEGMENT

Linefill i is a function of pipe diameter D, wall thickness e, Young's modulus of the pipe wall material E, thermal expansion coefficient of the pipe material α, reference density of the product ρ_0, pressure P, and temperature T. By definition:

$$i = \int_0^L \rho(x)\ A(x)\ dx \tag{4.1}$$

in which L = pipe length and $A(x)$ = cross-sectional area of the pipe,

$$L = L_o(1 + \Delta T) \tag{4.2}$$

$$A(x) = A_0\ (e^{\frac{Dc_1 P(x)}{Ee}} + 2\alpha\, \Delta T\ ) \tag{4.3}$$

where L_0 and A_0 are the pipe length and the cross-sectional area at the standard condition. ΔT denotes temperature departure from 15°C. In Eq. (4.3), the first term in the parenthesis is a fractional cross-sectional area change due to pressure departure from 1 atm. The "e" in the base denotes the natural logarithmic function. The "e" in the denominator of the exponent represents the thickness of the pipe wall. The dimensionless constant c_1 reflects the state of stress in the pipe wall. The second term in the parenthesis is the fractional change due to temperature departure from 15°C. A third term $(\alpha\Delta T)^2$ is very small compared with $2\alpha\Delta T$ and is neglected.

The value of c_1 depends on the state of stress in the pipe wall. When a pipe is allowed to extend freely, there is no longitudinal stress in the pipe wall. The constant c_1 equals unity, and the area expansion is the greatest for a given pressure rise. On the other hand, when a pipe is prevented from axial movement, no axial strain can develop. The constant c_1 becomes 1 - μ^2 where μ is the Poisson's ratio of the pipe wall material (Wylie and Streeter (1993)). The second condition yields the smallest area expansion. The state of stress in a cross-country pipeline is unknown but lies somewhere in between the two extremes. For D/e =100, P = 1000 psig, E = 300,000 psi, and μ = 0.35, the variation of pipe expansion between the two extremes is about 4 percent. The variation is smaller for smaller D/e and P.

In leak detection by volumetric mass balance, the uncertainty in c_1 has an negligible effect since c_1 is not a process variable and any uncertainty in c_1 remains unchanged over time. For simplicity, c_1 is assumed to be unity and is no longer explicitly spelled out in the equations.

For uniform temperature and pressure, the expression for linefill becomes

$$i = [\rho_0 \; C_T(1 - FP)^{-1}] \; [A_0(e^{\frac{Dp}{Ee}} + 2\alpha\Delta T)] \; [L_0(1 + \alpha\,\Delta T)] \tag{4.4}$$

where and C_T and F are defined in Eqs. (3. 2) and (3.5).

Unlike temperature, the pressure may vary significantly over distance. Assuming a linear pressure profile and uniform temperature, the integral for i in Eq. (4.1) has been evaluated numerically for common pipeline segments. Separately, linefill calculations using the average pressure over pipeline segments were carried out. Comparisons show that the linefill can be calculated accurately using the average pressure for pipelines about 50 miles in length. Longer lines can be broken into segments and Eq. (4.4) applied individually with average pressures.

The uncertainty in linefill di is expressed in terms of the uncertainty in each of the eight variables by

$$di = \frac{\partial i}{\partial D}dD + \frac{\partial i}{\partial e}de + \frac{\partial i}{\partial E}dE + \frac{\partial i}{\partial \alpha}d\alpha \frac{\partial i}{\partial L}dL + \frac{\partial i}{\partial \rho_0}d\rho_0 + \frac{\partial i}{\partial T}dT + \frac{\partial i}{\partial P}dP \tag{4.5}$$

where dD, de, dE, $d\alpha$, dL, $d\rho_0$, dT, and dP are regarded as uncertainties in the variables. The partial derivatives can be viewed as the sensitivity coefficients of linefill with respect to each of the variables. Algebraic expressions for the derivatives can be obtained from Eqs. (3.1), (3.2), and (4.3). Alternatively, the derivatives can be evaluated numerically. Because the algebraic expressions are lengthy, numerical derivatives are preferred.

The uncertainties in the seven variables are independent of each other. In estimating the most probable uncertainty in linefill as a result of the combined effects of the seven variables, the RSS procedure outlined in Section 3.6 is used to obtain

$$di \le \sqrt{(\frac{\partial i}{\partial D}dD)^2+(\frac{\partial i}{\partial e}de)^2+(\frac{\partial i}{\partial E}dE)^2+(\frac{\partial i}{\partial \alpha}d\alpha)^2+(\frac{\partial i}{\partial L}dL)^2+(\frac{\partial i}{\partial \rho_0}d\rho_0)^2+(\frac{\partial i}{\partial T}dT)^2+(\frac{\partial i}{\partial P}dP)^2} \quad (4.6)$$

The volumetric linefill V and its uncertainty dV in volumes of mass at the standard condition can be obtained by dividing the respective quantities with ρ_0

$$V = \frac{i}{\rho_0} \quad (4.7)$$

$$dV = \frac{di}{\rho_0} \quad (4.8)$$

4.2 LINEFILL AND ITS UNCERTAINTY IN SERIAL PIPES AND IN PIPES WITH MULTIPLE BATCHES

Changes in pipe diameter and pipe wall thickness are common in long pipelines. Multiple batches of products may be present in such pipelines at any given instant. In evaluating linefill, the pipeline is divided into segments so that the properties within each segment are uniform. The relationship presented in the previous section is used to establish the linefill and its uncertainty segment by segment. Summing up the linefill for individual segments yields the linefill for the whole pipeline.

The uncertainty of batch interface positions introduces another linefill uncertainty. Let n be the number of batches in the pipeline, ρ_i, A_i and L_i be the mass density, pipe cross-sectional area, and length, respectively, of the i-th segment. The linefill uncertainty resulting from the batch interface uncertainties alone is

$$di_{batch\ interfaces} \leq \sum_{i=1}^{n-1} |\rho_i A_i - \rho_{i+1} A_{i+1}| dL_i \qquad i=1,2,...n \qquad (4.9)$$

The corresponding volumetric uncertainty is

$$dV_{batch\ interfaces} \leq \sum_{i=1}^{n-1} \left|\frac{\rho_i A_i - \rho_{i+1} A_{i+1}}{MIN(\rho_i, \rho_{i+1})}\right| dL_i \qquad i=1,2,1...n \qquad (4.10)$$

The linefill uncertainty due to uncertainty in batch interfaces should be added to the sum of linefill uncertainties over all pipe segments.

4.3 CHANGE OF LINEFILL UNCERTAINTY OVER TIME

As shown previously, there are nine variables that influence the linefill. They are divided into three groups:

1. Pipeline parameters

    diameters, D
    wall thicknesses, e
    Young's Moduli of elasticity, E
    thermal expansion coefficients, α
    lengths, L

2. Process variables that are polled in every SCADA scan

    pressures, P
    temperatures, T

3. Process variables that are not polled in every SCADA scan

    reference mass density for each product batch, ρ_0
    batch interface positions

The effects of pipeline variables on changes of linefill uncertainty over time are considered first. The uncertainties of the pipeline variables do not change over time. For example, the pipe length may be too long or too short with respect to its true value. Whatever the case may be, the length remains constant. The sensitivity coefficients of linefill with respect to the system variables change continuously with the state of flow. Over a short time period or if the state of flow changes gradually, one should expect little change in these sensitivity coefficients. In the extreme, they should not change at all for true steady flow. In any event, the linefill uncertainties contributed by uncertainties in D, e, E, α,and L are all zero since these variables are not evaluated from one SCADA scan to next.

The effect of the process variables is more significant. Consider pressure and temperature first. They are scanned during each SCADA polling cycle. As such, they are subjected to uncertainty each time. It is possible that dP and/or dT in Eq. (4.6) may change sign from scan to scan. On the other hand, the respective sensitivity coefficients $\partial i/\partial P$ and $\partial i/\partial T$ vary continuously with the state of flow and should not change appreciably between two consecutive scans. Consequently, the uncertainty in the change of linefill as a result of the two scans is almost doubled. It should be doubled exactly if the flow is truly at steady-state since the sensitivity coefficients remain constant for steady flow.

As noted in Section 3 of Chapter 3, the reference mass density of a product batch is assigned, based on product type, before the batch enters the pipeline. Representative reference mass density based on sampling can be more accurate but its value can not be established until the product batch has advanced well into the pipeline. In either case, the reference mass density remains constant while the product is in transit. Therefore, like system variables, the uncertainty in the reference mass density does not change with time. Similarly, the uncertainty in batch interface positions, once assigned, should not change over small time intervals. Thus the linefill uncertainty change over time due to these two variables is expected to be negligible.

4.4 EXAMPLE OF LINEFILL SENSITIVITY

A 100 mile long steel pipe with a wall thickness of 0.3 inch is used to demonstrate the variability of some of the coefficients. The product considered is gasoline with a reference density of 700 kg/m^3. Six orthographic 3-dimensional plots are shown in Fig. 4.1. A pressure of 3500 kPa is specified for the figures in the left column. A temperature of 15°C is specified for the ones in the right column. Note that the surfaces shown are slightly warped. Therefore, the sensitivity of the linefill

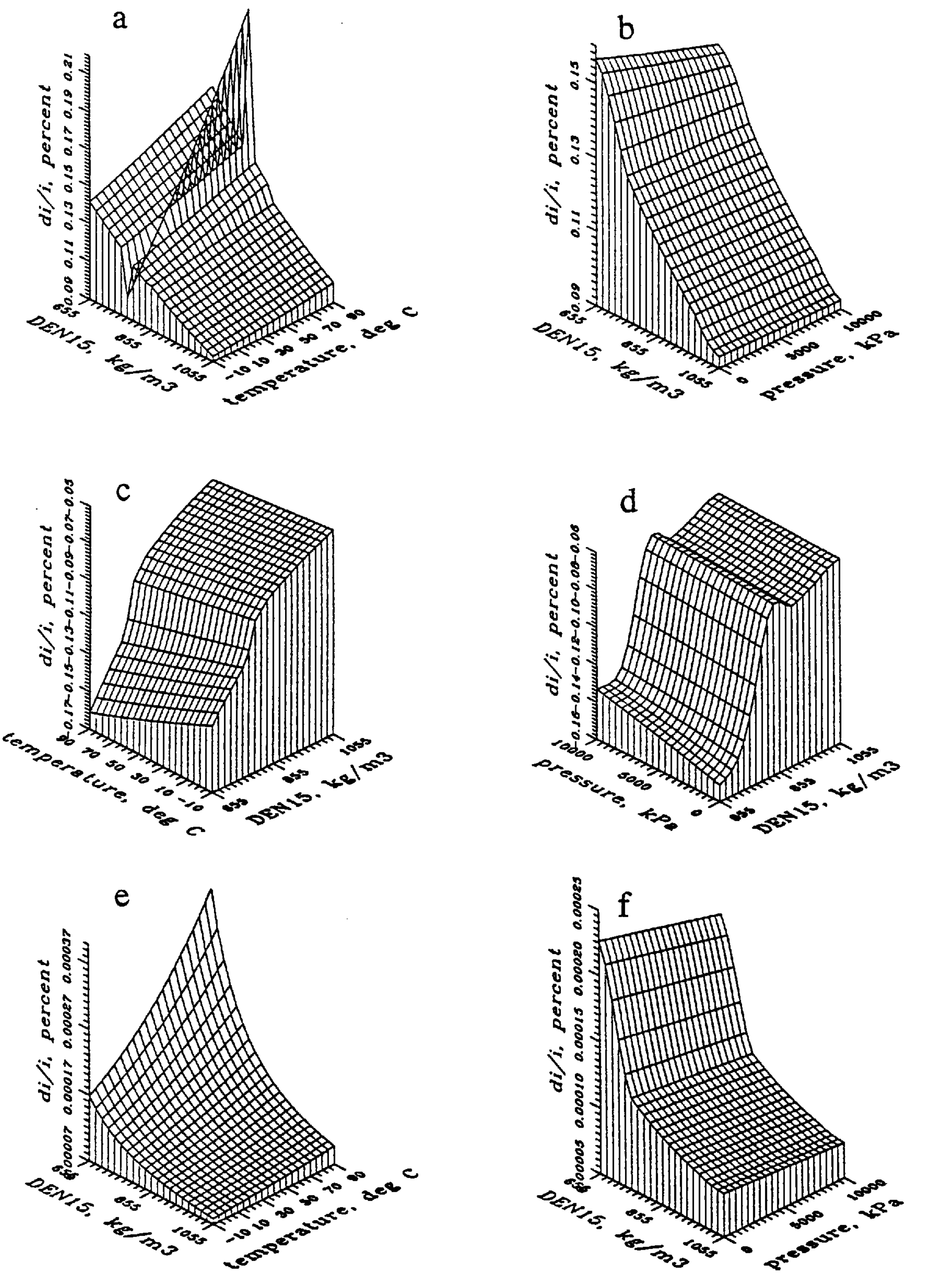

Fig. 4.1
Sensitivity of linefill with respect to reference density, pressure, and temperature

change is a nonlinear function of reference density, temperature, and pressure. The nonlinearity is more pronounced with reference density and temperature than with pressure.

Figs. 4.1a and 4.1b show the percent change in linefill as a result of a 1 kg/m^3 increase in the reference mass density. The sharp change in Fig. 4.1a at a reference mass density of 775 kg/m^3 is caused by the change in the form of the equation for α_T (see the change in β Eq. (3.3) and Table 3.2). This change is required by the steep slope in the α_T versus $1/\rho_0{}^2$ plot in the range of gasoline to jet fuel transition (ASTM (1980)). The percent change of linefill with respect to a 1°C temperature increase is shown in Figs. 4.1c and 4.1d. Figs. 4.1e and 4.1f show the percent change in linefill for a 1 kPa increase in pressure. Several trends are observed.

1) the density sensitivity is lower at high reference density, high pressure, and low temperature,

2) the temperature sensitivity is lower at low reference density, low pressure, and high temperature, and

3) the pressure sensitivity is lower at high density, high pressure, and low temperature.

Fig. 4.2 shows the relative importance of uncertainties in the variables discussed. The numbers in the top section are the assumed magnitude of the uncertainty in the variables. The middle section shows the percent change in linefill due to each of the seven errors. The bottom section shows the distribution of the linefill error among the seven variables. In the order of decreasing importance, the variables can be ranked as: relative density, temperature, diameter, length, pressure, wall thickness, and Young's modulus. The last two variables have equal but negligible effect on the linefill.

Of the seven variables, only temperature, pressure, and sometimes reference density are process variables. The remaining five variables remain unchanged over time. Note that the uncertainty in the reference density has the greatest impact on the uncertainty in linefill change. This is the case when the linefill is expressed in mass units, as in Fig. 4.2. However, when appropriate standard volumes are used to express linefill (a mass), the numerical value for the linefill change caused by an uncertain reference density is greatly reduced. Furthermore, under most circumstances, the reference density is not a process variable and will not affect uncertainty in linefill change. Therefore, temperature and pressure are the only two variables that are involved. Of the two, temperature is far more important.

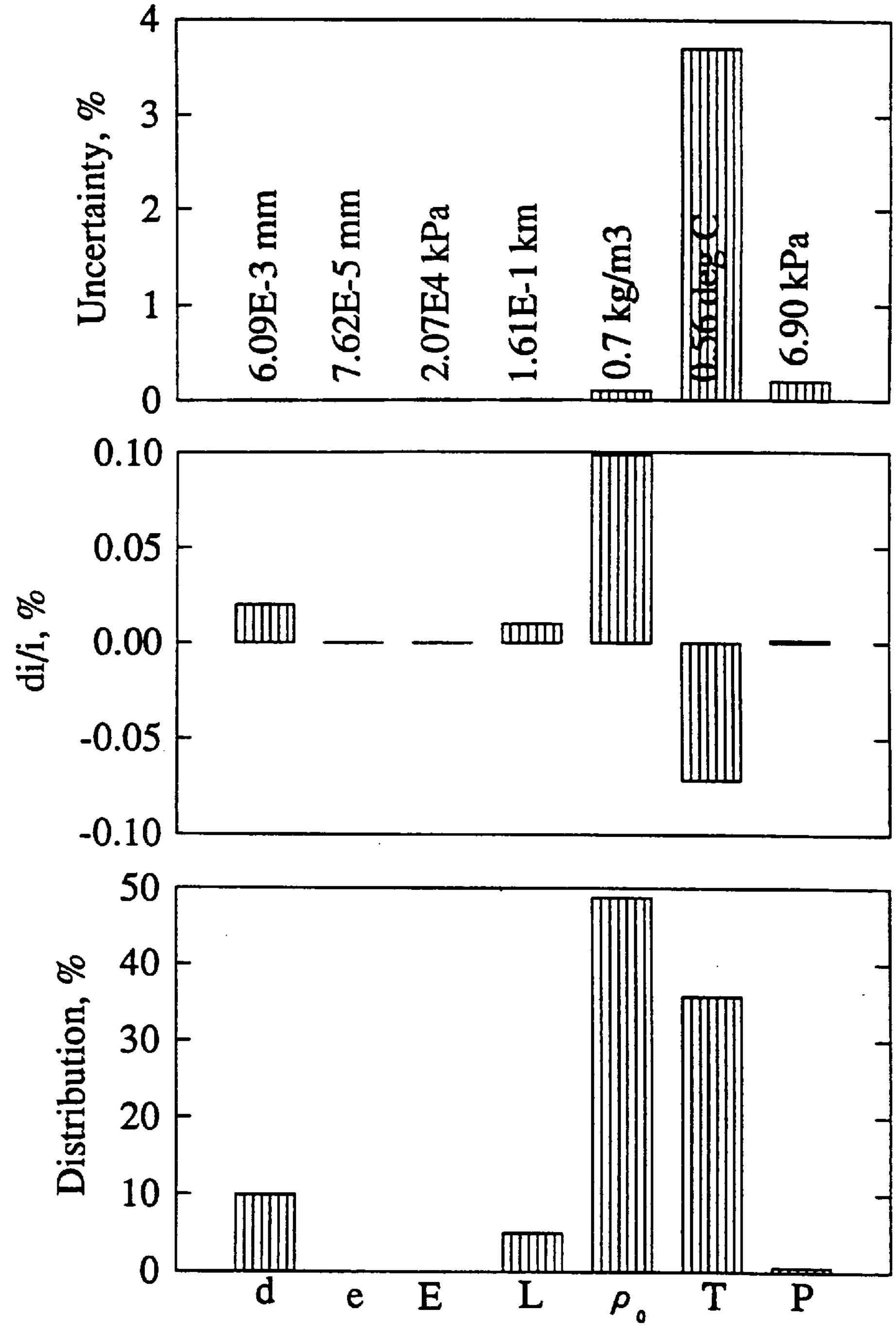

Fig. 4.2
Relative importance of uncertainties affecting linefill

Chapter 5

LEAK DETECTABILITY FOR STEADY-STATE FLOW BASED ON THE PRINCIPLE OF MASS CONSERVATION

5.1 MASS BALANCE AND LINEFILL UNCERTAINTIES

During a unit time interval, the measured mass of products, expressed in standard volumes, that enter a pipe may not be equal to the measured mass that has left. The difference is accounted for by uncertainties in flow measurements and in linefill change. Let Q_{in} be the measured inflow, and Q_{out} the measured outflow. Including the uncertainties, the principle of conservation of mass is stated as

$$| Q_{in} - Q_{out} | \leq dQ_m + \frac{dV_s}{\Delta t} \tag{5.1}$$

where dQ_m = bound of uncertainty in flow measurements and dV_s = bound of uncertainty in linefill change over a time interval Δt.

A leak, if it exists, can only be detected reliably if

$$Q_l = Q_{in} - Q_{out} > dQ_m + \frac{dV_s}{\Delta t} \tag{5.2}$$

where Q_l is the flow rate of the leak.

Flow measurements at the pipe inlet and outlet should be made with equipment of known and acceptable uncertainty. For each measurement, this uncertainty can be expressed as a fraction k of a reference flow rate Q_{ref} in standard volume per unit time. In general, dQ_m can be expressed as

$$dQ_m = Q_{ref}\sqrt{k_{in}^2 + k_{out}^2} \tag{5.3}$$

where the subscripts *in* and *out* denote the k values at the inlet and the outlet of a pipe segment. Since the two uncertainties in flow measurements are independent of each other, the RSS process (Section 3.6) is used to estimate the most probable uncertainty dQ_m. This estimation is more reasonable and less conservative than simply using the sum of the two component uncertainties.

The k values depend on the flow measurement equipment. If turbine meters are used over a 10:1 flow range, k can be set to the nonlinearity of the meter, which is typically about 0.002. However, if they are operated in a very narrow flow range, k can be equated to the repeatability of the meter, which is typically about 0.0002. Q_{ref} can be the steady-state or the maximum flow rate.

These flow measurement uncertainty values should be regarded as theoretical lower limits. In practice, the uncertainties can be considerably greater due to unknown bias errors and noise. This aspect is illustrated later in Sections 6.2 and 6.6.

The quantity dV_s is considered next. Use the dV defined in Eq. (4.7) to obtain

$$dV_s = dV_{t+\Delta t} - dV_t \tag{5.4}$$

Since the state of the flow does not change, the sensitivity coefficients of linefill with respect to the variables do not change. Following the discussion in Section 4.3 and using the RSS procedure, dV_s can be expressed as

$$dV_s = \sqrt{2\sum_{i=1}^{n} \frac{(\frac{\partial i}{\partial P}dP)^2 + (\frac{\partial i}{\partial T}dT)^2}{(\rho_0)^2}} \tag{5.5}$$

where n is the number of pipe segments. The partial derivatives are evaluated at the average pressure and temperature for the pipe segments. The incremental quantities

dP and dT are uncertainties in pressure and temperature for each segment. For true steady-state flow, they can be established from instrumentation specifications.

5.2 METHODOLOGY FOR STEADY FLOW

A leak becomes detectable when the volume of leakage exceeds the sum of volumetric uncertainties in flow measurements and in linefill change. Let Q_l be the flow rate of the leak. From Eqs. (5.2), (5.3) and (5.5), it can be shown that

$$\frac{Q_l}{Q_{ref}} \geq \sqrt{(k_{in}^2 + k_{out}^2) + (\frac{\Delta V_s}{\Delta t Q_{ref}})^2} \tag{5.6}$$

The ratio Q_l / Q_{ref} can be regarded as the minimum detectable leak over a time window Δt. Plotting Q_l / Q_{ref} against Δt results in a hyperbola that specifies the leak detection potential of the pipeline at steady flow. Two extreme conditions are of interest here. First, when $Q_l / Q_{ref} = 1$, the corresponding Δt can be regarded as a minimum response time. Second, when Δt approaches infinity, Q_l / Q_{ref} approaches the RSS uncertainty of the flow meters.

A special case of steady-state flow is a static or non-flowing line. When a pipeline is shut-in, the inflow and outflow are known to be zero with certainty. Eq. (5.6) is applicable to non-flowing pipes if k_{in} and k_{out} are set to zero. The choice of Q_{ref} for this case is immaterial as long as it is non-zero.

5.3 DATA BASE FOR RATES OF LINEFILL CHANGE

The analytical expressions for the partial derivatives in Eq. (5.5) are lengthy and not suitable for hand calculations. However, they are used, in conjunction with the fluid properties described in Chapter 3, to establish a data base that enables simple and accurate hand calculations to evaluate the partial derivatives.

Consider a single pipe segment. Let I be a scaled linefill defined as

$$I = \frac{i}{\rho_0 A_0 L_0} \tag{5.7}$$

The quantity $\rho_0 A_0 L_0$ represents the mass of the product contained in the pipe segment at standard conditions. Using a volume with a known reference mass density as a unit for mass, the magnitude for $\rho_0 A_0 L_0$ is simply $A_0 L_0$, or the dry volume of the pipe segment.

In terms of I, Eq. (5.5) is restated as

$$dV_s = \sqrt{2\sum_{i=1}^{n} (A_0 L_0)_i^2 [(\frac{\partial I}{\partial P} dP)^2 + (\frac{\partial I}{\partial T} dT)^2]} \tag{5.8}$$

Referring to Eq. (4.4), it is seen that I depends on the pipe inside diameter to wall thickness ratio, the thermal expansion coefficient and the Young's modulus of the pipe material, pressure, temperature, and the volume correction factors for pressure and for temperature. The latter two depend on fluid properties as well as on pressure and temperature. The thermal expansion coefficient and the Young's modulus are known with precision and are thus eliminated from the variable list.

Since each fluid group has its distinctive properties, product groups (see Table 3.1) are considered separately. Each product group is divided into a number of equal-length °API intervals so that the variations of reference mass density within each product group can be considered. For adequate resolutions, it was decided to represent gasoline with 7 intervals, gasoline-jet fuel transition with 1 interval, jet fuel with 3 intervals, fuel oils with 4 intervals, and crude oil with 15 intervals.

According to the set of representative pipeline data gathered by the API Pipeline Leak Detection Task Force, the ratio D/e varied from 15 to 126. D/e ratios of 15, 45, 75, and 105 are used to represent the D/e range.

The rate of change of the scaled linefill with pressure is a function of the D/e ratio, pressure, temperature, and reference mass density. The computed $\partial I/\partial P$ in psig^{-1} is shown in Fig. 5.1 for a gasoline with a reference mass density of 711.75 kg/m^3 (67.11°API). Six equidistant (evenly spaced) pressure and six equidistant temperature points are used to span 0 to 1500 psig and 0 to 120°F respectively.

Associated with each D/e ratio is a surface. The smoothness of the surfaces indicates that the number of pressure-temperature pairs used is adequate. The plots for the other three fluid groups are similar and are not presented here. For a fixed temperature, $\partial I/\partial P$ varies almost linearly with pressure. Alternatively, for a fixed pressure, $\partial I/\partial P$ varies with temperature in a non-linear fashion. With these observations, each surface is represented by an equation in the following form:

$$\frac{\partial I}{\partial P} x10^6 = a_0 + a_1 P + a_2 T + a_3 PT + a_4 T^2 \tag{5.9}$$

in which the coefficients a_0, a_1, a_2, a_3, and a_4 are constants. The units for P and T are psig and °F respectively. The values of the a's are determined by three-dimensional curve fitting. Table 5.1 shows the resulting a values. For each °API interval, a mid-range °API value is used. For the °API chosen, the coefficients are computed at the four D/e ratios stated above.

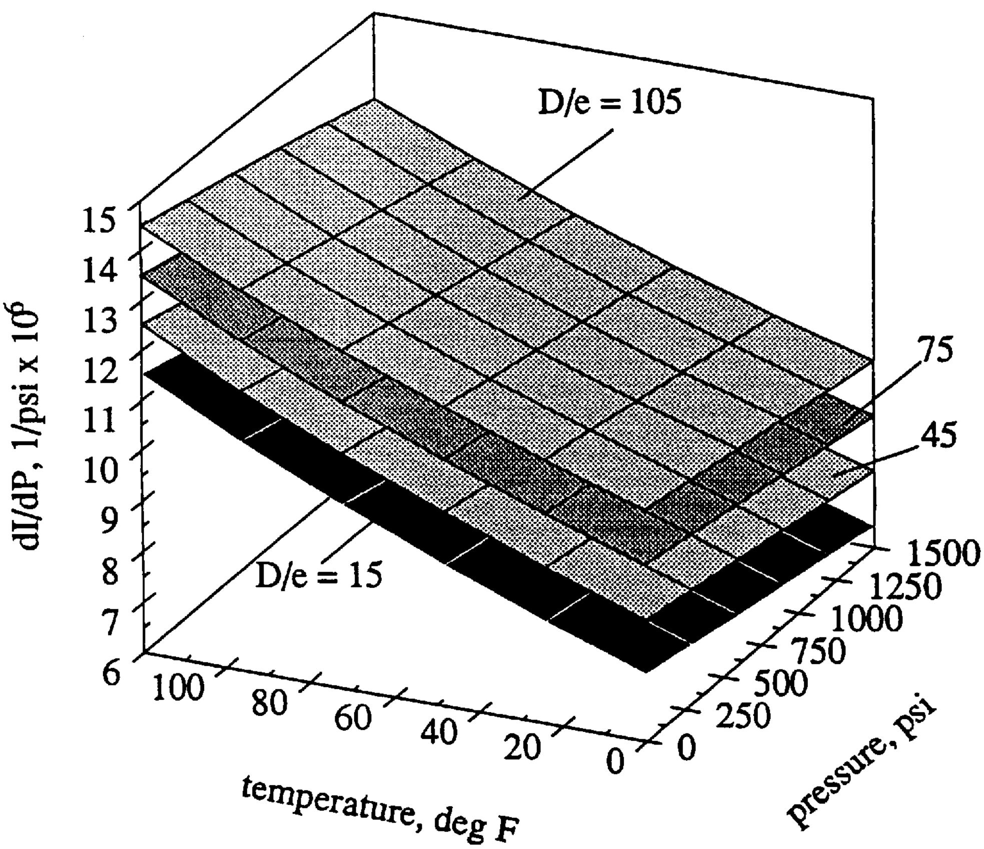

Fig. 5.1
Rate of scaled linefill change with pressure for gasoline

The rate of change of the scaled linefill with temperature is also a function of the *D/e* ratio, pressure, temperature, and reference mass density. The computed $\partial I/\partial T$, in °F^{-1}, is shown in Fig. 5.2 for the same gasoline.

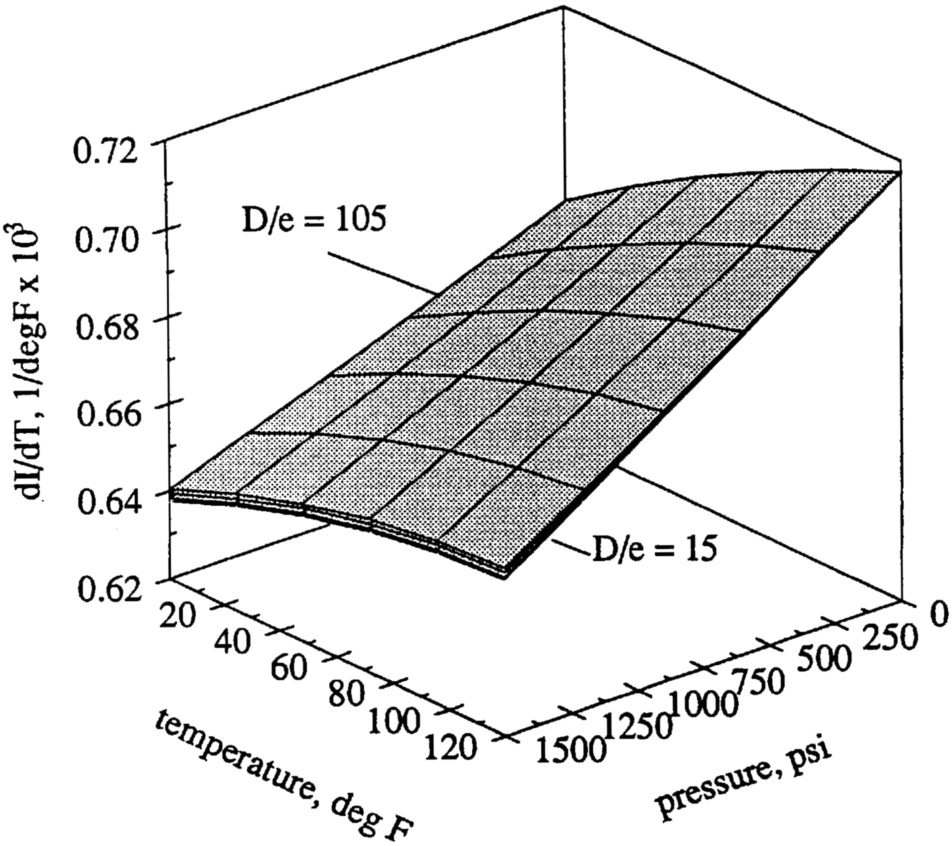

Fig. 5.2
Rate of scaled line fill change with temperature for gasoline

Note that, as before, $\partial I/\partial T$ varies linearly with pressure and nonlinearly with temperature. Thus a similar function relationship is used to represent the $\partial I/\partial T$ surface as

$$\frac{\partial I}{\partial T}x10^3 = b_0 + b_1 P + b_2 T + b_3 PT + b_4 T^2 \tag{5.10}$$

where b_0, b_1, b_2, b_3, and b_4 are coefficients determined by three-dimensional curve fitting. The units for P and T are psig and °F respectively. The values of the b's are shown in Table 5.2.

The a's and b's for gasoline-jet fuel transition, jet fuel, fuel oil, and crude oil are shown in Tables 5.3 through 5.10. Tables 5.1 through 5.10 constitute the data base for obtaining the rates of change of scaled linefill with pressure, temperature, and the D/e ratio. The ranges of the independent variables are as follows:

pressure: 0 - 1500 psig
temperature: 0 - 120°F
D/e ratio:15 - 105
reference mass density: 24 - 85 °API for refined products
0 - 86 °API for crude oil.

Table 5.1 Coefficients for the rate of scaled linefill change with pressure
Gasoline

°API Range	D/e	a_0	a_1	a_2	a_3	a_4
84.98 – 79.55	15	9.318×10^{0}	-7.549×10^{-4}	3.995×10^{-2}	-3.121×10^{-6}	1.220×10^{-4}
	45	1.040×10^{1}	-7.368×10^{-4}	3.912×10^{-2}	-3.016×10^{-6}	1.220×10^{-4}
	75	1.148×10^{1}	-7.163×10^{-4}	3.830×10^{-2}	-2.913×10^{-6}	1.220×10^{-4}
	105	1.257×10^{1}	-6.935×10^{-4}	3.748×10^{-2}	-2.811×10^{-6}	1.220×10^{-4}
79.54 – 74.39	15	8.553×10^{0}	-6.971×10^{-4}	3.485×10^{-2}	-2.883×10^{-6}	9.837×10^{-5}
	45	9.635×10^{0}	-6.803×10^{-4}	3.406×10^{-2}	-2.794×10^{-6}	9.832×10^{-5}
	75	1.072×10^{1}	-6.612×10^{-4}	3.327×10^{-2}	-2.707×10^{-6}	9.828×10^{-5}
	105	1.180×10^{1}	-6.398×10^{-4}	3.248×10^{-2}	-2.621×10^{-6}	9.824×10^{-5}
74.38 – 69.48	15	7.904×10^{0}	-6.472×10^{-4}	3.060×10^{-2}	-2.641×10^{-6}	8.019×10^{-5}
	45	8.983×10^{0}	-6.315×10^{-4}	2.984×10^{-2}	-2.565×10^{-6}	8.014×10^{-5}
	75	1.006×10^{1}	-6.135×10^{-4}	2.908×10^{-2}	-2.490×10^{-6}	8.008×10^{-5}
	105	1.114×10^{1}	-5.933×10^{-4}	2.832×10^{-2}	-2.417×10^{-6}	8.003×10^{-5}
69.47 – 64.80	15	7.347×10^{0}	-6.037×10^{-4}	2.703×10^{-2}	-2.409×10^{-6}	6.605×10^{-5}
	45	8.425×10^{0}	-5.890×10^{-4}	2.630×10^{-2}	-2.343×10^{-6}	6.600×10^{-5}
	75	9.503×10^{0}	-5.720×10^{-4}	2.557×10^{-2}	-2.279×10^{-6}	6.593×10^{-5}
	105	1.058×10^{1}	-5.528×10^{-4}	2.484×10^{-2}	-2.216×10^{-6}	6.586×10^{-5}
64.79 – 60.32	15	6.866×10^{0}	-5.655×10^{-4}	2.401×10^{-2}	-2.194×10^{-6}	5.492×10^{-5}
	45	7.942×10^{0}	-5.517×10^{-4}	2.331×10^{-2}	-2.137×10^{-6}	5.485×10^{-5}
	75	9.019×10^{0}	-5.356×10^{-4}	2.261×10^{-2}	-2.081×10^{-6}	5.478×10^{-5}
	105	1.010×10^{1}	-5.173×10^{-4}	2.191×10^{-2}	-2.026×10^{-6}	5.470×10^{-5}
60.31 – 56.05	15	6.448×10^{0}	-5.319×10^{-4}	2.145×10^{-2}	-1.998×10^{-6}	4.606×10^{-5}
	45	7.523×10^{0}	-5.189×10^{-4}	2.077×10^{-2}	-1.948×10^{-6}	4.598×10^{-5}
	75	8.598×10^{0}	-5.036×10^{-4}	2.010×10^{-2}	-1.899×10^{-6}	4.591×10^{-5}
	105	9.673×10^{0}	-4.860×10^{-4}	1.942×10^{-2}	-1.852×10^{-6}	4.583×10^{-5}
56.04 – 51.97	15	6.082×10^{0}	-5.022×10^{-4}	1.926×10^{-2}	-1.822×10^{-6}	3.893×10^{-5}
	45	7.156×10^{0}	-4.898×10^{-4}	1.860×10^{-2}	-1.778×10^{-6}	3.885×10^{-5}
	75	8.230×10^{0}	-4.751×10^{-4}	1.795×10^{-2}	-1.735×10^{-6}	3.877×10^{-5}
	105	9.303×10^{0}	-4.582×10^{-4}	1.729×10^{-2}	-1.693×10^{-6}	3.869×10^{-5}

Table 5.2 Coefficients for the rate of scaled linefill change with temperature
Gasoline

°API Range	D/e	b_0	b_1	b_2	b_3	b_4
84.98 - 79.55	15	7.552×10^{-1}	-3.798×10^{-5}	5.967×10^{-4}	-2.453×10^{-7}	-1.407×10^{-6}
	45	7.552×10^{-1}	-3.723×10^{-5}	5.969×10^{-4}	-2.453×10^{-7}	-1.408×10^{-6}
	75	7.552×10^{-1}	-3.649×10^{-5}	5.972×10^{-4}	-2.452×10^{-7}	-1.409×10^{-6}
	105	7.552×10^{-1}	-3.574×10^{-5}	5.974×10^{-4}	-2.452×10^{-7}	-1.410×10^{-6}
79.54 - 74.39	15	7.269×10^{-1}	-3.297×10^{-5}	5.410×10^{-4}	-1.976×10^{-7}	-1.198×10^{-6}
	45	7.270×10^{-1}	-3.225×10^{-5}	5.411×10^{-4}	-1.975×10^{-7}	-1.199×10^{-6}
	75	7.270×10^{-1}	-3.152×10^{-5}	5.413×10^{-4}	-1.975×10^{-7}	-1.200×10^{-6}
	105	7.270×10^{-1}	-3.080×10^{-5}	5.415×10^{-4}	-1.974×10^{-7}	-1.201×10^{-6}
74.38 - 69.48	15	7.004×10^{-1}	-2.884×10^{-5}	4.933×10^{-4}	-1.610×10^{-7}	-1.031×10^{-6}
	45	7.004×10^{-1}	-2.814×10^{-5}	4.935×10^{-4}	-1.609×10^{-7}	-1.032×10^{-6}
	75	7.004×10^{-1}	-2.744×10^{-5}	4.937×10^{-4}	-1.608×10^{-7}	-1.033×10^{-6}
	105	7.005×10^{-1}	-2.673×10^{-5}	4.938×10^{-4}	-1.607×10^{-7}	-1.034×10^{-6}
69.47 - 64.80	15	6.755×10^{-1}	-2.540×10^{-5}	4.522×10^{-4}	-1.326×10^{-7}	-8.953×10^{-7}
	45	6.755×10^{-1}	-2.472×10^{-5}	4.523×10^{-4}	-1.325×10^{-7}	-8.962×10^{-7}
	75	6.755×10^{-1}	-2.404×10^{-5}	4.524×10^{-4}	-1.323×10^{-7}	-8.969×10^{-7}
	105	6.755×10^{-1}	-2.335×10^{-5}	4.526×10^{-4}	-1.322×10^{-7}	-8.977×10^{-7}
64.79 - 60.32	15	6.520×10^{-1}	-2.251×10^{-5}	4.162×10^{-4}	-1.102×10^{-7}	-7.835×10^{-7}
	45	6.520×10^{-1}	-2.185×10^{-5}	4.163×10^{-4}	-1.101×10^{-7}	-7.842×10^{-7}
	75	6.520×10^{-1}	-2.119×10^{-5}	4.165×10^{-4}	-1.099×10^{-7}	-7.848×10^{-7}
	105	6.520×10^{-1}	-2.053×10^{-5}	4.166×10^{-4}	-1.098×10^{-7}	-7.856×10^{-7}
60.31 - 56.05	15	6.298×10^{-1}	-2.006×10^{-5}	3.846×10^{-4}	-9.239×10^{-8}	-6.903×10^{-7}
	45	6.298×10^{-1}	-1.943×10^{-5}	3.847×10^{-4}	-9.224×10^{-8}	-6.909×10^{-7}
	75	6.298×10^{-1}	-1.878×10^{-5}	3.848×10^{-4}	-9.209×10^{-8}	-6.914×10^{-7}
	105	6.298×10^{-1}	-1.814×10^{-5}	3.849×10^{-4}	-9.194×10^{-8}	-6.920×10^{-7}
56.04 - 51.97	15	6.089×10^{-1}	-1.798×10^{-5}	3.565×10^{-4}	-7.807×10^{-8}	-6.117×10^{-7}
	45	6.089×10^{-1}	-1.736×10^{-5}	3.566×10^{-4}	-7.791×10^{-8}	-6.123×10^{-7}
	75	6.089×10^{-1}	-1.674×10^{-5}	3.567×10^{-4}	-7.776×10^{-8}	-6.127×10^{-7}
	105	6.089×10^{-1}	-1.612×10^{-5}	3.568×10^{-4}	-7.760×10^{-8}	-6.132×10^{-7}

Table 5.3 Coefficients for the rate of scaled linefill change with pressure
Gasoline - Jet Fuel Transition

°API Range	D/e	a_0	a_1	a_2	a_3	a_4
51.96 | 48.00	15	5.744×10^{0}	-4.742×10^{-4}	1.754×10^{-2}	-1.689×10^{-6}	3.430×10^{-5}
	45	6.814×10^{0}	-4.624×10^{-4}	1.695×10^{-2}	-1.649×10^{-6}	3.424×10^{-5}
	75	7.884×10^{0}	-4.484×10^{-4}	1.636×10^{-2}	-1.610×10^{-6}	3.418×10^{-5}
	105	8.953×10^{0}	-4.321×10^{-4}	1.577×10^{-2}	-1.572×10^{-6}	3.412×10^{-5}

Table 5.4 Coefficients for the rate of scaled linefill change with temperature
Gasoline - Jet Fuel Transition

°API Range	D/e	b_0	b_1	b_2	b_3	b_4
51.96 | 48.00	15	5.467×10^{-1}	-1.635×10^{-5}	2.863×10^{-4}	-6.878×10^{-8}	-4.572×10^{-7}
	45	5.467×10^{-1}	-1.579×10^{-5}	2.864×10^{-4}	-6.856×10^{-8}	-4.575×10^{-7}
	75	5.467×10^{-1}	-1.523×10^{-5}	2.865×10^{-4}	-6.854×10^{-8}	-4.579×10^{-7}
	105	5.467×10^{-1}	-1.467×10^{-5}	2.865×10^{-4}	-6.843×10^{-8}	-4.584×10^{-7}

Table 5.5 Coefficients for the rate of scaled linefill change with pressure
Jet Fuel

°API Range	D/e	a_0	a_1	a_2	a_3	a_4
47.90 | 44.18	15	5.442×10^{0}	-4.490×10^{-4}	1.604×10^{-2}	-1.569×10^{-6}	3.042×10^{-5}
	45	6.508×10^{0}	-4.377×10^{-4}	1.552×10^{-2}	-1.532×10^{-6}	3.037×10^{-5}
	75	7.574×10^{0}	-4.243×10^{-4}	1.499×10^{-2}	-1.497×10^{-6}	3.033×10^{-5}
	105	8.640×10^{0}	-4.086×10^{-4}	1.447×10^{-2}	-1.463×10^{-6}	3.029×10^{-5}
44.17 | 40.51	15	5.185×10^{0}	-4.274×10^{-4}	1.460×10^{-2}	-1.439×10^{-6}	2.629×10^{-5}
	45	6.249×10^{0}	-4.166×10^{-4}	1.409×10^{-2}	-1.407×10^{-6}	2.625×10^{-5}
	75	7.314×10^{0}	-4.037×10^{-4}	1.359×10^{-2}	-1.375×10^{-6}	2.621×10^{-5}
	105	8.378×10^{0}	-3.885×10^{-4}	1.309×10^{-2}	-1.344×10^{-6}	2.617×10^{-5}
40.50 | 36.99	15	4.955×10^{0}	-4.080×10^{-4}	1.334×10^{-2}	-1.324×10^{-6}	2.286×10^{-5}
	45	6.018×10^{0}	-3.977×10^{-4}	1.285×10^{-2}	-1.294×10^{-6}	2.282×10^{-5}
	75	7.082×10^{0}	-3.851×10^{-4}	1.237×10^{-2}	-1.266×10^{-6}	2.278×10^{-5}
	105	8.145×10^{0}	-3.704×10^{-4}	1.189×10^{-2}	-1.238×10^{-6}	2.274×10^{-5}

Table 5.6 Coefficients for the rate of scaled linefill change with temperature
Jet Fuel

°API Range	D/e	b_0	b_1	b_2	b_3	b_4
47.90 | 44.18	15	4.856×10^{-1}	-1.493×10^{-5}	2.264×10^{-4}	-6.099×10^{-8}	-3.359×10^{-7}
	45	4.856×10^{-1}	-1.444×10^{-5}	2.264×10^{-4}	-6.090×10^{-8}	-3.362×10^{-7}
	75	4.856×10^{-1}	-1.394×10^{-5}	2.265×10^{-4}	-6.082×10^{-8}	-3.365×10^{-7}
	105	4.856×10^{-1}	-1.344×10^{-5}	2.265×10^{-4}	-6.073×10^{-8}	-3.368×10^{-7}
44.17 | 40.51	15	4.648×10^{-1}	-1.357×10^{-5}	2.068×10^{-4}	-5.270×10^{-8}	-2.916×10^{-7}
	45	4.648×10^{-1}	-1.310×10^{-5}	2.068×10^{-4}	-5.261×10^{-8}	-2.918×10^{-7}
	75	4.648×10^{-1}	-1.262×10^{-5}	2.069×10^{-4}	-5.253×10^{-8}	-2.921×10^{-7}
	105	4.648×10^{-1}	-1.214×10^{-5}	2.069×10^{-4}	-5.245×10^{-8}	-2.924×10^{-7}
40.50 | 36.99	15	4.452×10^{-1}	-1.239×10^{-5}	1.895×10^{-4}	-4.581×10^{-8}	-2.542×10^{-7}
	45	4.452×10^{-1}	-1.193×10^{-5}	1.895×10^{-4}	-4.573×10^{-8}	-2.545×10^{-7}
	75	4.452×10^{-1}	-1.147×10^{-5}	1.895×10^{-4}	-4.565×10^{-8}	-2.546×10^{-7}
	105	4.453×10^{-1}	-1.101×10^{-5}	1.896×10^{-4}	-4.557×10^{-8}	-2.548×10^{-7}

Table 5.7 Coefficients for the rate of scaled linefill change with pressure
Fuel Oil

°API Range	D/e	a_0	a_1	a_2	a_3	a_4
36.98 – 33.64	15	4.752×10^{0}	-3.907×10^{-4}	1.222×10^{-2}	-1.220×10^{-6}	1.993×10^{-5}
	45	5.814×10^{0}	-3.808×10^{-4}	1.176×10^{-2}	-1.193×10^{-6}	1.989×10^{-5}
	75	6.876×10^{0}	-3.686×10^{-4}	1.129×10^{-2}	-1.167×10^{-6}	1.985×10^{-5}
	105	7.939×10^{0}	-3.542×10^{-4}	1.083×10^{-2}	-1.142×10^{-6}	1.981×10^{-5}
33.63 – 30.42	15	4.570×10^{0}	-3.752×10^{-4}	1.124×10^{-2}	-1.125×10^{-6}	1.744×10^{-5}
	45	5.632×10^{0}	-3.656×10^{-4}	1.078×10^{-2}	-1.101×10^{-6}	1.740×10^{-5}
	75	6.693×10^{0}	-3.537×10^{-4}	1.033×10^{-2}	-1.078×10^{-6}	1.736×10^{-5}
	105	7.755×10^{0}	-3.397×10^{-4}	9.876×10^{-2}	-1.055×10^{-6}	1.732×10^{-5}
30.41 – 27.33	15	4.406×10^{0}	-3.611×10^{-4}	1.036×10^{-2}	-1.041×10^{-6}	1.533×10^{-5}
	45	5.467×10^{0}	-3.518×10^{-4}	9.921×10^{-3}	-1.019×10^{-6}	1.529×10^{-5}
	75	6.528×10^{0}	-3.402×10^{-4}	9.479×10^{-3}	-9.978×10^{-7}	1.525×10^{-5}
	105	7.589×10^{0}	-3.265×10^{-4}	9.037×10^{-3}	-9.772×10^{-7}	1.521×10^{-5}
27.32 – 24.35	15	4.258×10^{0}	-3.482×10^{-4}	9.586×10^{-3}	-9.659×10^{-7}	1.353×10^{-5}
	45	5.318×10^{0}	-3.392×10^{-4}	9.155×10^{-3}	-9.455×10^{-7}	1.349×10^{-5}
	75	6.378×10^{0}	-3.279×10^{-4}	8.724×10^{-3}	-9.259×10^{-7}	1.345×10^{-5}
	105	7.438×10^{0}	-3.144×10^{-4}	8.293×10^{-3}	-9.072×10^{-7}	1.341×10^{-5}

Table 5.8 Coefficients for the rate of scaled linefill change with temperature
Fuel Oil

°API Range	D/e	b_0	b_1	b_2	b_3	b_4
36.98 – 33.64	15	4.303×10^{-1}	-1.135×10^{-5}	1.766×10^{-4}	-3.994×10^{-8}	-2.265×10^{-7}
	45	4.303×10^{-1}	-1.090×10^{-5}	1.767×10^{-4}	-3.987×10^{-8}	-2.266×10^{-7}
	75	4.303×10^{-1}	-1.046×10^{-5}	1.767×10^{-4}	-3.979×10^{-8}	-2.268×10^{-7}
	105	4.303×10^{-1}	-1.001×10^{-5}	1.767×10^{-4}	-3.971×10^{-8}	-2.270×10^{-7}
33.63 – 30.42	15	4.188×10^{-1}	-1.043×10^{-5}	1.671×10^{-4}	-3.494×10^{-8}	-2.057×10^{-7}
	45	4.189×10^{-1}	-9.991×10^{-6}	1.671×10^{-4}	-3.486×10^{-8}	-2.058×10^{-7}
	75	4.189×10^{-1}	-9.556×10^{-6}	1.672×10^{-4}	-3.478×10^{-8}	-2.060×10^{-7}
	105	4.189×10^{-1}	-9.119×10^{-6}	1.672×10^{-4}	-3.470×10^{-8}	-2.062×10^{-7}
30.41 – 27.33	15	4.080×10^{-1}	-9.610×10^{-6}	1.584×10^{-4}	-3.071×10^{-8}	-1.875×10^{-7}
	45	4.080×10^{-1}	-9.186×10^{-6}	1.584×10^{-4}	-3.063×10^{-8}	-1.877×10^{-7}
	75	4.080×10^{-1}	-8.760×10^{-6}	1.584×10^{-4}	-3.055×10^{-8}	-1.878×10^{-7}
	105	4.080×10^{-1}	-8.334×10^{-6}	1.585×10^{-4}	-3.047×10^{-8}	-1.879×10^{-7}
27.32 – 24.35	15	3.976×10^{-1}	-8.886×10^{-6}	1.504×10^{-4}	-2.711×10^{-8}	-1.715×10^{-7}
	45	3.976×10^{-1}	-8.470×10^{-6}	1.504×10^{-4}	-2.703×10^{-8}	-1.717×10^{-7}
	75	3.976×10^{-1}	-8.054×10^{-6}	1.504×10^{-4}	-2.695×10^{-8}	-1.718×10^{-7}
	105	3.976×10^{-1}	-7.638×10^{-6}	1.505×10^{-4}	-2.687×10^{-8}	-1.719×10^{-7}

Table 5.9 Coefficients for the rate of scaled linefill change with pressure
Crude Oil

°API Range	D/e	a_0	a_1	a_2	a_3	a_4
85.98 | 76.89	15	$9.167x10^0$	$-7.433x10^{-4}$	$3.918x10^{-2}$	$-3.111x10^{-6}$	$1.197x10^{-4}$
	45	$1.025x10^1$	$-7.254x10^{-4}$	$3.839x10^{-2}$	$-3.086x10^{-6}$	$1.197x10^{-4}$
	75	$1.133x10^1$	$-7.052x10^{-4}$	$3.760x10^{-2}$	$-2.908x10^{-6}$	$1.196x10^{-4}$
	105	$1.241x10^1$	$-6.827x10^{-4}$	$3.681x10^{-2}$	$-2.808x10^{-6}$	$1.196x10^{-4}$
76.88 | 68.54	15	$7.974x10^0$	$-6.523x10^{-4}$	$3.136x10^{-2}$	$-2.711x10^{-6}$	$8.473x10^{-5}$
	45	$9.052x10^0$	$-6.365x10^{-4}$	$3.064x10^{-2}$	$-2.632x10^{-6}$	$8.470x10^{-5}$
	75	$1.013x10^1$	$-6.184x10^{-4}$	$2.992x10^{-2}$	$-2.555x10^{-6}$	$8,467x10^{-5}$
	105	$1.121x10^1$	$-5.981x10^{-4}$	$2.920x10^{-2}$	$-2.479x10^{-6}$	$8.464x10^{-5}$
68.53 | 60.83	15	$7.058x10^0$	$-5.804x10^{-4}$	$2.556x10^{-2}$	$-2.329x10^{-6}$	$6.183x10^{-5}$
	45	$8.132x10^0$	$-5.663x10^{-4}$	$2.490x10^{-2}$	$-2.267x10^{-6}$	$6.178x10^{-5}$
	75	$9.206x10^0$	$-5499x10^{-4}$	$2.423x10^{-2}$	$-2.206x10^{-6}$	$6.174x10^{-5}$
	105	$1.028x10^1$	$-5.312x10^{-4}$	$2.357x10^{-2}$	$-2.147x10^{-6}$	$6.169x10^{-5}$
60.82 | 53.69	15	$6.339x10^0$	$-5.227x10^{-4}$	$2.117x10^{-2}$	$-1.995x10^{-6}$	$4.627x10^{-5}$
	45	$7.410x10^0$	$-5.099x10^{-4}$	$2.055x10^{-2}$	$-1.946x10^{-6}$	$4.622x10^{-5}$
	75	$8.481x10^0$	$-4.948x10^{-4}$	$1.994x10^{-2}$	$-1.897x10^{-6}$	$4.617x10^{-5}$
	105	$9.552x10^0$	$-4.774x10^{-4}$	$1.933x10^{-2}$	$-1.850x10^{-6}$	$4.613x10^{-5}$
53.68 | 47.06	15	$5.764x10^0$	$-4.757x10^{-4}$	$1.779x10^{-2}$	$-1.717x10^{-6}$	$3.540x10^{-5}$
	45	$6.832x10^0$	$-4.639x10^{-4}$	$1.722x10^{-2}$	$-1.676x10^{-6}$	$3.535x10^{-5}$
	75	$7.901x10^0$	$-4.499x10^{-4}$	$1.665x10^{-2}$	$-1.636x10^{-6}$	$3.530x10^{-5}$
	105	$8.969x10^0$	$-4.336x10^{-4}$	$1.608x10^{-2}$	$-1.597x10^{-6}$	$3.525x10^{-5}$
47.05 | 40.89	15	$5.297x10^0$	$-4.369x10^{-4}$	$1.513x10^{-2}$	$-1.485x10^{-6}$	$2.760x10^{-5}$
	45	$6.363x10^0$	$-4.259x10^{-4}$	$1.461x10^{-2}$	$-1.451x10^{-6}$	$2.756x10^{-5}$
	75	$7.429x10^0$	$-4.127x10^{-4}$	$1.408x10^{-2}$	$-1.418x10^{-6}$	$2.751x10^{-5}$
	105	$8.495x10^0$	$-3.973x10^{-4}$	$1.355x10^{-2}$	$-1.386x10^{-6}$	$2.746x10^{-5}$
40.88 | 35.13	15	$4.913x10^0$	$-4.045x10^{-4}$	$1.303x10^{-2}$	$-1.293x10^{-6}$	$2.189x10^{-5}$
	45	$5.977x10^0$	$-3.942x10^{-4}$	$1.253x10^{-2}$	$-1.264x10^{-6}$	$2.185x10^{-5}$
	75	$7.041x10^0$	$-3.817x10^{-4}$	$1.204x10^{-2}$	$-1.236x10^{-6}$	$2.180x10^{-5}$
	105	$8.104x10^0$	$-3.670x10^{-4}$	$1.155x10^{-2}$	$-1.209x10^{-6}$	$2.175x10^{-5}$
35.12 | 29.75	15	$4.592x10^0$	$-3.771x10^{-4}$	$1.133x10^{-2}$	$-1.134x10^{-6}$	$1.762x10^{-5}$
	45	$5.654x10^0$	$-3.674x10^{-4}$	$1.087x10^{-2}$	$-1.109x10^{-6}$	$1.758x10^{-5}$
	75	$6.716x10^0$	$-3.556x10^{-4}$	$1.041x10^{-2}$	$-1.085x10^{-6}$	$1.753x10^{-5}$
	105	$7.778x10^0$	$-3.414x10^{-4}$	$9.945x10^{-3}$	$-1.063x10^{-6}$	$1.749x10^{-5}$

Table 5.9 continued

29.74 – 24.70	15	4.322×10^{0}	-3.538×10^{-4}	9.939×10^{-3}	-1.001×10^{-6}	1.437×10^{-5}
	45	5.382×10^{0}	-3.446×10^{-4}	9.508×10^{-3}	-9.795×10^{-7}	1.433×10^{-5}
	75	6.442×10^{0}	-3.332×10^{-4}	9.076×10^{-3}	-9.591×10^{-7}	1.429×10^{-5}
	105	7.503×10^{0}	-3.196×10^{-4}	8.645×10^{-3}	-9.395×10^{-7}	1.425×10^{-5}
24.69 – 19.96	15	4.092×10^{0}	-3.338×10^{-4}	8.794×10^{-3}	-8.894×10^{-7}	1.186×10^{-5}
	45	5.151×10^{0}	-3.250×10^{-4}	8.390×10^{-3}	-8.708×10^{-7}	1.182×10^{-5}
	75	6.209×10^{0}	-3.141×10^{-4}	7.984×10^{-3}	-8.531×10^{-7}	1.179×10^{-5}
	105	7.268×10^{0}	-3.009×10^{-4}	7.579×10^{-3}	-8.362×10^{-7}	1.175×10^{-5}
19.95 – 15.49	15	3.894×10^{0}	-3.165×10^{-4}	7.838×10^{-3}	-7.954×10^{-7}	9.891×10^{-6}
	45	4.951×10^{0}	-3.081×10^{-4}	7.458×10^{-3}	-7.790×10^{-7}	9.858×10^{-6}
	75	6.009×10^{0}	-2.975×10^{-4}	7.077×10^{-3}	-7.635×10^{-7}	9.825×10^{-6}
	105	7.066×10^{0}	-2.847×10^{-4}	6.696×10^{-3}	-7.487×10^{-7}	9.793×10^{-6}
15.48 – 11.29	15	3.723×10^{0}	-3.014×10^{-4}	7.034×10^{-3}	-7.155×10^{-7}	8.331×10^{-6}
	45	4.779×10^{0}	-2.933×10^{-4}	6.675×10^{-3}	-7.010×10^{-7}	8.301×10^{-6}
	75	5.835×10^{0}	-2.830×10^{-4}	6.317×10^{-3}	-6.873×10^{-7}	8.270×10^{-6}
	105	6.891×10^{0}	-2.705×10^{-4}	5.958×10^{-3}	-6.742×10^{-7}	8.240×10^{-6}
11.28 – 7.32	15	3.574×10^{0}	-2.881×10^{-4}	6.350×10^{-3}	-6.471×10^{-7}	7.078×10^{-6}
	45	4.628×10^{0}	-2.803×10^{-4}	6.012×10^{-3}	-6.341×10^{-7}	7.051×10^{-6}
	75	5.683×10^{0}	-2.703×10^{-4}	5.674×10^{-3}	-6.219×10^{-7}	7.023×10^{-6}
	105	6.738×10^{0}	-2.581×10^{-4}	5.335×10^{-3}	-6.103×10^{-7}	6.996×10^{-6}
7.31 – 3.56	15	3.443×10^{0}	-2.764×10^{-4}	5.765×10^{-3}	-5.882×10^{-7}	6.062×10^{-6}
	45	4.496×10^{0}	-2.689×10^{-4}	5.446×10^{-3}	-5.766×10^{-7}	6.037×10^{-6}
	75	5.550×10^{0}	-2.591×10^{-4}	5.126×10^{-3}	-5.657×10^{-7}	6.011×10^{-6}
	105	6.603×10^{0}	-2.472×10^{-4}	4.806×10^{-3}	-5.552×10^{-7}	5.986×10^{-6}
3.55 – 0	15	3.327×10^{0}	-2.661×10^{-4}	5.261×10^{-3}	-5.373×10^{-7}	5.230×10^{-6}
	45	4.380×10^{0}	-2.587×10^{-4}	4.958×10^{-3}	-5.267×10^{-7}	5.207×10^{-6}
	75	5.432×10^{0}	-2.492×10^{-4}	4.656×10^{-3}	-5.168×10^{-7}	5.184×10^{-6}
	105	6.485×10^{0}	-2.374×10^{-4}	4.353×10^{-3}	-5.075×10^{-7}	5.161×10^{-6}

Table 5.10 Coefficients for the rate of scaled linefill change with temperature
Crude oil

°API Range	*D/e*	b_0	b_1	b_2	b_3	b_4
85.98–76.89	15	7.224×10^{-1}	-3.721×10^{-5}	5.460×10^{-4}	-2.405×10^{-7}	-1.276×10^{-6}
	45	7.224×10^{-1}	-3.650×10^{-5}	5.462×10^{-4}	-2.405×10^{-7}	-1.277×10^{-6}
	75	7.224×10^{-1}	-3.579×10^{-5}	5.464×10^{-4}	-2.405×10^{-7}	-1.278×10^{-6}
	105	7.224×10^{-1}	-3.507×10^{-5}	5.467×10^{-4}	-2.405×10^{-7}	-1.279×10^{-6}
76.88–68.54	15	6.649×10^{-1}	-2.957×10^{-5}	4.474×10^{-4}	-1.702×10^{-7}	-9.388×10^{-7}
	45	6.649×10^{-1}	-2.891×10^{-5}	4.476×10^{-4}	-1.701×10^{-7}	-9.396×10^{-7}
	75	6.649×10^{-1}	-2.824×10^{-5}	4.477×10^{-4}	-1.701×10^{-7}	-9.405×10^{-7}
	105	6.649×10^{-1}	-2.758×10^{-5}	4.479×10^{-4}	-1.700×10^{-7}	-9.413×10^{-7}
68.53–60.83	15	6.136×10^{-1}	-2.398×10^{-5}	3.728×10^{-4}	-1.241×10^{-7}	-7.068×10^{-7}
	45	6.136×10^{-1}	-2.336×10^{-5}	3.723×10^{-4}	-1.240×10^{-7}	-7.074×10^{-7}
	75	6.136×10^{-1}	-2.274×10^{-5}	3.724×10^{-4}	-1.239×10^{-7}	-7.081×10^{-7}
	105	6.136×10^{-1}	-2.212×10^{-5}	3.725×10^{-4}	-1.238×10^{-7}	-7.877×10^{-7}
60.82–53.69	15	5.677×10^{-1}	-1.979×10^{-5}	3.134×10^{-4}	-9.283×10^{-8}	-5.421×10^{-7}
	45	5.677×10^{-1}	-1.921×10^{-5}	3.135×10^{-4}	-9.234×10^{-8}	-5.426×10^{-7}
	75	5.677×10^{-1}	-1.863×10^{-5}	3.136×10^{-4}	-9.264×10^{-8}	-5.430×10^{-7}
	105	5.677×10^{-1}	-1.806×10^{-5}	3.137×10^{-4}	-9.254×10^{-8}	-5.435×10^{-7}
53.68–47.06	15	5.266×10^{-1}	-1.658×10^{-5}	2.666×10^{-4}	-7.099×10^{-8}	-4.223×10^{-7}
	45	5.266×10^{-1}	-1.604×10^{-5}	2.667×10^{-4}	-7.089×10^{-8}	-4.226×10^{-7}
	75	5.266×10^{-1}	-1.550×10^{-5}	2.668×10^{-4}	-7.080×10^{-8}	-4.230×10^{-7}
	105	5.266×10^{-1}	-1.496×10^{-5}	2.668×10^{-4}	-7.070×10^{-8}	-4.234×10^{-7}
47.05–40.89	15	4.895×10^{-1}	-1.408×10^{-5}	2.288×10^{-4}	-5.534×10^{-8}	-3.332×10^{-7}
	45	4.895×10^{-1}	-1.358×10^{-5}	2.289×10^{-4}	-5.241×10^{-8}	-3.335×10^{-7}
	75	4.895×10^{-1}	-1.307×10^{-5}	2.289×10^{-4}	-5.515×10^{-8}	-3.337×10^{-7}
	105	4.900×10^{-1}	-1.257×10^{-5}	2.290×10^{-4}	-5.505×10^{-8}	-3.341×10^{-7}
40.88–35.13	15	4.560×10^{-1}	-1.210×10^{-5}	1.979×10^{-4}	-4.387×10^{-8}	-2.658×10^{-7}
	45	4.560×10^{-1}	-1.163×10^{-5}	1.979×10^{-4}	-4.378×10^{-8}	-2.661×10^{-7}
	75	4.560×10^{-1}	-1.116×10^{-5}	1.980×10^{-4}	-4.369×10^{-8}	-2.663×10^{-7}
	105	4.560×10^{-1}	-1.069×10^{-5}	1.980×10^{-4}	-4.360×10^{-8}	-2.665×10^{-7}
35.12–29.75	15	4.257×10^{-1}	-1.051×10^{-5}	1.723×10^{-4}	-3.530×10^{-8}	-2.143×10^{-7}
	45	4.257×10^{-1}	-1.007×10^{-5}	1.724×10^{-4}	-3.522×10^{-8}	-2.145×10^{-7}
	75	4.257×10^{-1}	-9.626×10^{-5}	1.724×10^{-4}	-3.514×10^{-8}	-2.146×10^{-7}
	105	4.257×10^{-1}	-9.183×10^{-5}	1.724×10^{-4}	-3.505×10^{-8}	-2.148×10^{-7}

Table 5.10 continued

29.74 – 24.70	15	3.981x10^{-1}	-9.215x10^{-6}	1.510x10^{-4}	-2.879x10^{-8}	-1.742x10^{-7}
	45	3.981x10^{-1}	-8.800x10^{-6}	1.510x10^{-4}	-2.871x10^{-8}	-1.743x10^{-7}
	75	3.981x10^{-1}	-8.384x10^{-6}	1.510x10^{-4}	-2.863x10^{-8}	-1.744x10^{-7}
	105	3.981x10^{-1}	-7.968x10^{-6}	1.511x10^{-4}	-2.855x10^{-8}	-1.746x10^{-7}
24.69 – 19.96	15	3.729 x10^{-1}	-8.148x10^{-6}	1.330x10^{-4}	-2.375x10^{-8}	-1.427x10^{-7}
	45	3.730x10^{-1}	-7.757x10^{-6}	1.331x10^{-4}	-2.368x10^{-8}	-1.429x10^{-7}
	75	3.730x10^{-1}	-7.366x10^{-6}	1.331x10^{-4}	-2.361x10^{-8}	-1.430x10^{-7}
	105	3.730x10^{-1}	-6.974x10^{-6}	1.331x10^{-4}	-2.353x10^{-8}	-1.430x10^{-7}
19.95 – 15.49	15	3.500x10^{-1}	-7.258x10^{-6}	1.178x10^{-4}	-1.981x10^{-8}	-1.178x10^{-7}
	45	3.500x10^{-1}	-6.890x10^{-6}	1.178x10^{-4}	-1.974x10^{-8}	-1.179x10^{-7}
	75	3.500x10^{-1}	-6.521x10^{-6}	1.179x10^{-4}	-1.968x10^{-8}	-1.179x10^{-7}
	105	3.500x10^{-1}	-6.152x10^{-6}	1.179x10^{-4}	-1.961x10^{-8}	-1.181x10^{-7}
15.48 – 11.29	15	3.289x10^{-1}	-6.511x10^{-6}	1.048x10^{-4}	-1.668x10^{-8}	-9.782x10^{-8}
	45	3.289x10^{-1}	-6.163x10^{-6}	1.049x10^{-4}	-1.662x10^{-8}	-9.792x10^{-8}
	75	3.289x10^{-1}	-5.815x10^{-6}	1.049x10^{-4}	-1.656x10^{-8}	-9.802x10^{-8}
	105	3.289x10^{-1}	-5.467x10^{-6}	1.049x10^{-4}	-1.650x10^{-8}	-9.811x10^{-8}
11.28 – 7.32	15	3.962x10^{-1}	-5.876x10^{-6}	9.370x10^{-5}	-1.417x10^{-8}	-8.175x10^{-8}
	45	3.962x10^{-1}	-5.548x10^{-6}	9.372x10^{-5}	-1.412x10^{-8}	-8.188x10^{-8}
	75	3.096x10^{-1}	-5.219x10^{-6}	9.373x10^{-5}	-1.406x10^{-8}	-8.187x10^{-8}
	105	3.096x10^{-1}	-4.889x10^{-6}	9.375x10^{-5}	-1.401x10^{-8}	-8.197x10^{-8}
7.31 – 3.56	15	2.918x10^{-1}	-5.333x10^{-6}	8.409x10^{-5}	-1.214x10^{-8}	-6.867x10^{-8}
	45	2.918x10^{-1}	-5.022x10^{-6}	8.410x10^{-5}	-1.208x10^{-8}	-6.876x10^{-8}
	75	2.918x10^{-1}	-4.711x10^{-6}	8.411x10^{-5}	-1.204x10^{-8}	-6.875x10^{-8}
	105	2.918x10^{-1}	-4.399x10^{-6}	8.413x10^{-5}	-1.199x10^{-8}	-6.889x10^{-8}
3.55 – 0	15	2.754x10^{-1}	-4.865x10^{-6}	7.576x10^{-5}	-1.047x10^{-8}	-5.804x10^{-8}
	45	2.754x10^{-1}	-4.571x10^{-6}	7.577x10^{-5}	-1.042x10^{-8}	-5.809x10^{-8}
	75	2.754x10^{-1}	-4.276x10^{-6}	7.577x10^{-5}	-1.378x10^{-8}	-5.812x10^{-8}
	105	2.754x10^{-1}	-3.981x10^{-6}	7.579x10^{-5}	-1.033x10^{-8}	-5.821x10^{-8}

5.4 PROCEDURE FOR ESTABLISHING LEAK DETECTION POTENTIAL

The materials presented so far can be used to establish leak detection potentials for pipeline systems. A step-by-step procedure to do this is given herein.

Step 1: Assemble Data

The whole pipeline may be divided into segments by the locations of discontinuities such as product batch interfaces, pipe diameter changes, and intermediate pressure and temperature measurement locations.

Pipeline Data

Dry volumes of pipeline segments at standard conditions of 15°C (60°F) and 1 atm. This volume can be in barrels or any other volume units.

Fluid Data

Product group (gasoline, gasoline-jet fuel transition, jet fuel, fuel oil, or crude oil) and °API values of all segments.

Operational Data

Volumetric flowrate in bbl/hr or any other volumetric flow units, Q_{ref}.
Average pressures in psig for all segments, P.
Average temperature in °F for all segments, T.

Uncertainties of Process Variable Measurements

Fractional uncertainty in flow rate measurement, k_{in}, k_{out} (dimensionless)
Uncertainty of pressure measurement in psig, dP.
Uncertainty of temperature measurement in °F, dT.

Step 2: Obtain the Rate of Linefill Change with Pressure

Based on the product group, look up a_0, a_1, a_2, a_3, and a_4 from Table 5.1, 5.3, 5.5, 5.7, or 5.9. Choose the values closest to the D/e ratio of the system in question. Compute $\partial I/\partial P$ according to Eq. (5.9). The result is psi^{-1}.

Step 3: Compute the Linefill Uncertainty Due to Pressure Uncertainty

Multiply the result from Step 2 by the pressure uncertainty dP and by the dry volume of the segment to obtain the volumetric linefill uncertainty due to pressure.

Step 4: Obtain the Rate of Linefill Change with Temperature

Based on the product group, lookup b_0, b_1, b_2, b_3, and b_4 from Table 5.2, 5.4, 5.6, 5.8, or 5.10. Choose the values closest to the D/e ratio of the system in question. Compute $\partial I/\partial T$ according to Eq. (5.10). The result is in $°F^{-1}$.

Step 5: Compute the Linefill Uncertainty Due to Temperature Uncertainty

Multiply the result from Step 4 by the temperature uncertainty dT and by the dry volume of the segment to obtain the volumetric linefill uncertainty due to temperature.

Step 6: Consider Multiple Pipeline Segments

Repeat Steps 2 to 5 for all segments.

Step 7: Compute the Uncertainty in Linefill Change Over a Time Window

Compute the uncertainty in volumetric linefill change dV_s according to Eq. (5.11).

Step 8: Establish the Response Time Corresponding to a 100 Percent Leak

Cmpute the minimum response time, Δt_{min}, as the minimum time required to detect a leak with a flowrate of Q_{ref} (i.e., a 100 percent leak). Define Δt_{min}

$$\Delta t_{min} = \frac{1}{\sqrt{1-k_{in}^2-k_{out}^2}}\frac{dV_s}{Q_{ref}} \tag{5.11}$$

where k_{in}, k_{out}, and Q_{ref} have been established in Step 1, and dV_s in Step 7.

Step 9: Establish the Leak Detection Potential

For any time window Δt greater than Δt_{min}, the fractional leak Q_l/Q_{ref} can be computed from Eq. (5.6). Compute several fractional leaks for several time windows to establish the leak detection potential curve.

5.5 APPLICATION EXAMPLE

Consider a 100 mile steel pipeline with an inside diameter of 12.54 inches and a pipe wall thickness of 0.203 inch. The dry volume of the pipe at standard conditions is 80,656 bbl. Suppose that at a certain instant the upstream 50,000 bbl contains 31°API fuel oil and the remaining volume contains 65°API gasoline. The steady-state flowrate is 2450 bbl/hr. Suppose the average pressure for the fuel oil and the gasoline batches are 752 and 352 psi respectively. Also suppose that the average temperature of the pipeline is 40°F.

Volumetric flowrate, pressure, and temperature are measured at the inlet and the outlet of this pipeline. An instrumentation analysis shows a 0.05% of reading uncertainty in each flow measurement, a 10 psi uncertainty in pressure measurement, and a 5°F uncertainty in temperature. What is the leak detection potential for this pipeline?

Step 1: Assemble Data

<u>Pipeline Data</u>

First segment:

Dry volume = 50,000 bbl
D/e = 12.54/0.203 = 61.8, the nearest D/e ratio in the tables is 75

Second segment:

Dry volume = 30,656 bbl
D/e = 61.8, the nearest D/e ratio in the tables is 75

<u>Fluid Data</u>

First segment:

Product group name = 31 °API fuel oil

Second segment:

Product group name = 65 °API gasoline

Operational Data

First segment:

Volumetric flowrate Q_{ref} = 2450 bbl/hr
Average pressure P = 752 psig
Average temperature T = 40 °F

Second segment:

Volumetric flowrate Q_{ref} = 2450 bbl/hr
Average pressure P = 352 psig
Average temperature T = 40 °F

Uncertainties of Process Variable Measurements

Fractional uncertainty in flow rate measurement $k_{in} = k_{out} = 0.0005$
Uncertainty of pressure measurement dP = 10 psi
Uncertainty of temperature measurement dT = 5 °F.

Step 2: Obtain the Rate of Linefill Change with Pressure

First segment:

Based on the product type, °API value, and D/e ratio, Table 5.7 is used to obtain a_0, a_1, a_2, a_3, and a_4 for the fuel oil as follows:

$a_0 = 6.693$
$a_1 = -3.537\text{x}10^{-4}$
$a_2 = 1.033\text{x}10^{-2}$
$a_3 = -1.078\text{x}10^{-6}$
$a_4 = 1.736\text{x}10^{-5}$

Using Eq. (5.9), $\partial I/\partial P = 6.836\text{x}10^{-6}$ psi^{-1}.

Step 3: Compute the Linefill Uncertainty Due to Pressure Uncertainty

Volumetric linefill uncertainty $=\partial I/\partial P\text{x}dP\text{x}$dry volume of the segment $= 6.836\text{x}10^{-6}$ psi^{-1} x10 psix50000 bbl = 3.418 bbl

Step 4: Obtain the Rate of Linefill Change with Temperature

From Table 5.8, b_0, b_1, b_2, b_3, and b_4 for the fuel oil are found to be

$b_0 = 4.189\text{x}10^{-1}$
$b_1 = -9.556\text{x}10^{-6}$
$b_2 = 1.672\text{x}10^{-4}$
$b_3 = -3.478\text{x}10^{-8}$
$b_4 = -2.060\text{x}10^{-7}$

Using Eq. (5.10), $\partial I/\partial T = 4.170\text{x}10^{-4}\,{}^{\circ}\text{F}^{-1}$.

Step 5: Compute the Linefill Uncertainty Due to Temperature Uncertainty

Volumetric linefill uncertainty $= \partial I/\partial T \text{x} dT \text{x}$dry volume of the segment
$= 4.170\text{x}10^{-4}\ {}^{\circ}\text{F}^{-1} \text{ x } 5^{\circ}\text{F x } 50000 \text{ bbl} = 1.043\text{x}10^{2}$ bbl

Step 6: Consider Multiple Pipeline Segments

Repeat Steps 2 through 5 for the gasoline batch and obtain the following:

$\partial I/\partial P = 1.040\text{x}10^{-5}$ psi^{-1}
Volumetric linefill uncertainty for pressure = 3.188 bbl
$\partial I/\partial T = 6.818\text{x}10^{-4}\ {}^{\circ}\text{F}^{-1}$
Volumetric linefill uncertainty for temperature = $1.045\text{x}10^{2}$ bbl

Step 7: Compute the Uncertainty in Linefill Change Over a Time Window

Use Eq. (5.8) with $n = 2$ to obtain

$$dV_s = \sqrt{2(3.418^2 + 104.3^2 + 3.188^2 + 104.5^2)} = 208.9 \ bbl$$

Step 8: Establish the Response Time Corresponding to a 100 Percent Leak

According to Eq. (5.11)

$$\Delta t_{\min} = \frac{1}{\sqrt{1-0.0005^2-0.0005^2}}\frac{208.9}{2450} = 8.53x10^{-2}\ hour$$

or 5.12 minutes.

Step 9: Establish the Leak Detection Potential

Using the equal sign in Eq. (5.6), the following data pairs are calculated.

Δt(minutes)	5.12	10	20	40	60	90	120	240
Q_l/Q_{ref}	1.00	0.511	0.256	0.128	0.085	0.054	0.043	0.021

The tabulated data is plotted as the solid curve in Fig. 5.3. For a specified time window size, the ordinate (vertical axis) of the curve gives the minimum detectable leak. For a specified fractional leak flowrate, the abscissa (horizontal axis) gives the minimum size of the time window needed to detect that leak.

5.6 SENSITIVITY WITH RESPECT TO TEMPERATURE AND PRESSURE UNCERTAINTIES

In the above example, most of the volumetric linefill uncertainty is attributable to the temperature uncertainty. If the field temperature measurement is upgraded so that the uncertainty is reduced from 5 to 2°F, the total volumetric linefill uncertainty is reduced from 208.9 bbl to 83.78 bbl and the leak detectability curve becomes

Δt (minutes)	2.05	10	20	40	60	90	120	240
Q_l/Q_{ref}	1.00	0.205	0.103	0.051	0.034	0.023	0.017	0.009

This curve is plotted in Fig. 5.3 as the dotted curve. It is seen that the temperature upgrade results in improved leak detection potential. On the other hand, if the pressure measurement is upgraded by an order of magnitude so that the pressure uncertainty is reduced from 10 to 1 psi, the volumetric linefill uncertainty is only reduced from 208.9 to 208.8 bbl. This upgrade hardly improves the leak detectability.

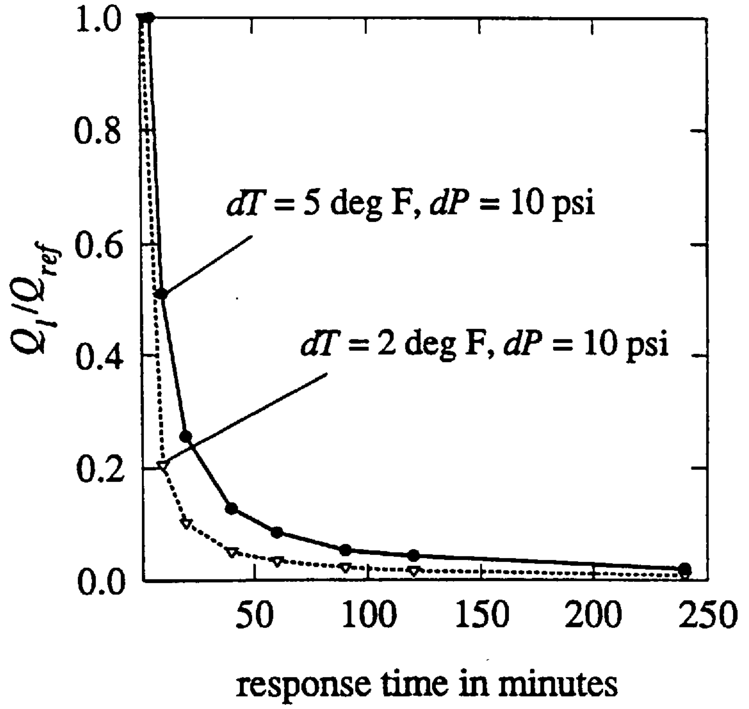

Fig. 5.3
Leak detectability curves for the example problem

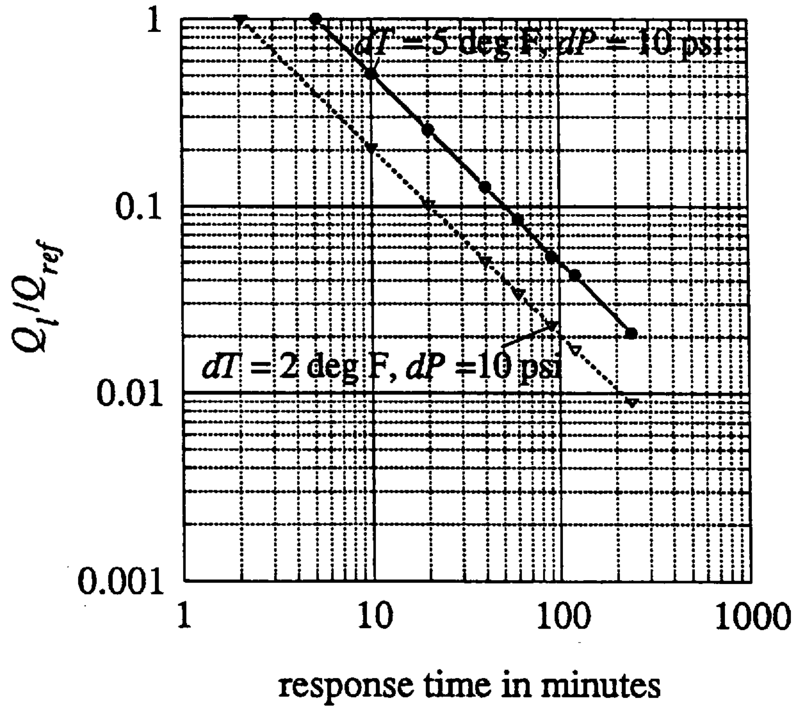

Fig. 5.4
Leak detectability curves for the example problem - logarithmic scales

The example demonstrates the general feature that leak detection potential is more sensitive to temperature uncertainty than pressure uncertainty.

Fig. 5.4 is a re-plot of Fig. 5.3 in a log-log scale. This plot better displays the rapid drop in Q_l / Q_{ref} for short response times. Such plots will be used for the rest of this report.

5.7 ACCURACY ASSESSMENT

Three sources of error exist for the proposed procedure. First, in establishing the tabulated coefficients, the three-dimensional curve fits do not yield exact values. Second and third, since a finite number of intervals are used to represent the reference mass density and the D/e ratio, discretization errors attributable to reference density and to the D/e ratio also exist.

To evaluate these errors for the example problem, the linefill uncertainty was recalculated using the equations in Chapters 4 and 5 directly. The results are free of curve-fitting and discretization errors and can be considered "exact". For a pressure uncertainty of 10 psi and a temperature uncertainty of 5°F, four cases were computed and the results are shown in Table 5.11. The change in the uncertainty of linefill is approximately 0.033 percent for the D/e ratio and 1.228 percent for the reference gravity. These percentages are indicative of the magnitude of discretization errors.

Table 5.11 "Exact" Linefill Uncertainties for Accuracy Assessment

case no.	°API of the fuel oil batch	°API of the gasoline batch	D/e	uncertainty in linefill, bbl
1	31	65	75	206.08
2	31	65	61.8	206.01
3	32.025	67.135	75	208.61
4	32.025	67.135	61.8	208.54

Case 2 reflects the D/e ratio and the reference gravity of the example problem: the 206.01 bbl uncertainty is the "exact" answer. The step-by-step procedure, which uses mid-range reference mass densities and a nearest D/e ratio, yields a slightly higher uncertainty estimation of 208.9 bbl. The 2.9 bbl or 1.4 percent difference is attributable to the three errors.

To break this error down one can compare 208.9 bbl (procedure) with 208.61 bbl (case 3). The 0.29 bbl difference is attributable to the errors in the three-dimensional curve fitting that established the coefficients for Eqs. (5.9) and (5.10). The 0.07 bbl difference between 208.61 bbl (case 3) and 208.54 (case 4) is attributable to discretization error in the D/e ratio. The 2.53 bbl difference between 208.54 (case 4) and 206.01 (case 2) is attributable to discretization error in the reference mass density.

In general, it is expected that the total error in linefill uncertainty obtained from the proposed procedure will not exceed 2 percent.

The impact of the error in linefill uncertainty on leak detectability can be evaluated from Eq. (5.6). Let $q = Q_l / Q_{ref}$ and view q as a function of ΔV_s and Δt. It can be shown that

$$\frac{dq}{q} = \frac{\Delta V_s}{(q Q_{ref} \Delta t)^2} d\Delta V_s - \frac{\Delta V_s^2}{(q Q_{ref} \Delta t)^2 \Delta t} d\Delta t \tag{5.14}$$

in which dq, $d\Delta V_s$, and $d\Delta t$ are viewed as errors in q, ΔV_s, and Δt respectively. Furthermore,

$$\frac{dq}{q} \leq \frac{d\Delta V_s}{\Delta V_s} - \frac{d\Delta t}{\Delta t} \tag{5.15}$$

In the above, the equality holds when $k_{in}^2 + k_{out}^2$ is much less than $(\Delta V_s / \Delta t Q_{ref})^2$ and is neglected. Eq. (5.15) indicates that for a specified response time (i.e., $d\Delta t = 0$), the fractional error in q is less than the fractional error in ΔV_s. Similarly, for a specified leak size (i.e., $dq = 0$), the fractional error in the response time is less than the fractional error in ΔV_s. Therefore, the error in the leak detectability from the procedure does not exceed 2 percent, either in leak size or in response time.

5.8 EFFECTS OF THE STATE OF FLOW

The volumetric mass balance method assumes steady-state flow. When starting and stopping pipelines, significant changes in linefill occur. If these changes have not been considered in establishing the leak detectability, then the leak detection scheme needs to be suspended to avoid false alarms. Often, however, relatively small and unexpected changes in pressure and flow may not be avoidable and the flow may not be strictly at a steady-state. The leak detection scheme described in this chapter still may be used if the flowrate and pressure uncertainties caused by flow unsteadiness are included in the k_{in} and k_{out} of Eq. (5.11) and in the dP of Eq. (5.8). This optimistic view is supported by two observations. First, the above example and previous sensitivity calculations (Liou, Brockway, and Miller 1992) showed that linefill is much more sensitive to temperature than to pressure. When temperature measurement uncertainties exist, small pressure fluctuations are relatively unimportant. Second, as will be seen in the next chapter, k_{in} and k_{out} have a dominating effect on leak detectability only when the leak flowrate is small.

Chapter 6

FIELD TRIALS : STEADY-STATE FLOW

6.1 FACILITY DESCRIPTION AND MEASUREMENT UNCERTAINTIES: SITE 1

Two sets of actual leak test data were used to judge the reasonableness of the proposed methodology and the validity of the data base. Field leak tests at site 1 were conducted for this study. These tests and comparisons are described first. Using existing data from earlier field tests at site 2, additional comparisons were carried out. The characteristics of the two pipeline systems are quite different. They offer different settings for verifying the methodology and the data base.

The pipeline of site 1 is a long petroleum products pipeline in a hilly terrain. The pipeline has a uniform outside diameter of 8.625 inches and a length of approximately 140 miles. The pipe wall thickness varies from 0.219 inches to 0.5 inches, depending on the local conditions. Fig. 6.1 shows the profiles of pipe wall thickness and elevation. There is a pump station at the inlet end and a flow regulator at the receiving station. Eight tests were conducted where near-steady flow was maintained before the onset of a leak. The actual flow was not strictly at steady-state, mainly because of a small-amplitude cyclic movement of the flow regulator. Simulated leaks with various flowrates were created at a point 61 miles from the inlet.

The representative flowrate during the test period was about 650 barrels per hour. Several products with distinct properties were simultaneously present during the tests. The outlet pressure was maintained at approximately 175 psig. The inlet pressure was about 1350 psig and varied slightly as the configuration of the products changed. The inlet and the outlet temperatures were 65.9°F and 51.5°F respectively, and remained essentially constant.

The flowrates were measured by a turbine meter at the inlet and by positive displacement meters at the outlet and at the leak site. The estimated inaccuracy for individual volumetric flowrate measurements is 0.25% of reading. The meters have been in service since 1949 and there is not sufficient data to separate bias errors from nonrepeatabilities. Based on the measured flowrate trace at the inlet, a nonrepeatability of 0.15% of reading was estimated.

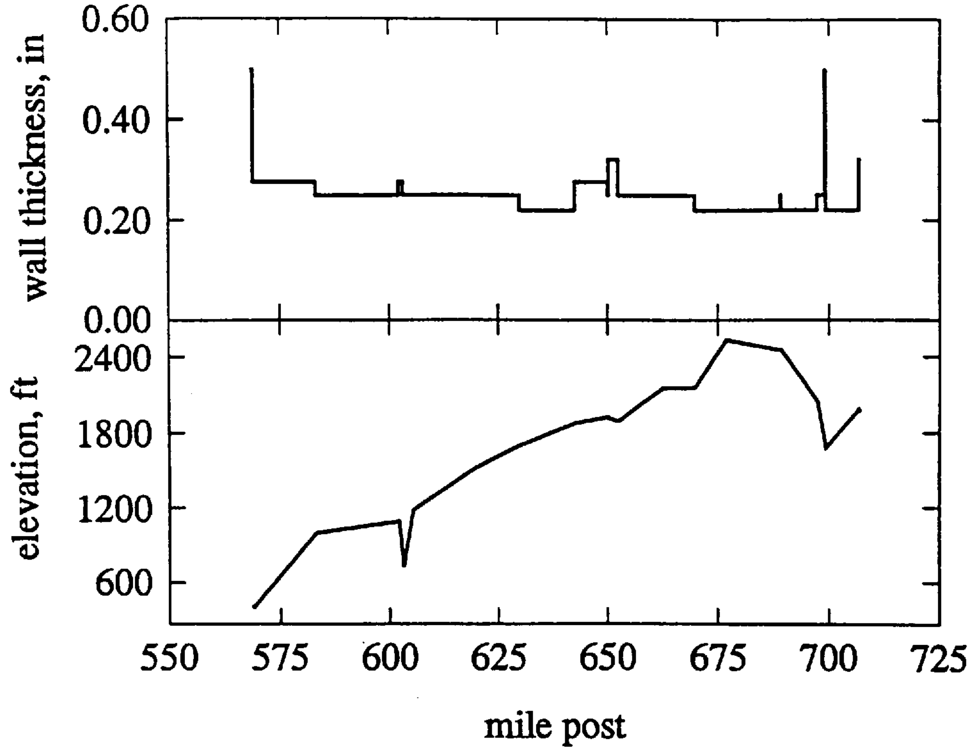

Fig. 6.1
Pipe wall thickness and elevation profiles - site 1

The inlet and outlet pressures were measured by pressure transmitters. The performance specifications of the transmitters indicate an inaccuracy of ±0.25% of the calibrated span, which is 0 to 2000 psi at the inlet and 0 to 200 psi at the outlet. This inaccuracy includes hysteresis, nonlinearity, and nonrepeatability of the pressure sensor. Contributions from each source were not stated in the specifications. Assuming equal contribution from the three sources, the calculated nonrepeatabilities are ±2.89 psi at the inlet and 0.289 psi at the outlet. The outputs from the pressure transmitters are analog 4-20 mA signals.

The inlet and outlet temperatures were measured by Resistance-Thermal-Detectors (RTD's) and temperature transmitters. The inlet temperature was measured upstream from the pumps. The temperature of the liquid at the pump station discharge was higher but no measurement was made there. Based on the inaccuracy of the data representing the worst-case condition, the platinum RTD's have an inaccuracy of 0.09°F at 0°F and 0.27°F at 200°F. These inaccuracies include hysteresis, repeatability, and inaccuracy of calibration equipment. The individual contributions are unknown and equal contribution from each source was assumed. The temperature nonrepeatability at measured values is then obtained by linear interpolation. At 50 °F, the computed nonrepeatability is ±0.078°F or ± 0.78% of the calibrated span of 0 to 100°F for both the inlet and the outlet RTD's. No nonrepeatability error is stated in the performance specifications of the temperature transmitters although analog-to-digital conversion errors do exist. Like the pressure transmitters, the outputs of the temperature transmitters are analog 4-20 mA signals.

Because linefill uncertainty is very sensitive to temperature uncertainty, three temperature traces were collected several months after the tests. By then the ambient temperature was colder. Nonetheless, the nonrepeatability should not change appreciably. To see the effect of the transmitter, the temperature data were read at the termination end of the transmitter and are shown in Fig. 6.2. The standard deviation σ computed from the three data sets is 0.0287°F. The variability represented by $\pm 2\sigma$ is 0.0574°F or ±0.072% of the calibrated span of 80°F (changed from 0-100 to 20-100°F). The "horizontal gap" seen in Fig. 6.2 is due to discretization of the analog signal from the RTD by the transmitter electronics. It appears that the transmitter did not add nonrepeatability to the measurements. A quantity equaling ±0.072% of the calibrated span of 100°F or 0.072°F was taken as the nonrepeatability for temperature measurements.

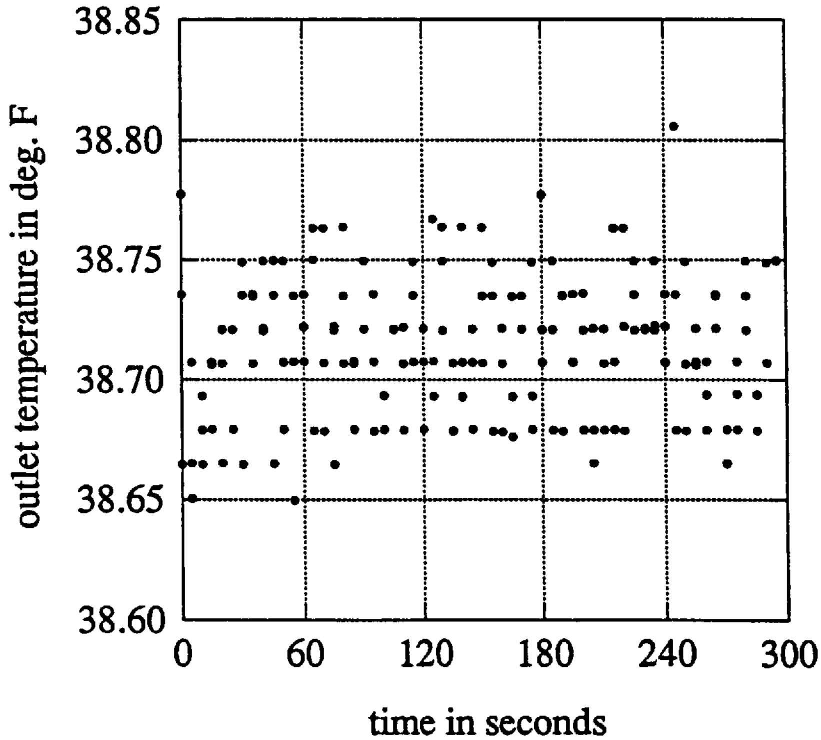

Fig. 6.2
Temperature measurement nonrepeatability at the outlet - site 1

The analog pressure and temperature signals from the transmitters at the inlet and outlet are digitized by Remote Terminal Units (RTU's) using an 11-bit A/D conversion. The calibrated span of each measurement is represented by integers ranging from 1 to 2048 (2^{11}). Strings of integers are brought to the control center by the SCADA system. The integer value for each variable is not updated unless a difference of 5 or more occurs. This process filters out small fluctuations in the signal reaching the control center. After updating, the digital signals are converted to pressures, temperatures, and flowrates in engineering units for further processing. This filtering causes the appearance of a constant outlet temperature recorded to two decimal places. Because truncations took place, the last digit or 0.01°F was viewed as a "measured" nonrepeatability of the outlet temperature measurement.

6.2 REPRESENTATIVE TEST DATA AND THEIR UNCERTAINTIES: SITE 1

Eighteen tests were conducted in a two-day period. In eight of these tests, a leak was initiated when the flow was as close to steady-state as possible. For the remaining tests, a leak was started during transients produced by pump starts and stops. Only "steady-state" tests are addressed in this chapter.

Shown in Fig. 6.3 are the measured pressure and flow at the inlet and the outlet for a test D1. The data was polled by the SCADA system at a regular interval of 15 seconds. Data logging began at 9:58:13 AM. A 5.2 gallon per minute leak was initiated at 10:11:00 AM and terminated at 10:43:12 AM. At the receiving terminal, the regulator constantly attempted to match a pressure set-point and caused the observed cycles in the outlet pressure and flowrate.

Due to frictional damping, the cycles of oscillations are absent in the pressure and flowrate traces at the inlet. The first 50 scans are free of the perturbation of the imposed leak and hence represent a "steady-state." The standard deviations for the 50 scans were computed for pressure, temperature, and flowrate measurements at the inlet and the outlet. Double the standard deviations were taken as the measured nonrepeatabilities. These nonrepeatabilities are tabulated in Table 6.1, together with those inferred from instrumentation specifications.

Note that the measured nonrepeatabilities come from uncertainties in the state of flow as well as in instrumentation. This explains why the nonrepeatabilities in the pressure and the flowrate at the outlet are relatively large. Since there was no hydraulic-caused fluctuations at the inlet, the measured flowrate nonrepeatability at the inlet can be used to approximate the nonrepeatability of the flow meters.

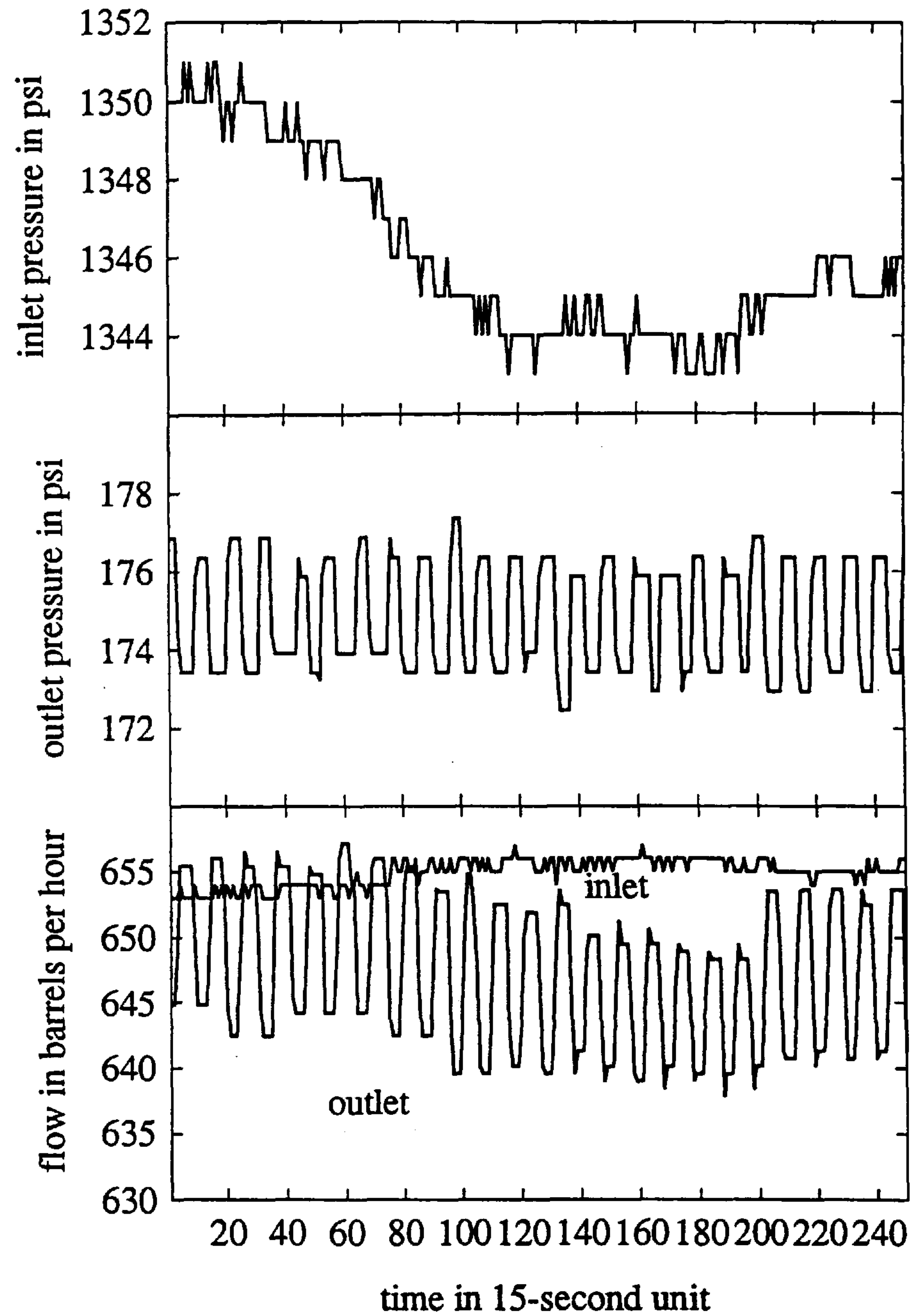

Fig. 6.3
Measured pressures and flowrates at pipe inlet and outlet for test D1 - site 1

Table 6.1 Summary of Process Variable Nonrepeatabilities: Site 1

Variables	Inferred from Spec.	Measurements
P_{in} psi	2.890	1.358
P_{out} psi	0.289	2.946
T_{in} °F	0.072	0.076
T_{out} °F	0.072	0.010
Q_{in} % of reading	not available	0.154
Q_{out} % of reading	not available	1.678

The small uncertainty in the measured outlet temperature is caused by the filtering at the control center described earlier. The same filtering process made the uncertainty in the measured inlet pressure smaller than that estimated from the pressure transmitter specification.

6.3 LEAK DETECTION POTENTIAL: SITE 1

Eqs. (4.4) and (5.8) were used to compute linefill and the uncertainty in linefill change. These equations require pressures and temperatures at interior locations. For each test, the interior pressures were estimated by finding a Darcy-Weisbach friction factor that produced a pressure drop matching the measured data. Variations in elevation and product batch densities were considered in these computations. For interior temperature estimations, an exponential decrease from inlet to the outlet was assumed.

Leak detectability curves are established and shown in Fig. 6.4 for two cases:

Case 1: Storage uncertainty computed from Eq. (5.8). Total probable uncertainty computed by the RSS procedure using the measured nonrepeatabilities (column 3 of Table 6.1). Uncertainties from flow unsteadiness are included.

Case 2: Storage uncertainty computed from Eq. (5.8). Total probable uncertainty computed by the RSS procedure using the inferred nonrepeatabilities (column 2 of Table 6.1) for pressure and temperature measurements and the measured inlet flowrate nonrepeatability for flowrate measurements. Uncertainties from flow unsteadiness are not included.

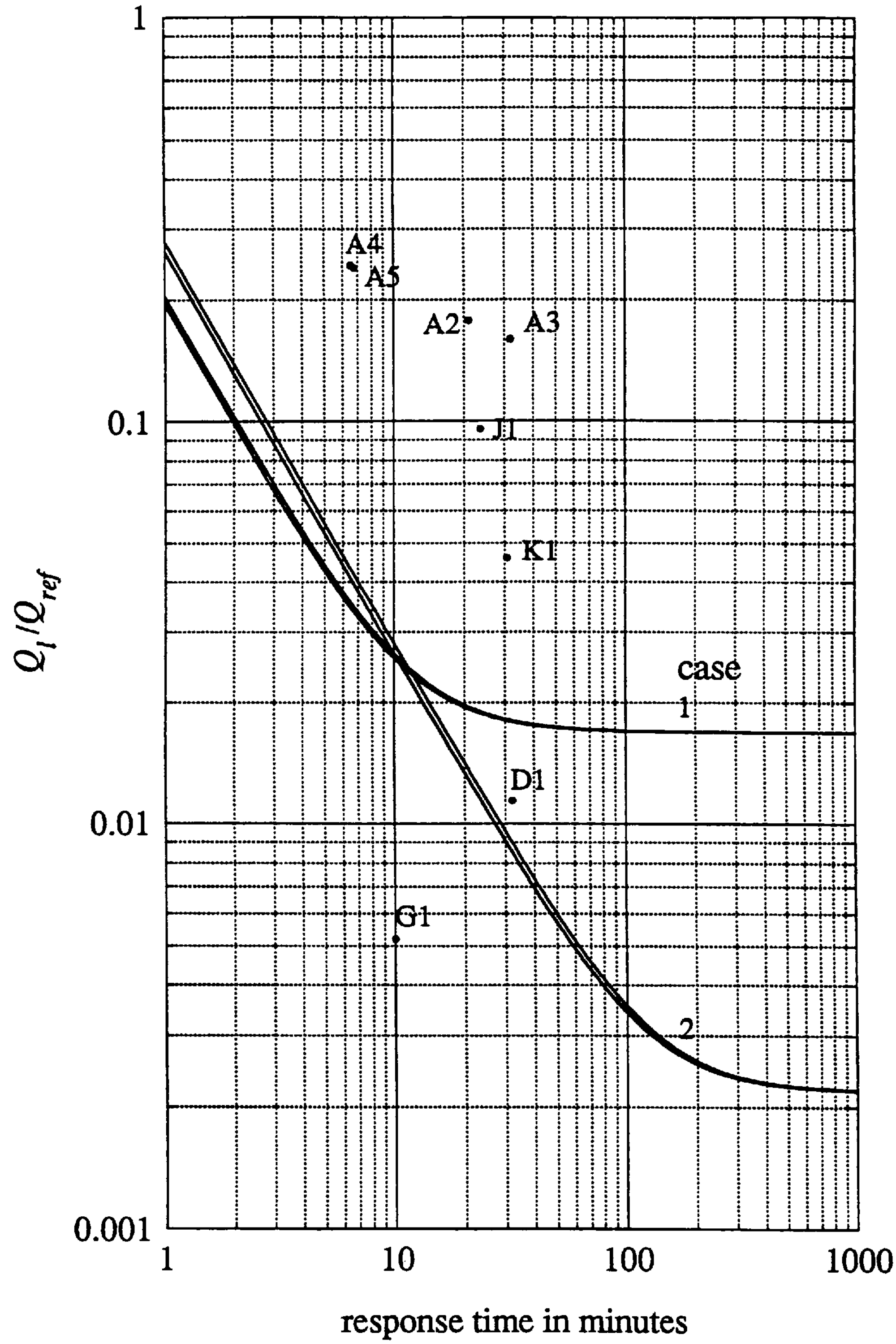

Fig. 6.4
Leak detectability curves and field test results - site 1

Two curves are used to represent case 1 and case 2. For each case, the two curves represent different products batch configurations (see Section 11.1). They bracketed the leak detectability curves for all the "steady-state" tests. The narrow space between the two indicates that batch configuration is not a sensitive parameter for leak detection by volumetric mass balance.

The labeled dots in Fig. 6.4 represent the field test results. For tests A2, A3, A4, A5, J1, and K1, the leaks were detected by the pipeline operator, using leak thresholds based on their experience. For these tests, the dots represent the leak flowrates and the response time, or the elapsed time between the start of the leak to the moment when the leak was first detected. For tests D1 and G1, the leaks were not found. The time coordinates for these two dots represent the duration of the leaks imposed instead of the response time.

6.4 DISCUSSION: SITE 1

The two families of curves in Fig. 6.4 exhibit the general trend of leak detectability by the mass balance method. Larger leaks can be detected in shorter time. For large leaks (large Q_l/Q_{ref}), the uncertainty in linefill over-shadows the uncertainties in flowrate measurements in their impact on leak detectability. For small leaks, the curves approach asymptotes that can be established by flowrate uncertainties alone. Therefore, accurate flow meters with small nonrepeatabilities are required for detecting small leaks over a long time period.

This general trend explains the cross-over of the leak detectability curves for the two cases at approximately 10 minutes. Case 1 has a smaller uncertainty in linefill but larger uncertainties in the flowrates.

6.5 FACILITY DESCRIPTION AND MEASUREMENT UNCERTAINTIES: SITE 2

This facility is a 12.75-inch outside diameter steel pipe with variable wall thickness. The length of the pipe is approximately 550 miles. Fig. 6.5 shows the wall thickness and elevation profiles of the pipeline. Three pump stations and a receiving terminal are also indicated. The pipeline transports light crude continuously at a constant flowrate of about 250 m^3/hr. The crude oil can enter the pipeline at two locations. Besides the main inlet at the very upstream of the pipeline, there is a side line near the receiving terminal that can inject crude into the pipeline. The pipeline has only one outlet: the receiving terminal. Custody transfer metering with dedicated provers are used at all inflow and outflow points.

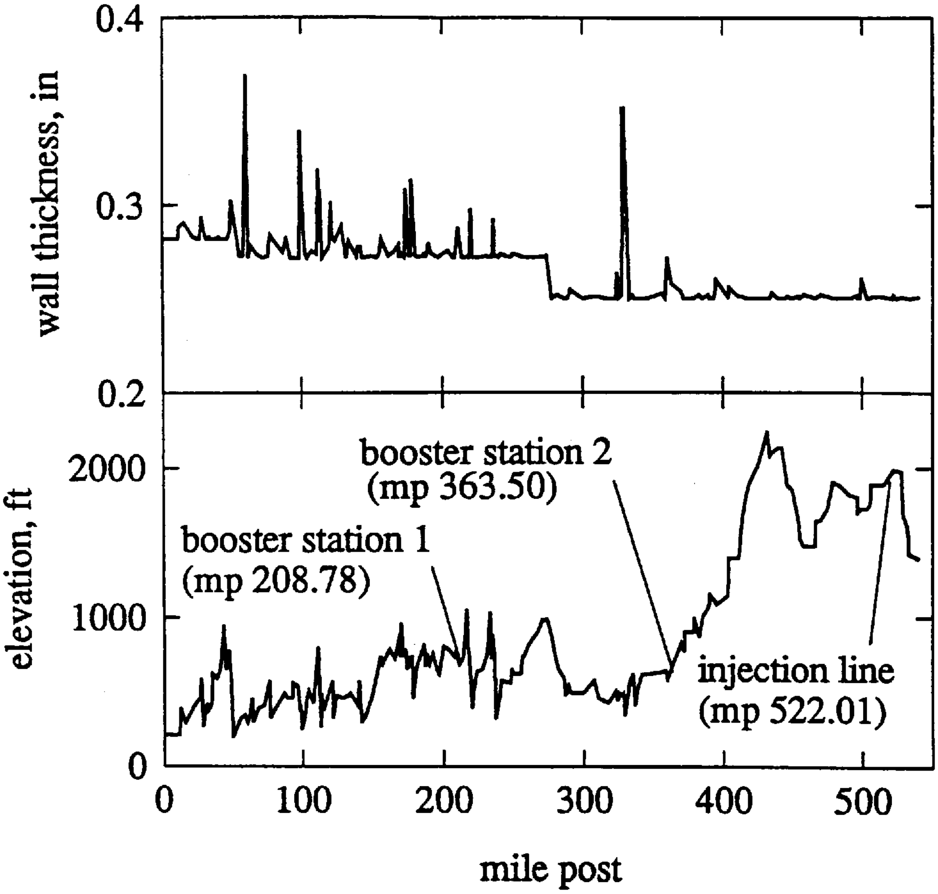

Fig. 6.5
Pipe wall thickness and elevation profiles - site 2

Flow measurements are made by positive displacement meters. The flow meters are proven weekly at the origin station with dedicated provers, monthly at the injection site and at the receiving terminal with a portable prover. The estimated accuracy for flowrate measurements is about normally 0.1%, although the maximum inaccuracy can be as great as 0.25%. The nonrepeatability is estimated at about 0.01%.

Pressure at stations and at several valve sites are measured by pressure transmitters. The performance specifications of the transmitters indicate an inaccuracy of ±0.25% of span, which is 0 to 12000 kPa(gauge) at all locations. The stated inaccuracy includes the combined effects of nonlinearity, hysteresis and nonrepeatability. The outputs from the transmitters are 4-20 mA analog signals.

Temperature measurements are made by 100 R_0 Platinum RTDs and temperature transmitters. The nonrepeatability of the RTDs is 0.025% of operating range or ±0.05 °C, whichever is greater. The transmitters have an inaccuracy of ±0.2% of calibrated span from -20°C to 20°C or 0.08°C. This inaccuracy includes combined effects of nonlinearity, hysteresis, and nonrepeatability. The outputs from the transmitters are also 4-20 mA analog signals.

All 4-20 mA analog signals are digitized by RTUs using 12 bit converters. The SCADA system polls the data from the RTUs at a time interval of about 20 seconds and converts them into physical units. Time stamping occurs at the control center. Temperature and flowrates are reported every scan. The pressure data is reported by exception using a dead-band of about 10 psi. The converted temperature data was rounded to the nearest one-tenth of one degree C.

6.6 REPRESENTATIVE TEST DATA AND THEIR UNCERTAINTIES: SITE 2

Five sets of data were available. All of them contain leaks (one each) of known size. The flows were at steady-state prior to the leaks. Fig. 6.6 shows the recorded pressures and flows at the origin station (inlet) and at the receiving terminal (outlet) while the injection line was valved off. It is apparent that, aside from noise, the flow was at steady-state. The noise levels in both the pressure and flow were higher at the inlet because of the proximity of the pump station. Other data that are available but not shown in this figure are temperature at the inlet and the outlet, and temperature and pressure at the booster stations and at several valve sites.

As shown in Fig. 6.5, there are two booster pump stations which separate the pipeline into three segments. Pressure and temperature measurements were made at both the suction and the discharge of the booster stations. Assuming that the inlet flow data is applicable to each segment, the leak detectability for the three segments can be evaluated individually.

Alternately, one can use the data received at the control center to establish variable nonrepeatabilities. In Fig. 6.6, the dip of the inlet flow at approximately 68600 seconds could not be explained. However, the first 344 time steps (prior to 68539 seconds) should represent a steady-state. The standard deviations in this portion of the data set were computed and doubled. The resulting values were used as measured nonrepeatabilities for pressure, temperature and flowrate. They are shown in Table 6.2, together with the nonrepeatabilities inferred from instrumentation specifications.

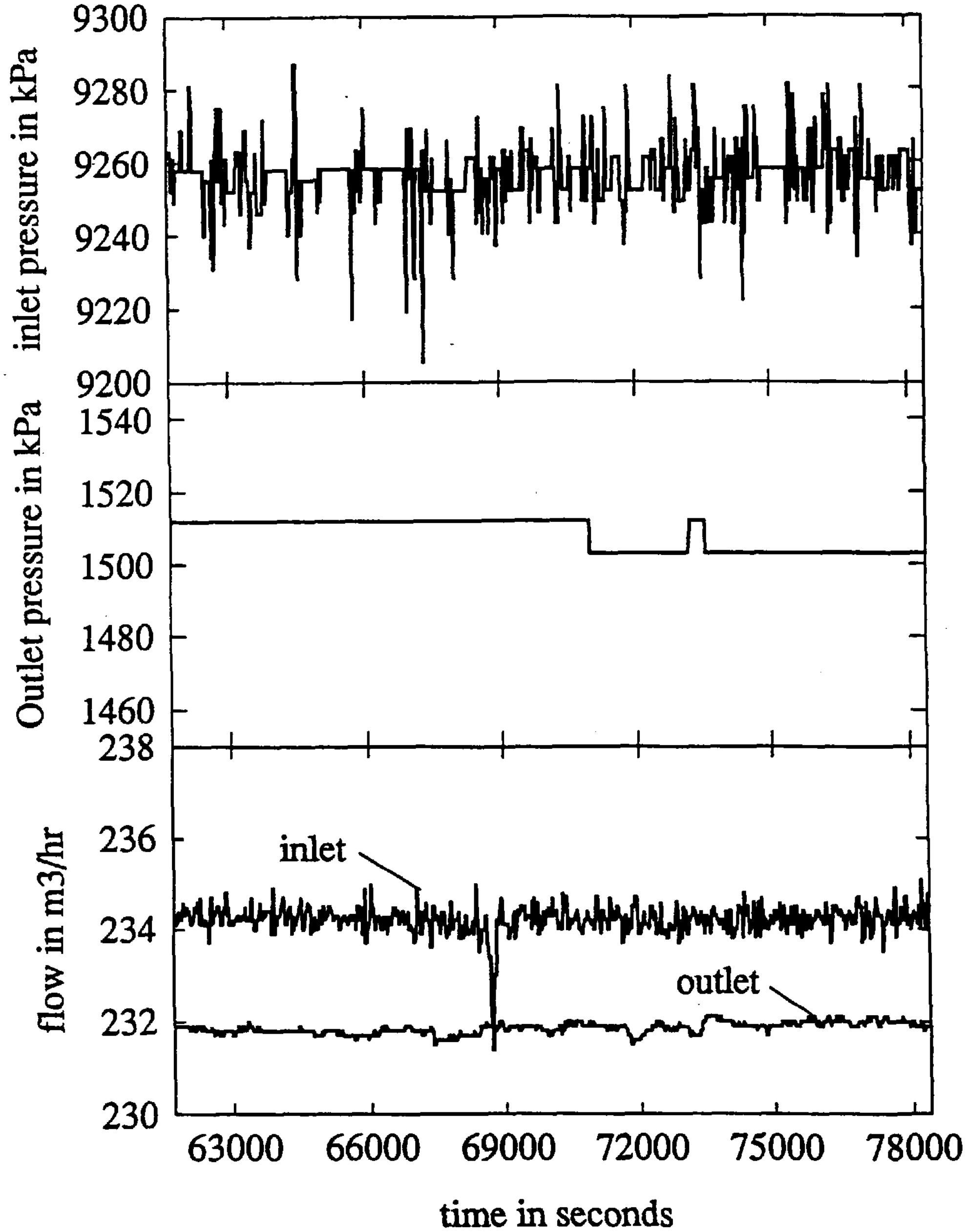

Fig. 6.6
Measured pressures and flowrates at pipe inlet and outlet - site 2

Table 6.2 Summary of Process Variable Nonrepeatabilities: Site 2

Variables	Inferred From Specifications	Measured Segment 1	Segment 2	Segment 3
P_{in} psi	2.010	2.545	1.120	4.109
P_{out} psi	2.010	1.013	3.812	0.145
T_{in} °F	0.13	0.309	0.180	0.180
T_{out} °F	0.13	0.180	0.180	0.180
Q_{in} %	0.01	0.204	0.204	0.204
Q_{out} %	0.01	0.204	0.204	0.204

As for site 1, the measured nonrepeatabilities come from uncertainties in the state of flow as well as in instrumentation. The RTU and SCADA system may filter out some fluctuations. Measured uncertainties greater than those estimated from instrument specifications are caused by noise in the data. Measured uncertainties smaller than those from specifications are due to filtering at either the RTU or the SCADA levels.

6.7 LEAK DETECTION POTENTIAL: SITE 2

Using the uncertainties in Table 6.2, the resulting leak detection potentials for the three pipe segments are shown in Fig. 6.7. Also shown are the five leak data points. Each point represents the size of the leak and the time it took to detect it, using thresholds established by the pipeline operator.

6.8 DISCUSSION: SITE 2

The leak detectability curves established appear to be reasonable as the detectable leaks fall above the curves. For data points labeled leak1 and leak2, the leak flowrates were reported as less than 2 m^3/hr while the detection times were 310 and 180 minutes respectively. Presumably, the resolution of the meter used to measure the leak flowrate could not discern differences below 2 m^3/hr. 2 m^3/hr was taken as the leak flowrate to establish Q_l / Q_{ref}. The true leak flowrate for leak1 might be smaller than that of leak2.

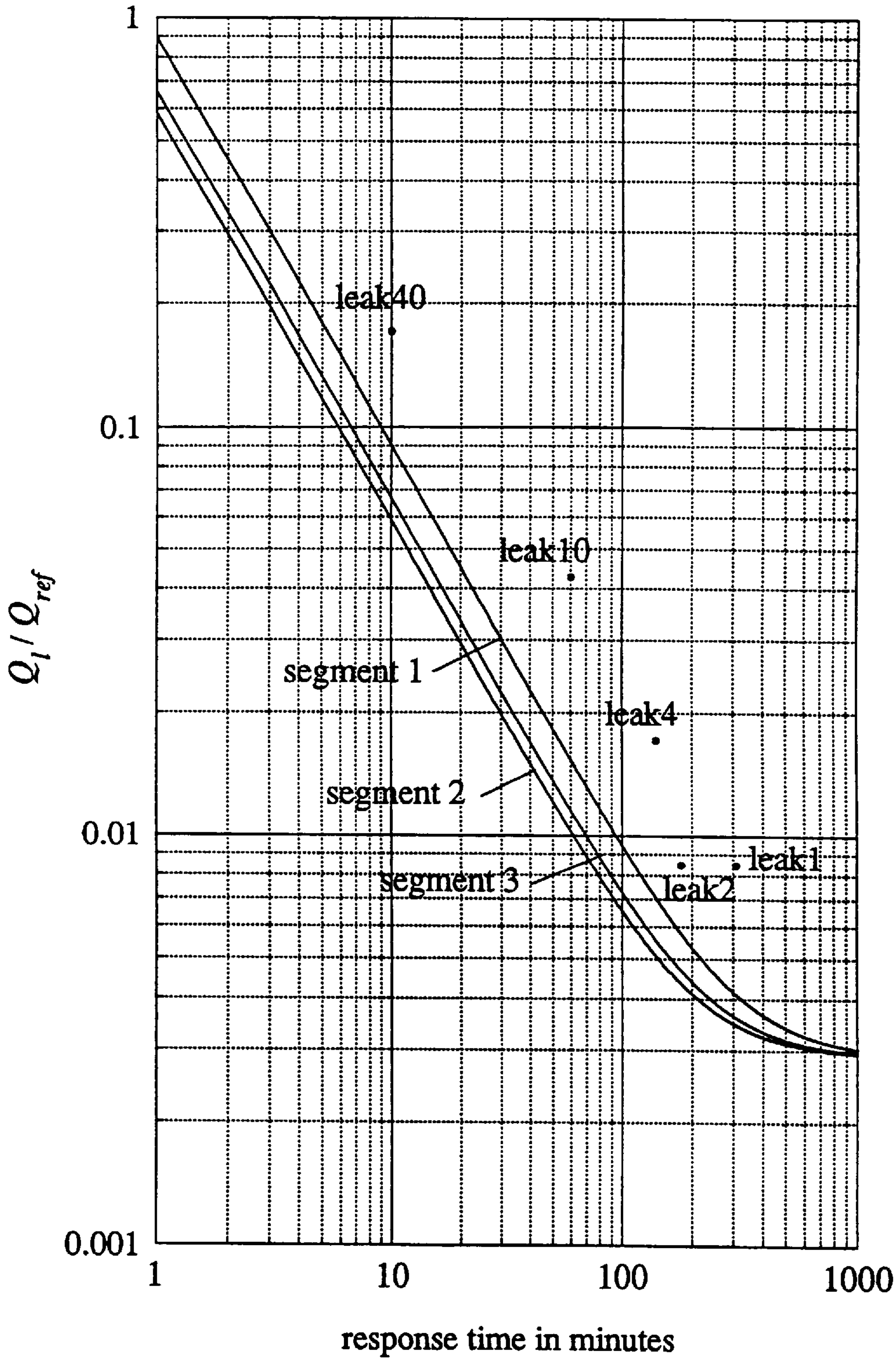

Fig. 6.7
Leak detectability curves and field test results - Site 2

This set of test data covers a wide range of leak flowrates. The leaks were detected by the pipeline operator within the time intervals indicated. Meanwhile, all the test points fall above the leak detectability curves established independently by using the procedure and data base described in Chapter 5.

6.9 DISCUSSION AND CONCLUSION

Detected leaks at two sites with different characteristics were investigated. In both cases, the pipeline operators used their own logic and experience to set the threshold for leak alarms. These thresholds were set as tight as possible without triggering false alarms, thus they represent practical bounds for leak detectability.

On the other hand, leak detectabilities for the sites were predicted based on variable uncertainties. For each site, all the test data points associated with detectable leaks fall above the predicted leak detectability curve. In addition, the test data points of detectable leaks follow the trend of the leak detectability curves. This is a strong indication that the methodology and the data base established in this study are valid.

It should be emphasized that variable uncertainties are not deterministic quantities. Although not always explicitly stated, the uncertainties are usually set at two or three times the sample standard derivations established from test data sets. Hence it is possible that a detectable leak test data point falls below the corresponding detectability curve. However, such an occurrence is not likely. For a qualitative estimation, if the frequency of uncertainties is normally distributed and the uncertainties are at two times the standard deviation, then the probability of detecting a leak underneath the detectability curve is less than 4.54 percent.

Chapter 7

RANKING OF VARIABLES AND THEIR SENSITIVITIES

7.1 GENERALIZED LEAK DETECTABILITY CURVE

In Figs. 5.4, 6.4, and 6.7, Q_l / Q_{ref} are plotted against Δt to establish leak detectability curves for particular pipelines. To facilitate variable ranking, it becomes necessary to find a more general way to represent leak detectability. This can be accomplished by combining Eqs. (5.6) and (5.8) to obtain

$$\frac{Q_l}{Q_{ref}} = \sqrt{k_{in}^2 + k_{out}^2 + 2\left(\frac{A_0 L_0}{\Delta t Q_{ref}}\right)^2 \left[\left(\frac{\partial I}{\partial P} dP\right)^2 + \left(\frac{\partial I}{\partial T} dT\right)^2\right]} \tag{7.1}$$

If we plot Q_l / Q_{ref} against $\Delta t \ Q_{ref} / A_0 L_0$ instead of Δt, then the resulting leak detectability curve becomes valid for a family of pipelines with common $\Delta t Q_{ref} / A_0 L_0$. This generalized leak detectability curve greatly simplifies the representation of the ranking of the uncertain variables.

7.2 SENSITIVITY COEFFICIENTS

Eq. (7.1) shows that mass balance based leak detectability depends on the characteristics of the pipeline system and the uncertainties associated with four process variables: inlet flow, outlet flow, pressure, and temperature. The sensitivity coefficients of leak detectability are obtained by taking partial derivatives of Q_l / Q_{ref} in Eq. (7.1) with the four process variables. Define q and λ as follows to simplify the notations

$$q = \frac{Q_l}{Q_{ref}} \tag{7.2}$$

$$\lambda = \frac{\Delta t Q_{ref}}{A_0 L_0} \tag{7.3}$$

and obtain

$$\frac{\partial q}{\partial k_{in}} = \frac{k_{in}}{q} \tag{7.4}$$

$$\frac{\partial q}{\partial k_{out}} = \frac{k_{out}}{q} \tag{7.5}$$

$$\frac{\partial q}{\partial dP} = \frac{2}{q\lambda^2}\left(\frac{\partial I}{\partial P}\right)^2 dP \tag{7.6}$$

$$\frac{\partial q}{\partial dT} = \frac{2}{q\lambda^2}\left(\frac{\partial I}{\partial T}\right)^2 dT \tag{7.7}$$

7.3 GENERAL TRENDS OF SENSITIVITY COEFFICIENTS

As seen in Eqs. (7.5), (7.6), and (7.7), the sensitivity coefficients are themselves dependent on the magnitude of uncertainty. An indication of the level of uncertainties that are likely to exist in practice is needed. The range of uncertainties established by the API Pipeline Leak Detection Task Force were shown in Table 3.3. Extracted from that table are the following maximum uncertainties for the four process variables:

inlet flow, k_{in}:	± 0.05
outlet flow, k_{out}:	± 0.05
pressure, dP:	± 15 psi
temperature, dT:	± 5°F

Consider an example pipeline which conveys a 55°API gasoline at an average pressure of 700 psig and an average temperature of 60°F. The pipeline has a D/e ratio of 45. From Tables 5.1 and 5.2, the following coefficients are established:

$a_0 = 7.156\text{x}10^{0}$, a_1=-4.898x10^{-4}, a_2=1.860x10^{-2}, a_3=-1.778x10^{-6}, a_4=3.885x10^{-5}

$b_0 = 6.089\text{x}10^{-1}$, b_1=-1.736x10^{-5}, b_2=3.566x10^{-4}, b_3=-7.791x10^{-8}, b_4=-6.123x10^{-7}

Next, use Eqs. (5.9) and (5.10) with P = 700 psig and T = 60°F to obtain

$\partial I/\partial P = 7.9943\text{x}10^{-6}$ psi^{-1}

$\partial I/\partial T = 6.1267\text{x}10^{-4}$ °F^{-1}

The sensitivity coefficients for the example can now be calculated as a function of λ. The results are shown in Fig. 7.1. It is apparent that:

1. The sensitivity coefficients for k_{in} and k_{out} are independent of λ. For a fixed amount of improvement in flow measurement, the gain in the reduction of the minimum detectable leak size is not affected by the response time, the reference flow, the pipe size, and the pipe length.

2. The sensitivity coefficient for dT decreases as λ increases. For a fixed amount of improvement in temperature measurement, the resulting reduction in the size of the minimum detectable leak diminishes as the response time becomes smaller, the reference flow becomes smaller, the pipe size becomes greater, and the length becomes greater. The same trend can be observed for dP.

These trends are not particular to this example, but hold in general.

7.4 APPLICATION EXAMPLE

Suppose the diameter and the length of the pipeline in Section 7.3 are 13.5 inches and 50 miles, and that the flowrate of the gasoline is 3500 bbl/hr. For a 10-minute response time, what are the magnitude of the sensitivity coefficients?

Using the data given in Section 7.3, a q of 0.35 is computed from Eqs. (7.1) and (7.2) and λ of 0.012 is computed from Eq. (7.3). The sensitivity coefficients for a 10-minute response time are then computed from Eqs. (7.5), (7.6) and (7.7) as

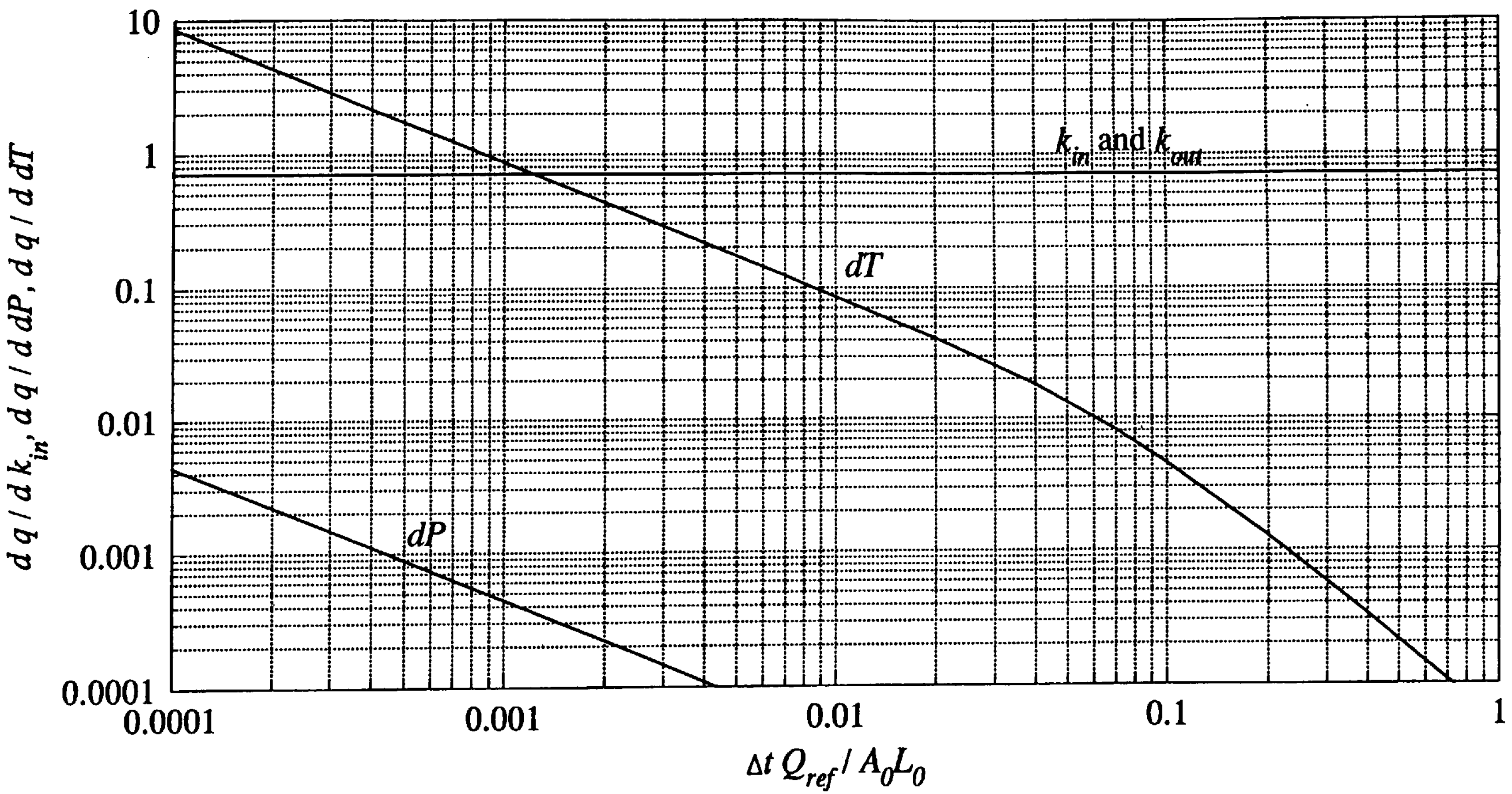

Fig. 7.1
Sensitivity coefficients for a 55°API gasoline at 700 psig and 60°F with pipeline *D/e* of 45. Uncertainty levels: dT = 5°F, dP = 15 psi, $k_{in} = k_{out} = 0.05$

$$\partial q/\partial k_{in} = \partial q/\partial k_{out} = 1.41\text{x}10^{-1}$$
$$\partial q/\partial dP = 3.47\text{x}10^{-5} \text{ per psi}$$
$$\partial q/\partial dT = 6.80\text{x}10^{-2} \text{ per °F}$$

Suppose one desires to reduce the minimum detectable leak size from 35% to 25% of Q_{ref} at a response time of 10 minutes, which measurement should be upgraded? Note that the maximum amount of improvements is $0.05Q_{ref}$ for inlet or outlet flow ($0.1Q_{ref}$ for both), 15 psi for pressure, and 5°F for temperature. Setting $\partial k_{in} = 0.05$, a ∂q of 0.0075 can be computed according to the sensitivity coefficient computed above. Similarly, $\partial q = 0.0005$ for $\partial dP = 15$ psi and 0.34 for $\partial dT = 5$°F. Since only the ∂q for temperature measurement exceeds 0.1 (or 10% of Q_{ref}), improvements in flowrate and pressure measurements will not improve leak detectability. The objective can only be achieved by improving the temperature measurement. The amount of improvement is simply 0.1 / $6.7984\text{x}10^{-2}$ or 1.47°F.

For a greater response time of 60 minutes, q is reduced to 0.091 and λ is increased to 0.075. The sensitivity coefficients for a 60-minute response time are

$$\partial q/\partial k_{in} = \partial q/\partial k_{out} = 5.47\text{x}10^{-1}$$
$$\partial q/\partial dP = 3.74\text{x}10^{-6} \text{ per psi}$$
$$\partial q/\partial dT = 7.33\text{x}10^{-3} \text{ per °F}$$

The $\partial q's$ for k_{in}, dP, and dT are 0.027, 0.000056, and 0.037 respectively. Suppose one desires to reduce the minimum detectable leak size by 5% (i.e., $\partial q = 0.05$) at a 60-minute response time. Since 0.05 > 0.037, improvement in temperature measurement alone is no longer sufficient. Flow measurements must be improved as well. Improvement in pressure measurement will not be helpful since the sensitivity coefficient for dP is very small. Other considerations, such as cost, enter at this point in determining the amount of improvement for flowrate and temperature measurements.

By patterning after this example and using Tables 5.1 to 5.10, similar information can be derived for other pipelines conveying crude oils and refined products. This information is useful in determining the best strategy for upgrading.

7.5 RANKING OF PROCESS VARIABLES

To rank the process variables according to their influence on leak detectability, the contributions of individual uncertainties to the leak detectability are examined. Plotted in Figs. 7.2, 7.3, and 7.4 are the individual and the combined effects of the three sets of uncertainties stated in the figure captions. Based on the trends exhibited by these figures it can be stated that:

1. Independent of $\Delta t Q_{ref} / A_0 L_0$ and the magnitude of the uncertainty levels, the magnitude of q attributed to dT alone is about one order of magnitude greater than that attributed to dP. Allowing for reasonable proportional increase in pressure uncertainty, the effect of temperature uncertainty is still greater. Therefore, in general, temperature uncertainty is ranked over pressure uncertainty.

2. For very small $\Delta t Q_{ref} / A_0 L_0$, the combined effect curve coincides with the dT curve. In other words, when the pipe dry volume is large, the throughput small, the leak response time short, or any combination of the above, the uncertainties in flowrates and in pressure become unimportant. The leak detectability can be determined based on temperature uncertainty alone.

3. For very large $\Delta t Q_{ref} / A_0 L_0$, the combined curve coincides with the k_{in} and k_{out} curve. This means that when the pipe dry volume is small, the throughput large, the leak response time long, or any combination of the above, the uncertainties in temperature and in pressure become unimportant. The leak detectability can be determined based on uncertainties in flowrate measurements alone.

4. Observations 2 and 3 hold true at all magnitudes of uncertainty levels.

5. Pressure uncertainty becomes important only when the temperature uncertainty is small and $\Delta t Q_{ref} / A_0 L_0$ is large.

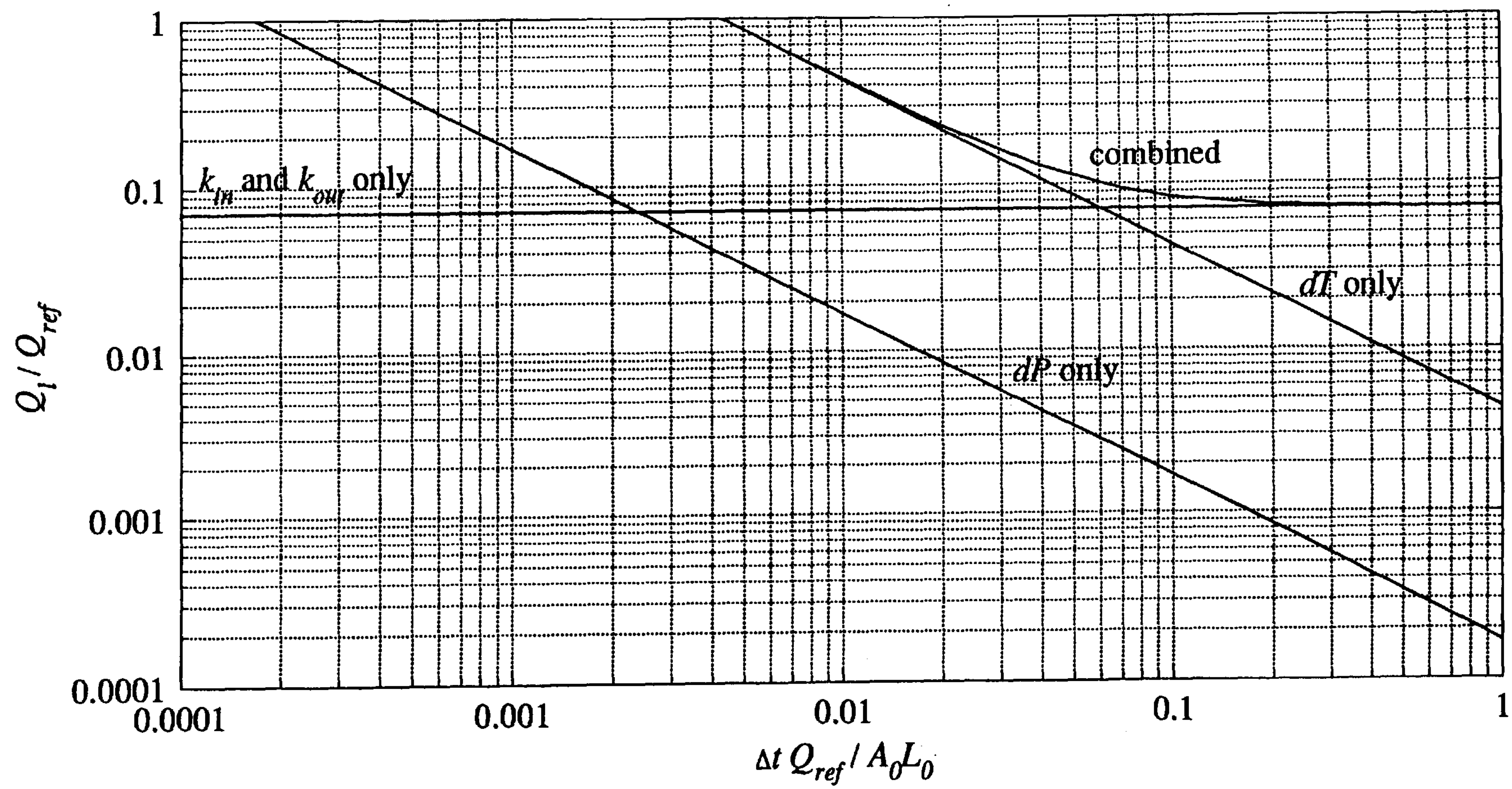

Fig. 7.2
Generalized leak detectability curve and its components for a 55°API gasoline at 700 psig and 60°F with pipeline *D/e* of 45. Uncertainty levels: dT = 5°F, dP = 15 psi, $k_{in} = k_{out}$ = 0.05

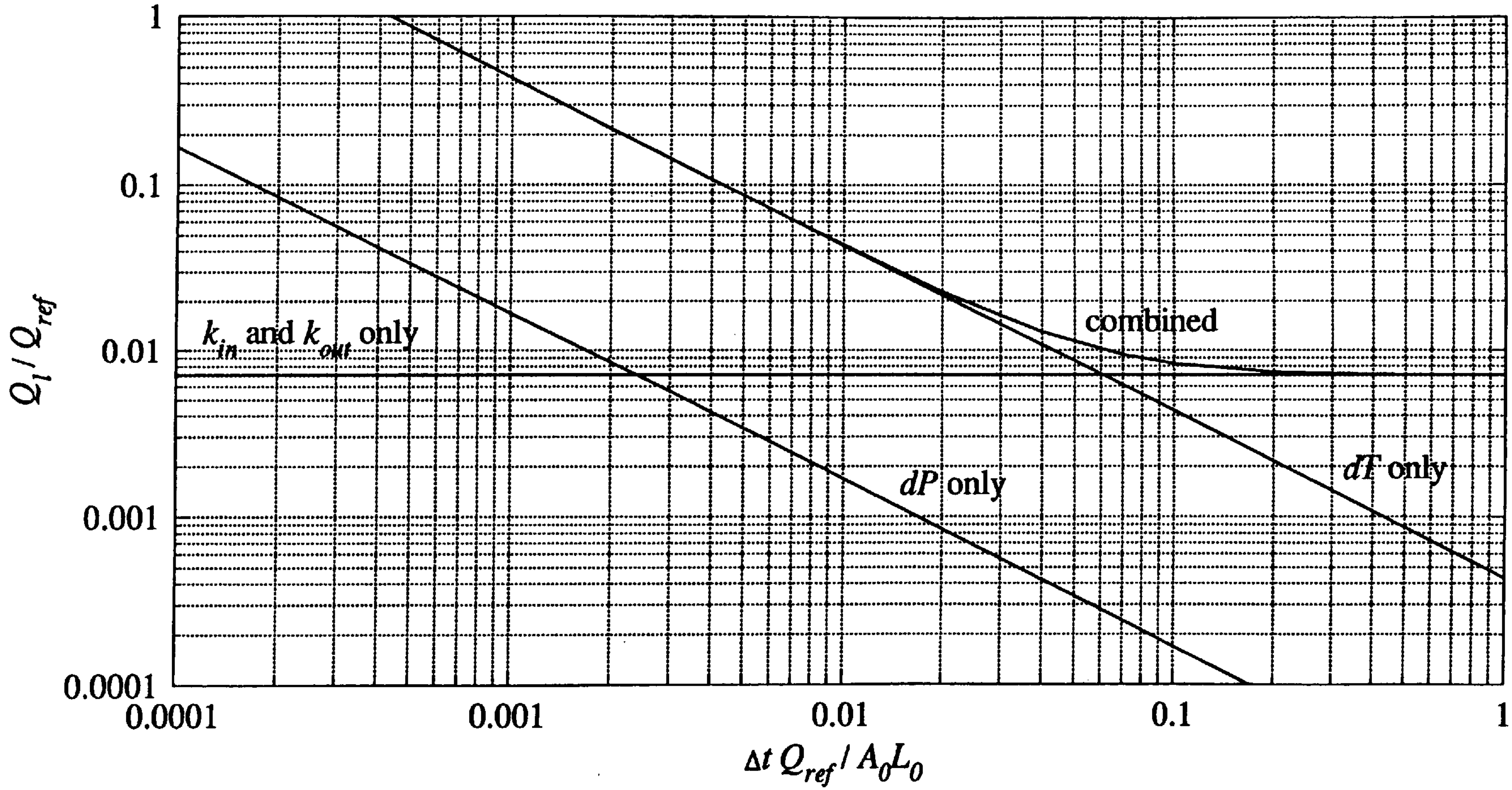

Fig. 7.3
Generalized leak detectability curve and its components for a 55°API gasoline at 700 psig and 60°F with pipeline D/e of 45. Uncertainty levels: dT = 0.5°F, dP = 1.5 psi, $k_{in} = k_{out} = 0.005$

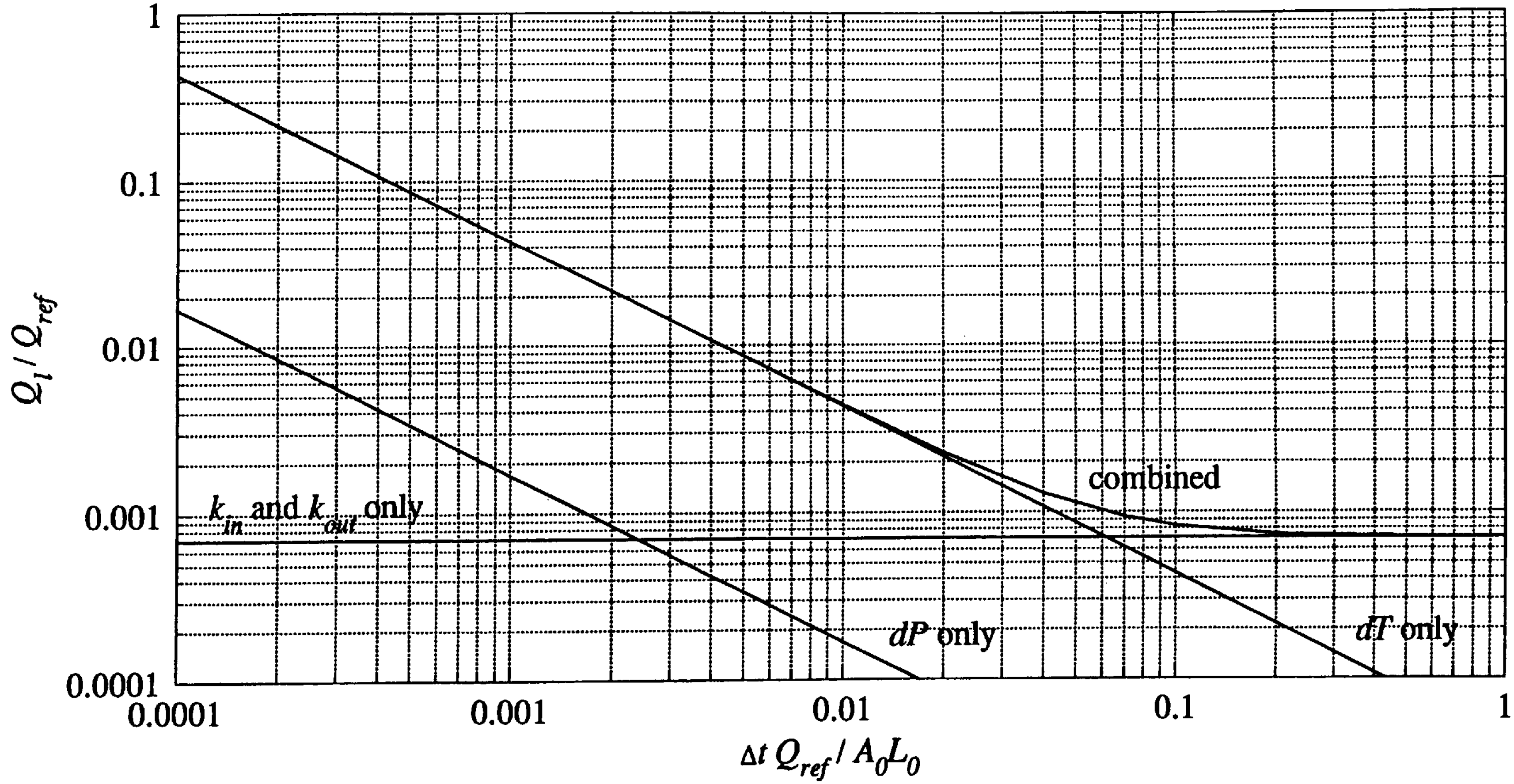

Fig. 7.4

Generalized leak detectability curve and its components for a 55°API gasoline at 700 psig and 60°F with pipeline *D/e* of 45. Uncertainty levels: $dT = 0.05$°F, $dP = 0.15$ psi, $k_{in} = k_{out} = 0.0005$

Chapter 8

TRANSIENTS MODELING AND SYSTEM CHARACTERIZATION

8.1 TRANSIENTS AND CHANGES IN LINEFILL

Transients arise by operations such as valving and pump starts or shutdowns. Depending on the cause, the severity of transients varies from mild to severe. Transients result in line fill changes that must be accounted for in leak detection.

The length, diameter, and flow conditions of petroleum products pipelines vary over a wide range. To deal with line fill change systematically, we need to characterize pipelines and transient severity. The governing equations for transient flow provide essential information on this aspect.

8.2 GOVERNING EQUATIONS FOR TRANSIENT FLOW

The principle of mass conservation and the equation of motion can be expressed in terms of pressure P and discharge velocity V by:

$$\frac{1}{\rho}\frac{\partial P}{\partial x}+V\frac{\partial V}{\partial x}+\frac{\partial V}{\partial t}+\frac{fV|V|}{2D}+g\sin\alpha=0 \tag{8.1}$$

$$\frac{1}{\rho a^2}\left(\frac{\partial P}{\partial t}+V\frac{\partial P}{\partial x}\right)+\frac{\partial V}{\partial x}=0 \tag{8.2}$$

in which P = pressure, V = velocity, D = pipe diameter, A = cross-sectional area of the pipe, g = gravitational acceleration, f = Darcy-Weisbach friction factor, x = distance, t = time, α = the upward angle between the pipe and the horizontal, and a = pressure wave speed of the liquid-pipe system given by:

$$a = \sqrt{\frac{K/\rho}{1 + KDc_1/(Ee)}} \tag{8.3}$$

where c_1 is a constant that reflects the state of stress in the pipe wall (see Section 4.1).

These two equations form a set of hyperbolic equations and thus can be transformed into a pair of total differential equations:

$$\frac{dV}{dt} \pm \frac{1}{\rho a}\frac{dP}{dt} + g\sin\alpha + \frac{fV|V|}{2D} = 0 \tag{8.4}$$

which are valid along curves defined by

$$\frac{dx}{dt} = V \pm a \tag{8.5}$$

in the distance versus time plane (x - t plane). These curves are called characteristics.

The mass density appearing in the coefficient of dP/dt in Eq. (8.4) is pressure - dependent and needs to be approximated during integration. To avoid this approximation, the pressure in Eq. (8.4) is replaced by piezometric head H

$$H = \frac{1}{g}\int_0^P \frac{dP}{\rho(P)} + Z \tag{8.6}$$

where Z is the elevation of the pipe with respect to a datum. Eq. (8.4) now becomes

$$\pm\frac{g}{a}\frac{dH}{dt} + \frac{dV}{dt} + \frac{fV|V|}{2D} \mp \frac{g\sin\alpha}{a}V = 0 \tag{8.7}$$

valid only along the characteristics defined by Eq. (8.5).

Eqs. (8.5) and (8.7) together with prescribed boundary conditions completely specify the transient flow in a pipe segment. Generally, analytical solutions to these equations can not be found and numerical solution procedures, such as the method of characteristics (Wylie and Streeter, (1993)), must be used. The slopes of tangents to the characteristics vary when velocity and wave speed change. These changes make interpolations necessary in the numerical solution process. Simplification is sought.

8.3 SIMPLIFICATIONS - WATERHAMMER EQUATIONS

When the convective terms $V\partial V/\partial x$ and $V\partial P/\partial x$ in the governing equations are small and neglected, the governing equations are simplified to (Wylie and Streeter, 1993):

$$g\frac{\partial H}{\partial x}+\frac{1}{A}\frac{\partial Q}{\partial t}+\frac{fQ|Q|}{2DA^2}=0 \qquad (8.8)$$

$$\frac{\partial H}{\partial t}+\frac{a^2}{gA}\frac{\partial Q}{\partial x}=0 \qquad (8.9)$$

These equations are commonly known as the waterhammer equations. When the wave speed is treated as a constant, the characteristics are straight lines that make the numerical solution straight forward.

The use of a constant wave speed while allowing mass density to vary with pressure is justifiable by data uncertainties. Table 8.1 shows the variations in ρ, K, and a at 15°C as percentages of the respective variables at 0 kPa.

Table 8.1 Property variations in percent between 0 and 7000 kPa.

ρ_0, kg/m^3	700	800	900	1000
ρ	0.90	0.60	0.40	0.34
K	5.40	5.40	5.40	5.40
a	2.20	2.40	2.40	2.50

From Eqs. (3.1), (3.7), and (3.8), the uncertainty bounds for mass density and wave speed can be established as

$$\frac{d\rho}{\rho} \leq \frac{P}{K-P}\frac{|dK|}{K} + \frac{|dC_T|}{C_T} \tag{8.10}$$

$$\frac{da}{a} \leq \frac{1}{2}\left(\frac{|dK|}{K} + \frac{|d\rho|}{\rho}\right) \tag{8.11}$$

Using $dC_T/C_T = \pm 0.05\%$ and $dK/K = dF/F = \pm 6.5\%$ (see Section 3.1), the percentage uncertainties in mass density, bulk modulus, and wave speed are computed and are shown in Tables 8.2, 8.3, and 8.4.

Table 8.2 Bound for density uncertainties (%)

ρ_0, kg/m^3	700	800	900	1000
0 kPa	0.050	0.050	0.050	0.050
3500 kPa	0.080	0.069	0.064	0.061
7000 kPa	0.108	0.087	0.077	0.072

Table 8.3 Bound for bulk modulus uncertainties (%)

ρ_0, kg/m^3	700	800	900	1000
all levels	6.5	6.5	6.5	6.5

Table 8.4 Bound for wave speed uncertainties (%)

ρ_0, kg/m^3	700	800	900	1000
0 kPa	3.263	3.263	3.263	3.263
3500 kPa	3.290	3.285	3.282	3.281
7000 kPa	3.304	3.294	3.289	3.286

Tables 8.1 and 8.2 show that, over the pressure range considered and in percentages, the mass density changes significantly exceed the uncertainties in the density data. Thus the mass density should be treated as a variable.

Table 8.1 shows that the percentage changes in bulk modulus and wave speed exceed that of density. However, as seen in Tables 8.3 and 8.4, the percentage changes in bulk modulus and wave speed fall within the associated data uncertainty limits. In the face of data uncertainty, the wave speed can be viewed as a constant. Uncertainty limits for modeling results due to the wave speed uncertainty will be considered separately. Because the wave speed is specified, the bulk modulus and its uncertainty do not affect the model results directly. The consequence of neglecting the convective terms will be discussed in Section 8.5 after the concept of similitude is introduced.

8.4 SIMILITUDE

Represent the steady-state volumetric flow rate by Q_0 and the head rise due to sudden and complete stoppage of the velocity V_0 (= Q_0/A) by H_0. This head rise, called potential surge, can be expressed as (Wylie and Streeter (1993))

$$H_0=\frac{aV_0}{g} \tag{8.12}$$

Let $v = Q/Q_0$, $h = H/H_0$, $x' = x/L$, and $t' = at/L$, L being the length of the pipe. Eqs. (8.8) and (8.9) take the following dimensionless form

$$\frac{\partial h}{\partial x'}+\frac{\partial v}{\partial t'}+Rv|v|=0 \tag{8.13}$$

$$\frac{\partial h}{\partial t'}+\frac{\partial v}{\partial x'}=0 \tag{8.14}$$

where

$$R=\frac{fLV_0}{2aD} \tag{8.15}$$

Eqs. (8.13) and (8.14) together with two boundary conditions completely specify any transient flow. For leak detection, the boundary conditions are measured flow and pressure (and thus head) histories at the pipe inlet and outlet. These boundary conditions need to be scaled by dividing head H with H_0, flow Q with Q_0, and time t with L/a.

In Eqs. (8.13) and (8.14), all system parameters are grouped into the single constant R. Thus R can be viewed as a parameter that characterizes a series of similar systems. That is, two pipelines with the same R value and with identical scaled head and flow histories will behave identically in terms of scaled variables. Once we have characterized the transients of a particular system, we can predict the transients in many similar but physically different pipelines. Shown in Fig. 8.1 is a distribution of the R values for a set of representative oil pipeline data gathered by the API leak detection task force.

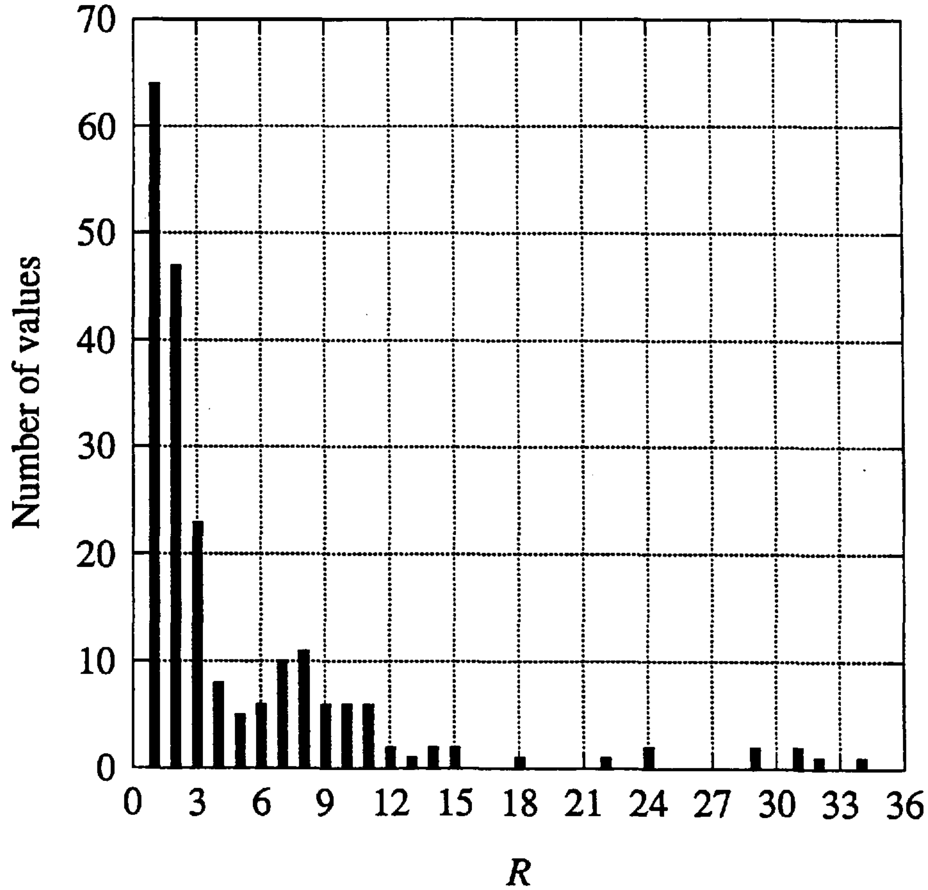

Fig. 8.1
Distribution of R values for oil pipelines

The first utility of the similitude parameter R is to generalize simulation results. A single R value encompasses infinitely many sets of f, L, V_0, a, and D as long as these five variables yield the same R. For example, suppose that two pipelines have identical f, V_0, and a values, and that one of them has a diameter and a length twice that of the other. The transient flow, expressed in terms of scaled variables, should be identical if the scaled boundary conditions imposed are the same. Hence, if we know the transient response of a particular pipeline to an upset, we can predict the transient response of all pipelines with the same R value and subject to the same scaled upset. The prediction is accomplished by simply re-scaling the known and scaled transient response to a particular pipeline. The need to simulate individual cases is eliminated.

The second utility of R is to simplify variable uncertainty analysis. A 5% uncertainty in f and, separately, a 5% uncertainty in V_0 result in the same amount of uncertainty in R. Equal sensitivity of leak detection potential with respect to the uncertainties in f and in V_0 should be expected. In other words, instead of considering the uncertainties in each of the five variables f, L, V_0, a, and D, it is sufficient to consider the uncertainty in R alone.

The R parameter is also useful in quantifying the mass imbalance error of the waterhammer equations. This is addressed in the next section.

8.5 MASS IMBALANCE ERROR OF WATERHAMMER EQUATIONS

The waterhammer equations can be used to compute changes in line fill. However, by neglecting the convective terms, the waterhammer equations introduce a mass imbalance error at steady-state flow. Why this happens and a way to judge the adequacy of the waterhammer equations in computing linefill changes are discussed in this section.

For steady-state flow, there should be no change in local pressure over time and $\partial P/\partial t = 0$. According to Eq. (8.2) and with $V\partial P/\partial x$ dropped, $\partial P/\partial t = 0$ implies $\partial V/\partial x = 0$. Thus the waterhammer equations give identical velocities at the pipe inlet and outlet. Meanwhile, pipe inlet pressure is different and usually higher than outlet pressure. This pressure difference causes the mass density and the pipe cross-sectional area to be different (see Eqs. (3.1), (3.7), and (4.3)) between the inlet and outlet. Since mass flux equals the product of velocity, mass density, and pipe cross-sectional area, identical velocities at the pipe ends result in a mass inflow different from mass outflow. Since in real-time monitoring there is no clear demarcation between steady-state and transient flows, does this mass imbalance error render the waterhammer equations useless in oil pipeline leak detection?

Liou (1993) quantified this mass imbalance error. It was demonstrated that the mass imbalance error depends on the R value of the pipeline and the inlet Mach number $Ma_i = (V/a)_i$. Let U be the mass imbalance error divided by the steady state mass flow rate. It can be shown (Liou (1993)) that

$$U = \frac{1}{\sqrt{1-2RMa_i}} - 1 \tag{8.16}$$

There is uncertainty in U itself. In the context of evaluating the mass imbalance error, the uncertainty in U is caused by uncertainties in f and a. Using the root-sum-square procedure, the total probable error dU as a result of uncertainties df in f and da in a can be expressed as

$$dU = \sqrt{\left(\frac{RMa_i}{(1-2RMa_i)^{1.5}}\frac{df}{f}\right)^2 + \left(\frac{2RMa_i}{(1-2RMa_i)^{1.5}}\frac{da}{a}\right)^2} \tag{8.17}$$

U and its uncertainty are plotted in Fig. 8.2 as a function of Ma_i and R. A 3 percent uncertainty in f and in a are used to establish the band of uncertainty between the dotted lines for each R value. The mass imbalance error is significant when R and/or Ma_i are large. In the same work, Liou demonstrated that this error is significant (as shown in Fig. 8.2) only when the flow is at or near a steady-state. During transients, the magnitude of changes in linefill is large and renders the mass imbalance error insignificant.

With the mass imbalance error quantified and knowing when it is significant, the waterhammer equations are used in estimating linefill changes (Chapter 9), and in transient flow simulation based leak detection (Chapter 10).

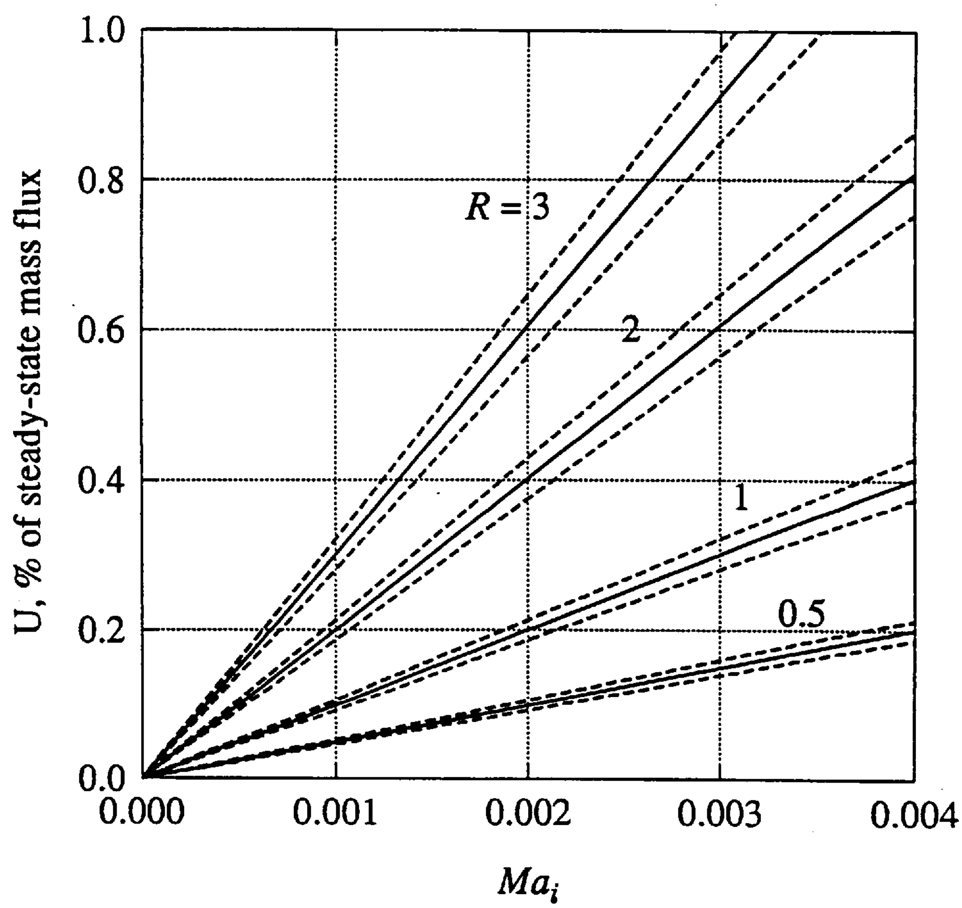

Fig. 8.2
Mass imbalance error of the waterhammer equations

Chapter 9

LINEFILL CORRECTION FOR TRANSIENTS

9.1 ESTIMATION OF THE SEVERITY OF TRANSIENTS

A number of pipeline operations and accidents can cause transients. The severity of the transients varies over a wide range. A measure to characterize the severity of transients in the context of leak detection is needed.

Fig. 9.1 shows a plot of mass flow at the pipe inlet against that at the pipe outlet. Each point on this plot represents a state of flow. Since mass inflow equals mass outflow at steady state, all steady flows must fall on the 45-degree line as shown. A curve, starting and ending at the 45-degree line, represents the transition from one steady flow to another. For example, let A designate an initial steady state. Suppose the operation demands a transition to a new steady state at a lower flow rate (point B). This transition may be accomplished by partially closing a valve at the outlet. If the valve is throttled very very slowly, the trajectory of the transition should follow the 45-degree line AB. If the valve is throttled down a little faster, the transition may be represented by the curve ADB. If the valve is throttled down instantaneously, the transition may look like ACB.

The line segments AB and ACB enclose all possible transitions from A to B for transients caused by flow reduction at the outlet. One "measure" for the severity of transients is the maximum horizontal distance between the 45-degree line and the trajectory of the transients in question over the range of outflow. When this distance is zero, the transient is extremely slow and generates no appreciable change in linefill. When the distance equals the difference between inflow and outflow, the transient is instantaneous and produces the greatest change in linefill.

The same idea works for transients caused by flow increase at the outlet as well as for flow changes initiated at the inlet.

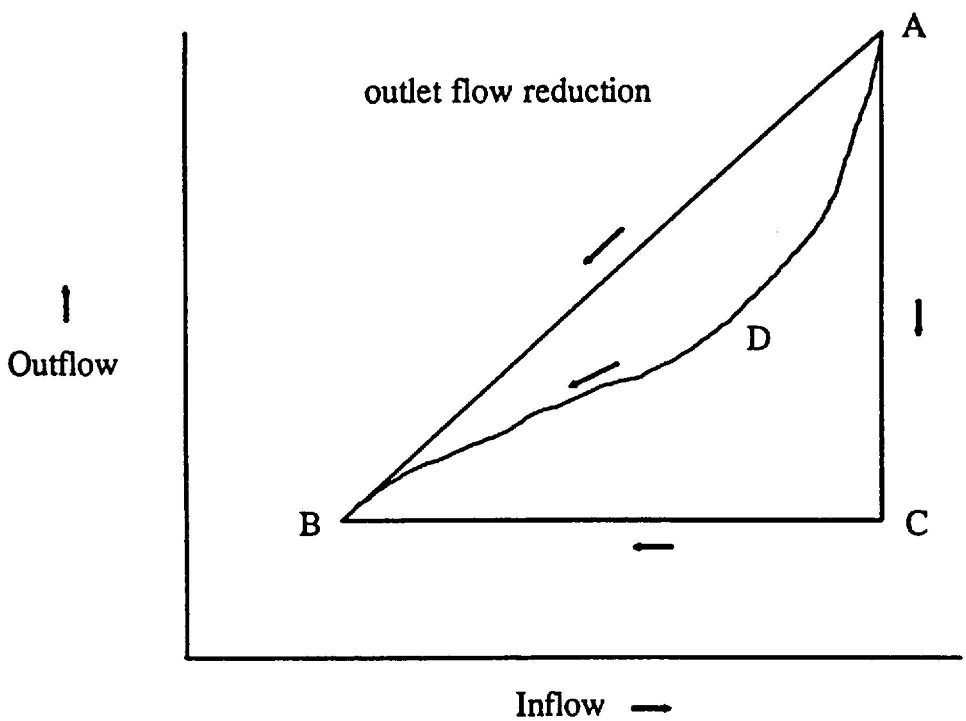

Fig. 9.1
Characterization of the severity of transients

With the motivation given above, transient severity *TSV* is defined as

$$TSV = \frac{MAX(|Q_{in} - Q_{out}|)}{Q_{ref}} \tag{9.1}$$

where the symbol *MAX* is to be understood as the maximum of the absolute value of the difference between Q_{in} and Q_{out} over the entire range of outflow. Q_{ref} is a reference flow, and can be taken as the initial steady-state flow or the flow corresponding to the maximum flow in the pipeline.

Shown in Fig. 9.2 are the trajectories of scaled inflow versus outflow for a series of transients in pipelines with an R value of 2. The transients were created by linearly reducing the outlet flow to zero while holding the inlet head constant. Ten cases with different transition times, the time ussed to ramp the outlet velocity to zero, were used. The inlet flow was calculated by solving Eqs. (8.8) and (8.9) numerically using the method of characteristics (Wylie and Streeter, (1993)). It is seen that the trajectories approach the 45-degree line as the transition period is lengthened.

For each case, the severity of the transient is determined according to Eq. (9.1) during the numerical solution process. It can also be determined graphically from Fig. 9.2 after completing the numerical solutions. The severities for the ten cases are shown in Table 9.1.

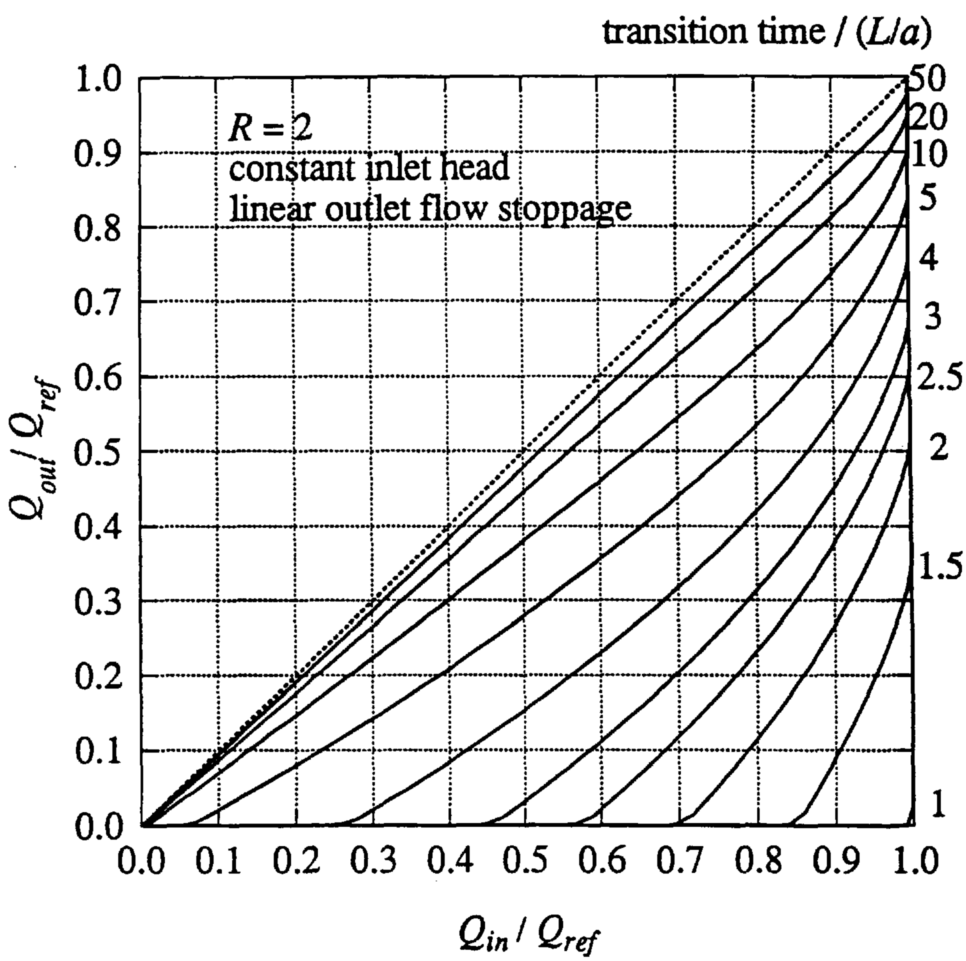

Fig. 9.2
Example of determining the severity of transients

For a specified transient scenario, there is a one-to one correspondance between transient severity and transition time. Thus one may simply use the transition time as an indicator for transient severity. However, when considering different transient scenarios, the transition time is no longer a good indicator. That is, the shortest transition time under one scenario may very likely be different from the shortest transition time under a different scenario. In general, the transition time alone can not characterize transient severity. Pipe system characteristics and boundary conditions must be known as well. The transient severity defined by Eq. (9.1) reflects the transient time as well as the effects of system characteristics and boundary conditions. For a given pipeline system, many transient scenarios can be simulated to establish the relationship between the transition time and the severity of transients.

Table 9.1 Example transients severity versus transition time

transition time/(L/a)	Severity
1	0.99
1.5	0.84
2	0.70
2.5	0.58
3	0.50
4	0.38
5	0.27
10	0.17
20	0.09
50	0.04

9.2 TYPE OF TRANSIENTS CONSIDERED

Three types of flow conditions were considered in this study. They are: steady state, flow increase over time, and flow decrease over time. Constant head at the inlet (or outlet), and variable flow at the outlet (or inlet) with a fixed rate of change over a specified period were used as the boundary conditions for the transient cases.

Only the transients in the pipeline will be modeled. The dynamics of pumps and valves are not modeled. This is consistent with common leak detection practice. Measurements of flow, pressure, and temperature at the ends of a pipe segment are available as the boundary conditions for transient flow modeling. These data completely capture the relevant dynamics of the equipment at an accuracy not achievable by directly modeling the behavior of pumps and valves.

9.3 ADJUSTMENT OF UNCERTAINTY IN LINEFILL CHANGE TO ACCOUNT FOR TRANSIENTS

Recall that the dV_s term in Eq. (5.1) represents a bound for line fill change over a time interval Δt in steady flow. In the mass balance method, changes in linefill by transients are regarded as uncertainties. This view is motivated by the fact that transients may occur unexpectedly and that the transient flow conditions may be unknown. Let dV_t be the uncertainty in the time rate of change in linefill due to transients. Include this uncertainty in dV_s to obtain

$$dV_s = dv_{t+\Delta t} - dv_t + dV_t \tag{9.2}$$

Note that in evaluating the dv terms in Eq. (9.2), the sensitivity coefficients (see Eq. (4.5)) at t and $t+\Delta t$ may be different although the process variable uncertainties dP and dT remain the same over time.

To improve the leak detection potential, dV_t needs to be reduced. One way to do so is to make corrections for linefill change according to pressure change. It can be shown that for a pipe segment with length Δx and over time Δt,

$$[(\rho AV)_{out} - (\rho AV)_{in}] \approx \frac{\Delta P \; \Delta x \; A}{a^2 \; \Delta t} \tag{9.3}$$

where V denotes velocity and ΔP is the average pressure change in Δx over Δt. The approximation becomes better as Δx and Δt become smaller.

A crude correction for linefill change can be made by using the two measured pressures at the pipe ends. To improve the approximation, a third pressure measurement is added at the mid-length of the pipe. This improves the linefill correction by using two shorter pipe segments. If two additional pressure measurements are added at 1/4 and 3/4 length (5 total), even better corrections can be made. This process can continue with more and more pressure measurements. Of course, too many pressure measurements may not be implemented in practice. However, the pressure meassurements can be substituted with a real-time transient flow model.

Define the linefill uncertainty due to transients as the absolute value of the maximum difference between the two sides of Eq. (9.3) during a transient episode

$$dV_t = \sum_{j=1}^{n} \left(MAX \left[(\rho A V)_{out} - (\rho A V)_{in} - \frac{\Delta x}{\Delta t} \sum \frac{\Delta P A}{a^2} \right] / \rho_0 \right) \qquad (9.4)$$

where n = number of pipe segments used in computing dV_t.

Fig. 9.3 shows dV_t, scaled by Q_{ref}, as a function of transient severity for the example in Section 9.1. The values of dV_t were computed from the numerical solutions to Eqs. (8.8) and (8.9) according to Eq. (9.4). When no correction is made, dV_t = MAX ($|Q_{in}$ - $Q_{out}|$), and the result is the 45-degree line. As more pressures are used for linefill correction, dV_t decreases. When the number of pressure measurements approaches the numer of pressure points used in the transient flow model, the uncertainty in linefill change approaches the error of the numerical solution, which can be very small. Therefore, a transient flow model is an effective substitute for additional pressure measurements in computing linefill changes.

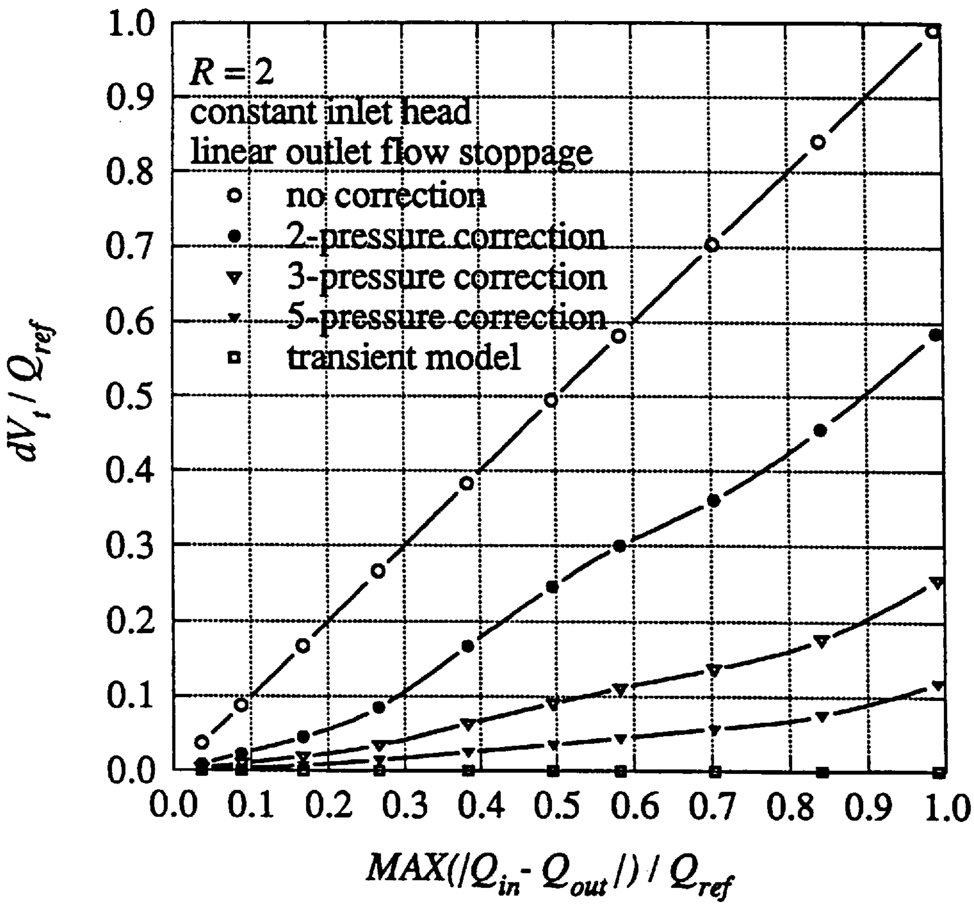

Fig. 9.3
Transients induced linefill uncertainty

9.4 LEAK DETECTION POTENTIAL WITH CORRECTION FOR LINEFILL CHANGE

How the correction for transient-induced linefill change improves the leak detection potential is demonstrated next. Suppose the transient severity is 0.2. From Fig. 9.3, we obtain the dV_t / Q_{ref} values for five cases: no correction for linefill change induced by transients, correction with two pressures, correction with 3 pressures, correction with 5 pressures, and correction with a transients flow model. Then, with Eq. (5.6), the five corresponding leak detection potentials are established and are show in Fig. 9.4. It is seen that the first two corrections significantly improve the leak detectability. The benefit of additional improvements diminishes as the linefill corrections become more refined.

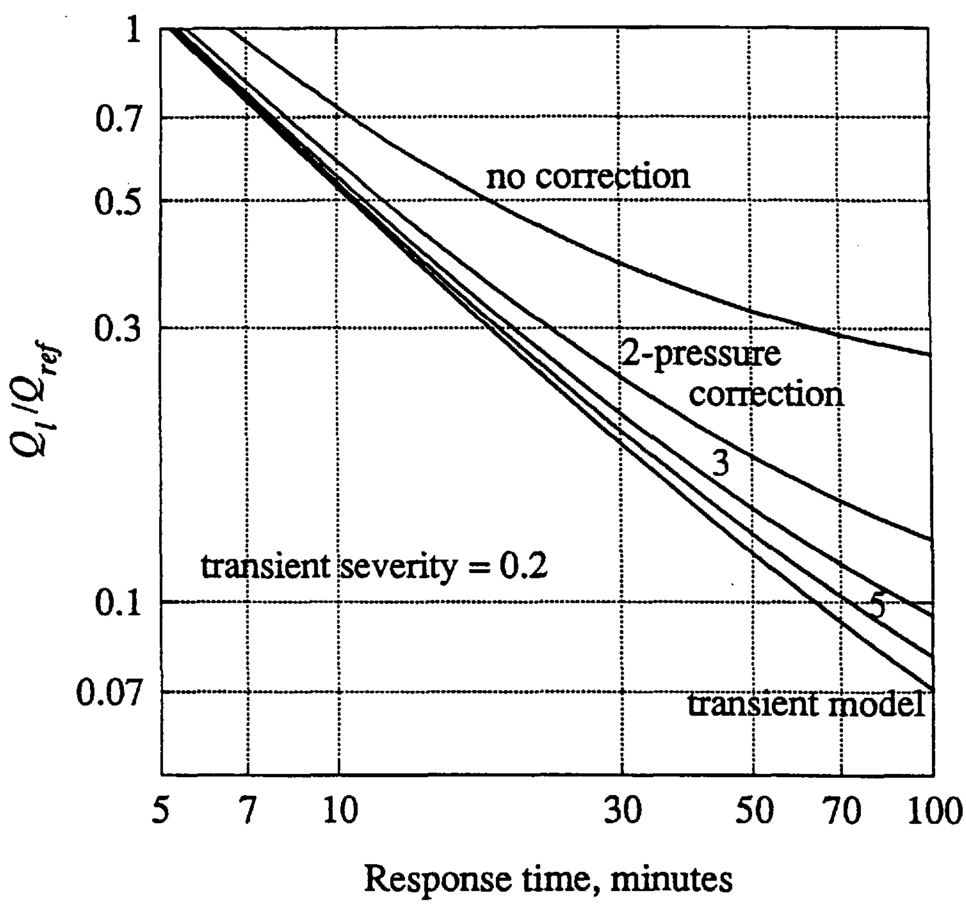

Fig. 9.4
Effects of linefill correction on leak detectability

Note that the demonstrated method of correcting linefill to reduce the uncertainty imposes a larger penalty for detecting smaller leaks (at longer response times). If the transients are known as a function of time, one can make dV_t diminish with time instead of staying at the maximum value as defined in Eq. (9.1). However, transients can be unexpected and not fully defined. To avoid false alarms, one may opt to be conservative by using larger dV_t estimates at the expense of lowering leak detectability. This is the major drawback of the mass balance method. An alternative approach that automatically accounts for line fill change over time will be discussed in Chapter 10.

Because there are infinite numbers of combinations of pipeline configuration, boundary conditions, and transition time, a universal data base for correcting transient-induced linefill changes is not possible. For a given pipeline system, transient flow simulations need to be made for all probable transients in order to establish a figure like Fig. 9.3, which provides a basis for correcting transients-induced linefill uncertainty. The rationale and the example provided in this chapter show how such corrections can be made.

Chapter 10

LEAK DETECTION BY MASS CONSERVATION AND LAW OF MOTION

10.1 BASIS OF LEAK DETECTION BY TRANSIENT FLOW SIMULATIONS

Shown in Fig. 10.1 is a time versus distance plane on which the numerical solution to the governing eqquations of transient flow can be carried out. Suppose that the pressure and flow measurements at pipe ends are measured in real-time by a SCADA system. Using the measured pressure and flow at the inlet between time t_1 and t_4, the pressure and flow at the outlet between time t_2 and t_3 can be calculated. Thus there are two sets of pressure and flow data at the outlet between t_2 and t_3, one measured and one calculated. In a similar manner, there are two sets of pressure and flow data at the inlet between t_2 and t_3.

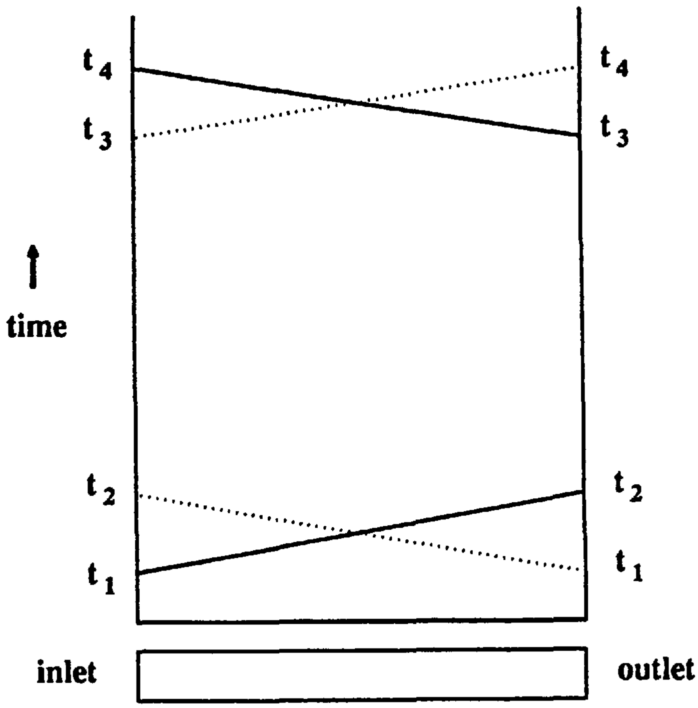

Fig. 10.1
Wave propagations and computations in the *x-t* plane

The pipeline is assumed to be intact in the calculations. The calculated pressure and flow should match the measured ones if the pipe is indeed intact. Otherwise, a leak is suspected. The logic used here is that a leak generates its own transients or signals. The leak-caused pressure and flow waves propagate to the pipe ends and imprint the leak signal in the measured data. When the measured data with the imprinted leak signal is used in the computations that assume no leak exists, the calculated pressure and flow at the pipe ends are unreal and diverge from the measured values. Discrepancy patterns between the measured and the calculated values emerge. A leak is declared once a discrepancy pattern specific to a leak is recognized. Further explanation of this approach can be found in Liou (1991). The finite difference equations used to implement this idea and some laboratory test results can be found in Liou (1990).

The ability to recognize the leak discrepancy pattern is hampered by uncertainties in measured data and in system parameters. A leak can be detected reliably only if the leak discrepancy pattern can be recognized amongst noise and bias errors.

The response time in leak detection by transient flow simulation is the time needed for the acoustic waves to travel from leak location to pressure and flow measurement sensors. This travel time is independent of the size of the leak. In leak detection by mass balance (Chapters 4 and 5), the response time is the sum of the acoustic wave travel time and the time interval over which one can discern a change in linefill amongst uncertainties. The length of the time interval needed to overcome uncertainties in linefill change depends on the size of the leak. It is very long for small leaks and makes the wave travel time insignificant. In general, leak detection by transient flow simulations is much more rapid than leak detection by mass balance.

10.2 GENERATING DISCREPANCY TRACES

Two transient flow models are developed for this purpose. The first one is a system model where a leak can be imposed at any computational node at any time. This model is driven by a specified flow (or head) at the inlet and a specified head(or flow) at the outlet. Inlet head (or flow) and outlet flow (or head) are then calculated over time. The head and flow pairs at the pipe ends are regarded as the "measured" values from an imaginary pipeline.

The second model is a leak detector. The computations in the detector assume the pipe to be intact. The "measured" inlet head and flow are used to drive the detector to compute head and flow at the outlet. In a second pass, the detector is driven by the "measured" head and flow at the outlet to compute the head and flow at the inlet.

After the second pass of the detector, eight traces exist: measured and calculated inlet head, measured and calculated inlet flow, measured and calculated outlet head, and measured and calculated outlet flow. From these, four discrepancy traces (measured value minus calculated value) for the inlet head, inlet flow, outlet head, and outlet flow are established.

10.3 SIMULATING UNCERTAINTIES IN MEASUREMENTS AND IN SYSTEM VARIABLES

Before searching for a leak discrepancy pattern, the measured data are processed by adding bias and noise, if needed. A normalized random number generator was used to create the noise.

The system parameters include pipe length, diameter, reference velocity, friction factor, and wave speed. Because of the similitude parameter R (see Eq. (8.15)), these five parameters need not be dealt with individually. It is sufficient to consider the uncertainty in R only. An error in R can be attributed to an error in a single variable, or be distributed among several or all the five parameters as long as the combined effect is the same. The parameter R offers considerable simplification in the variable uncertainty analysis.

10.4 DISCREPANCY PATTERNS SPECIFIC TO LEAK

An example is used to show discrepancy patterns that are specific to the onset of a leak. Since the advantage of leak detection by transient flow simulation is the ability to account for linefill changes, a leak is imposed during a transient flow period. Fig. 10.2 shows a set of representative discrepancy traces. The horizontal axis represent dimensionless time, which is time in seconds divided by L/a. The vertical axis represents measured minus calculated values, divided by the potential surge H_0 (Eq. (8.12)) for head discrepancies and by Q_{ref} for flow discrepancies. No bias nor noise in the head and flow measurements is introduced. Both are important and will be addressed in Chapter 11.

In Fig. 10.2, the flow is initially at steady-state and there is no discrepancy between the measured and the calculated head and flow at either end of the pipe. A 20% error in R is then imposed in the detector. The purpose of imposing the R error is to investigate the effect of variable uncertainties on leak detectability. The *R* error upsets the computed head and flow and discrepancies develop. After an initial excursion, the discrepancy traces become constant. These *R* error-generated discrepancies are not caused by physical disturbances but are unavoidable in this investigation. However, after the traces level out, the picture presented resembles a leak detector that is out of tune. A flow stoppage is then initiated and completed in 60 seconds. Except for the initial excursion in the inlet flow discrepancy, all four traces are moving toward zero. This is so because the lower velocity (due to flow stoppage) reduces the effect of the *R* error. While the pressure waves are propagating in the pipeline, a 10% leak is imposed at the mid-length of the pipeline. A third set of discrepancy patterns emerges.

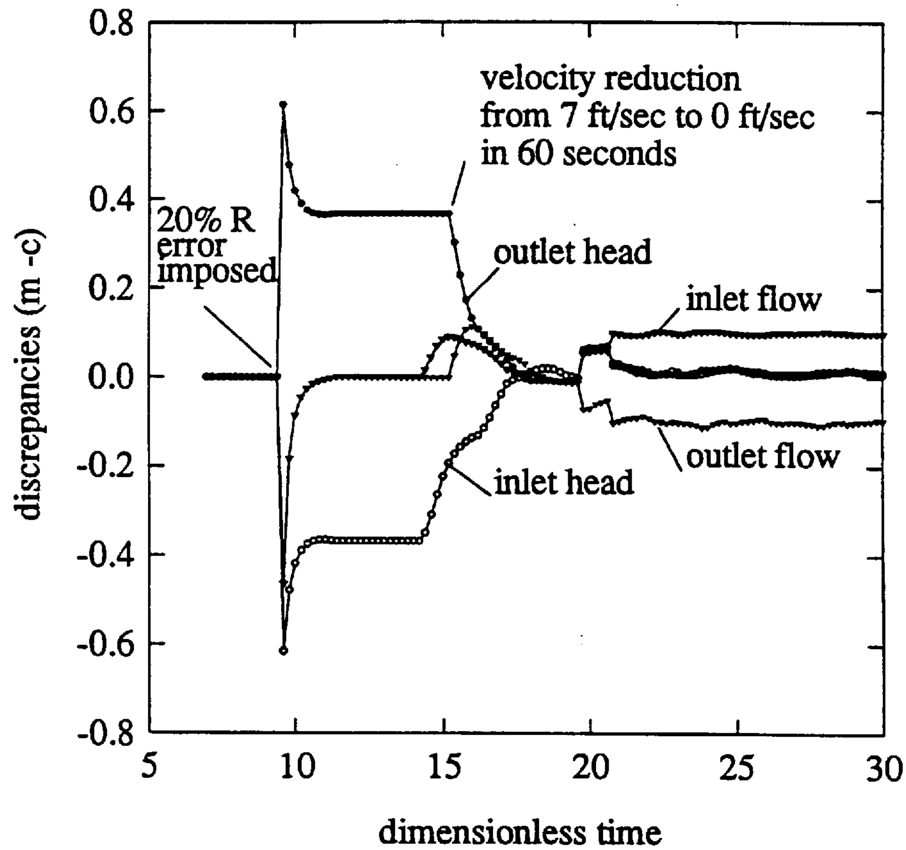

Fig. 10.2
Example discrepancy pattern specific to the onset of a leak

The leak induced discrepancies are characterized by an immediate increase (more positive) in the discrepancies (measured - calculated) for inlet head, outlet head, and inlet flow. Simultaneously, there is an immediate decrease (more negative) in the discrepancy in the outlet flow. The discrepancies persist for several time steps, depending on the leak location and the number of computational reaches used in the detector. In the example shown, 10 computational reaches were used and the discrepancies stay for 5 steps. Afterwards, the head discrepancies diminish while the flow discrepancies persist.

The discrepancy pattern indicates the location of the leak as well. For the example used above, had the leak occurred at two computational reaches from the inlet instead of at the mid-length, the starting time for the discrepancy traces at the inlet would be different from those at the outlet. In addition, the inlet discrepancies would persist for only 2 steps while the outlet ones would persist for 8 steps. The discrepancy patterns just described result from the propagation nature of the transient flow equations (Eqs. (8.1) and (8.2)).

Discrepancy patterns that match the following four conditions are considered leak discrepancy patterns (also see Section 11.5).

1. Immediate and simultaneous rise in the discrepancy (measured value minus calculated value) of inlet head and inlet flow.

2. Immediate rise in the discrepancy of outlet head. Immediate and simultaneous fall in the discrepancy of outlet flow.

3. The difference in the timing of the sudden changes in discrepancy traces at the pipe ends must indicate the location of the leak, and

4. The sum of the number of consecutive time steps with discrepancies at the pipe ends equals the number of computational reaches used in the detector.

The leak discrepancy patterns were investigated for negative errors in R instead of positive ones, for steady state flow, for transients with inlet flow increase instead of outlet flow decrease, and for various leak locations and timing. All cases yield the same type of leak discrepancy patterns.

Satisfying any subset of the above four conditions is an indication of a leak occurrence. For example, one may choose to impose the four conditions on flow only. However, for reliability, all four conditions for both head and flow are required to be met before a leak is announced.

How likely is it that the leak discrepancy patterns will occur by accident? Without imposing a leak, simulations were made using R errors from 0 to 50%, and noise from 0 to 5%. Many combinations of error, flow noise, and head noise (see Section 10.6) were used in an attempt to "trick" the detector into triggering a false alarm. At no point was the detector fooled - it never detected a leak when none existed. It is believed that the discrepancy pattern described is specific to leaks, and that no realistic combination of variable uncertainties and data noise is likely to produce a similar pattern.

10.5 DEGRADATION OF LEAK DETECTABILITY DUE TO UNCERTAINTIES IN SYSTEM VARIABLES

The influence of uncertainty in R on leak detectability was investigated for three types of flow: steady-state, flow increase, and flow stoppage. Fig. 10.3 shows typical results for systems with an R value of 1.83. One realization of this R is a 2 ft diameter, 40 mile long pipeline with a wave speed of 3417 ft/sec and a reference velocity of 7 ft/sec. The pipeline carries gasoline and has a Darcy-Weisbach friction factor of 0.017. In the flow increase case, the inlet velocity was increased linearly from 2 ft/sec to 7 ft/sec in 600 seconds. For the flow stoppage case, the flow was cut off at the outlet instantaneously. In generating the "measured data", leaks with different magnitudes were imposed at the mid-length of the pipeline.

The results indicate that the leak detectability degrades with greater uncertainties in R. Leak detectability is the greatest for steady-state flow, where the occurrence of very small leaks can be detected despite large uncertainty in R.

10.6 DEGRADATION OF LEAK DETECTABILITY DUE TO ATTENUATION

The four conditions of Section 10.4 result from the wave propagation nature of transient flow. For large R, the propagation of the leak signal is significantly attenuated. Leak detectability degrades when the leak signal is smeared through attenuation.

The dependence of leak detectability on the magnitude of R itself is shown in Fig. 10.4 for a flow increase transient, and in Fig. 10.5 for a flow reduction transient. As in Fig. 10.3, the "measured" data used to generate Figs. 10.4 and 10.5 had leaks imposed at the mid-length of a pipeline. Two trends are apparent. First, the leak detectability decreases for greater R. In other words, to detect the occurrence of a leak with a given size, pipelines with a lower R value can tolerate a greater uncertainty in

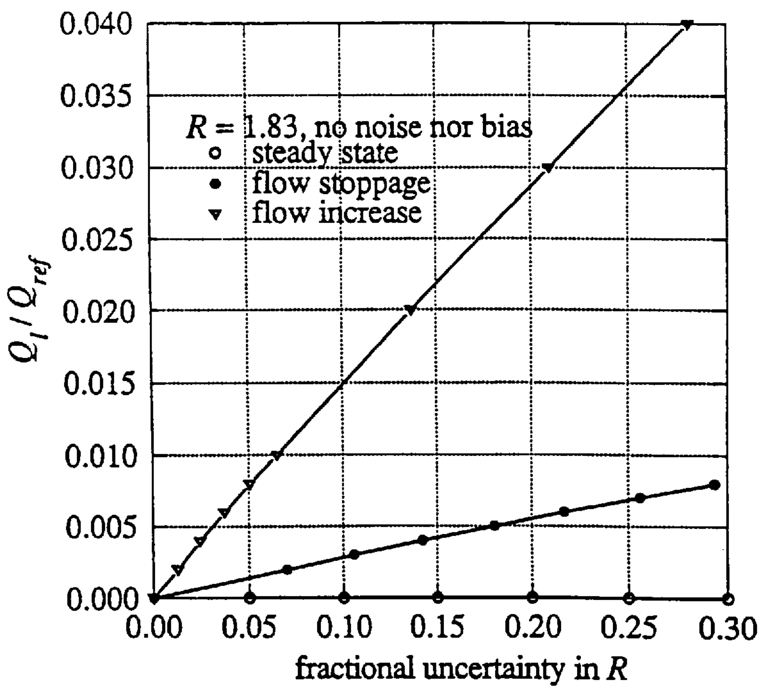

Fig. 10.3
Example leak detectability for different states of flow

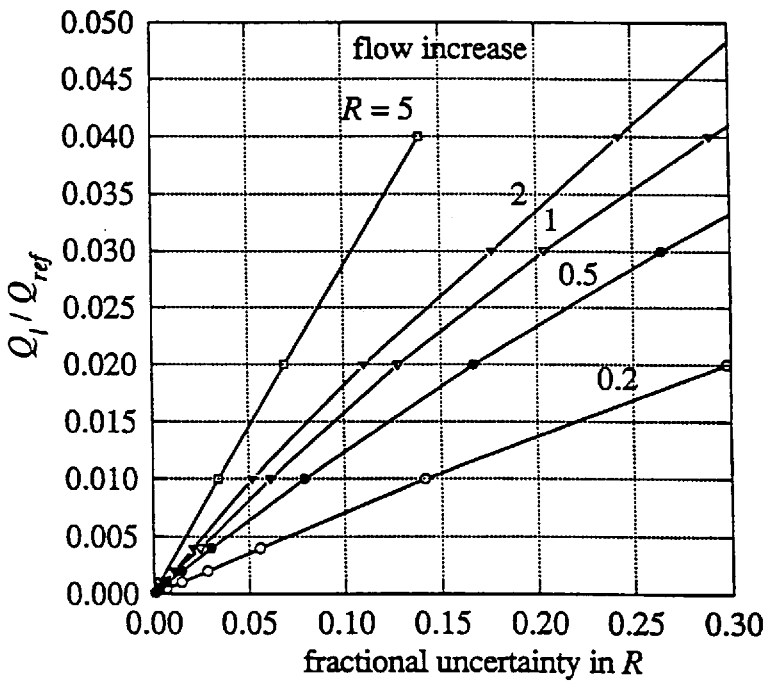

Fig. 10.4
Leak detectability as a function of R values. Leak occurs in flow increase transients

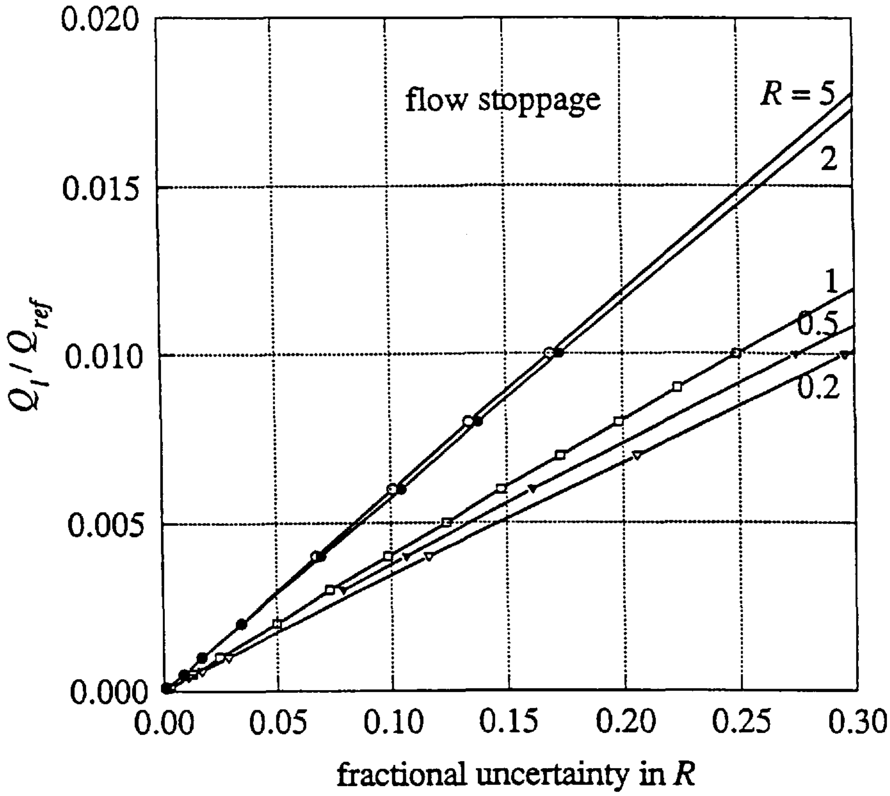

Fig. 10.5
Leak detectability as a function of R values. Leak occurs in flow stoppage transients

R. Second, leak detectability is greater for transients that create lower velocity. The latter trend is due to the fact that lower velocity diminishes the importance of frictional resistance to flow (see Eq. (8.13)). Consequently, the importance of R and its uncertainty is diminished.

Actual data noise was encountered during field trials (see Chapter 11). It was found that the leak discrepancy patterns becomes increasingly more difficult to recognize as R becomes greater. As a result, the highest R values shown in Figs. 10.4 and 10.5 are 5 while greater R values may be encountered (see Fig. 8.1). The cause and a modification to the leak discrepancy pattern for high R values are addressed in Sections 11.3 and 11.4.

An example of the dependency of leak detectability on leak location is shown in Fig. 10.6. The pipeline system is the same as the one used for Fig. 10.3. The leak detectability curves for leaks imposed at 10, 30, and 50 percent of the pipe length from

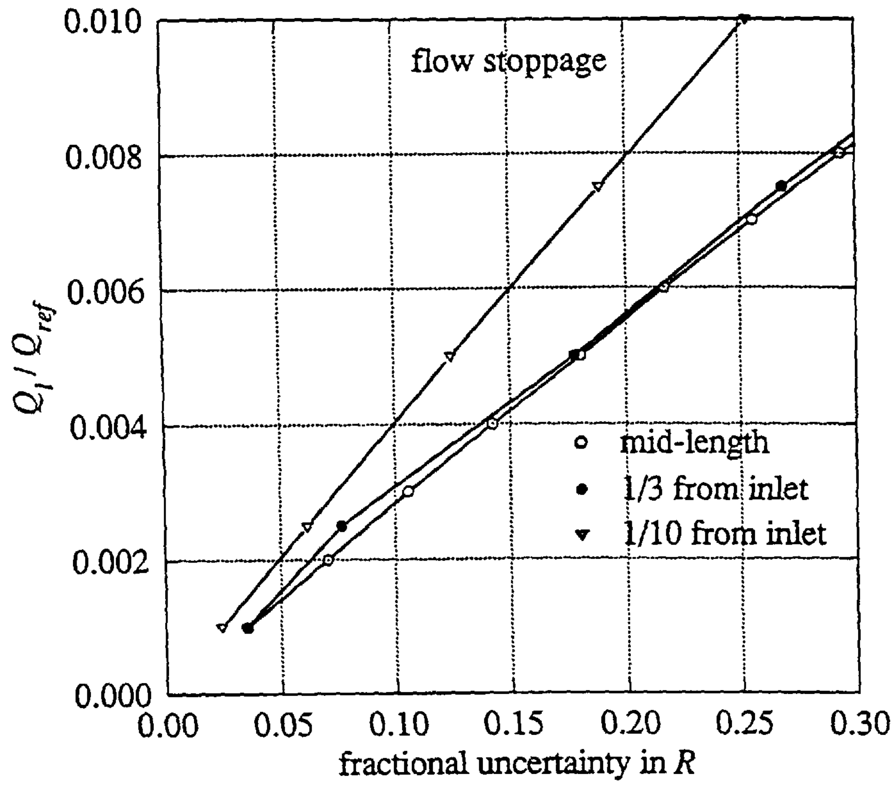

Fig. 10.6
Effect of leak location on leak detectability

the inlet are presented. It is seen that the leak detectability is greater for leaks occurring near the middle of the pipeline. The reason for this trend is that the closer a leak occurs to one end of the pipeline, the longer the leak signal has to travel to reach the opposite end, resulting in more attenuation and smearing of the leak signal. Consequently, the last condition becomes more difficult to satisfy and leak detectability is degraded.

10.7 DEGRADATION OF LEAK DETECTABILITY BY DATA NOISE AND BIAS

The recognition of the leak discrepancy pattern may be hampered by noise in the head and flow measurements. To see how noise affects leak detectability, noise was imposed to the "measured" head and flow before they were used to drive the detector. A normalized random number generator was used to produce a sequence of noise which was added to the "measured" data points over time. The minimum detectable leak versus R uncertainty calculations were repeated many times, using a different seed in the random number generator each time, until the average minimum detectable leak versus R error curve stabilized. Fig. 10.7 shows the results for the flow increase case. Here a mean of zero (i.e. no bias) and a standard deviation of 0.083 percent of the final steady state flow were used for the flow noise. No head noise was imposed for this illustration. Comparing with the flow increase curve in Fig. 10.3, it is seen that the flow noise downgraded the leak detectability by about 4 percent over the range of R errors shown. Further discussion on the effect of noise is given in Section 11.3.

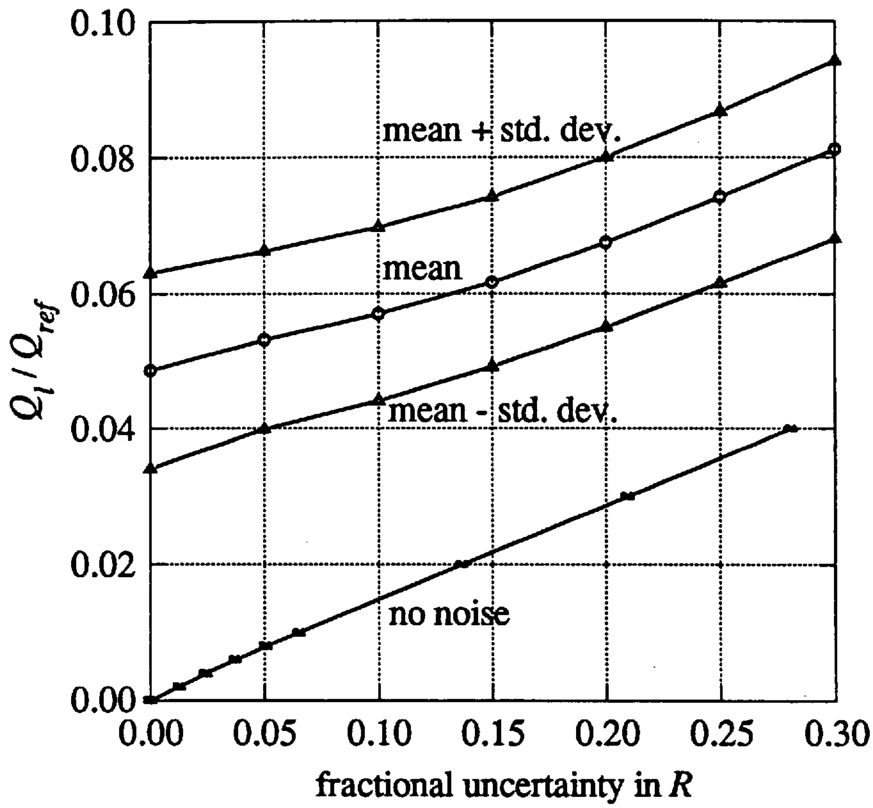

Fig. 10.7
Example degradation of leak detectability caused by flow noise

The effect of flow bias on leak detectability was investigated using a non-zero mean in the noise generation. Results indicate that leak detectability is not sensitive to bias errors.

Chapter 11

FIELD TRIALS - TRANSIENT FLOW

11.1 DESCRIPTION OF FACILITY AND TEST DATA

Field leak tests during transients were conducted on the 140 mile products pipeline described in Section 6.1. Simulated leaks were diverted from the pipeline 61 miles downstream from the inlet. Three centrifugal pumps were running in series at the inlet. A regulator was used at the receiving terminal to maintain an outlet pressure of approximately 175 psig. Transients were created by pump stops and starts. About 8.7 hours of uninterrupted data on pressure, temperature, and flow were collected by a SCADA system at a fixed interval of 15 seconds.

Pressures were measured at the inlet, at the leak site, at an intermediate location between the leak site and the receiving terminal, and at the receiving terminal. The performance specifications of the pressure transmitters used are described in Section 6.1. Fig. 11.1 shows the recorded pressure traces.

Volumetric flow rates were measured at the upstream side of the pumps by a turbine flow meter, and at the receiving terminal by a positive displacement meter. As discussed in Section 6.1, the performance specifications of these meters are not completely known, and a nonrepeatability of 0.15 percent of reading was assumed. Fig. 11.2 shows the recorded flow traces.

Because of the large scale used for the vertical axes in Figs. 11.1 and 11.2, the recorded pressure and flow traces appear to be smooth. Closer examination shows that the measured data are quite noisy (see Fig. 6.3). The regulator-caused pressure and flow oscillations at the receiving end are apparent even in the large-scale plots.

The measured inlet temperature essentially stayed at 65.9°F. The measured outlet temperature varied from 51.5°F at the beginning of the tests to 51.3°F toward the end of the tests. The nonrepeatability of the temperature measurements are described in Section 6.1. In leak detection by transient flow simulation, temperature is not directly involved and thus will not be discussed further.

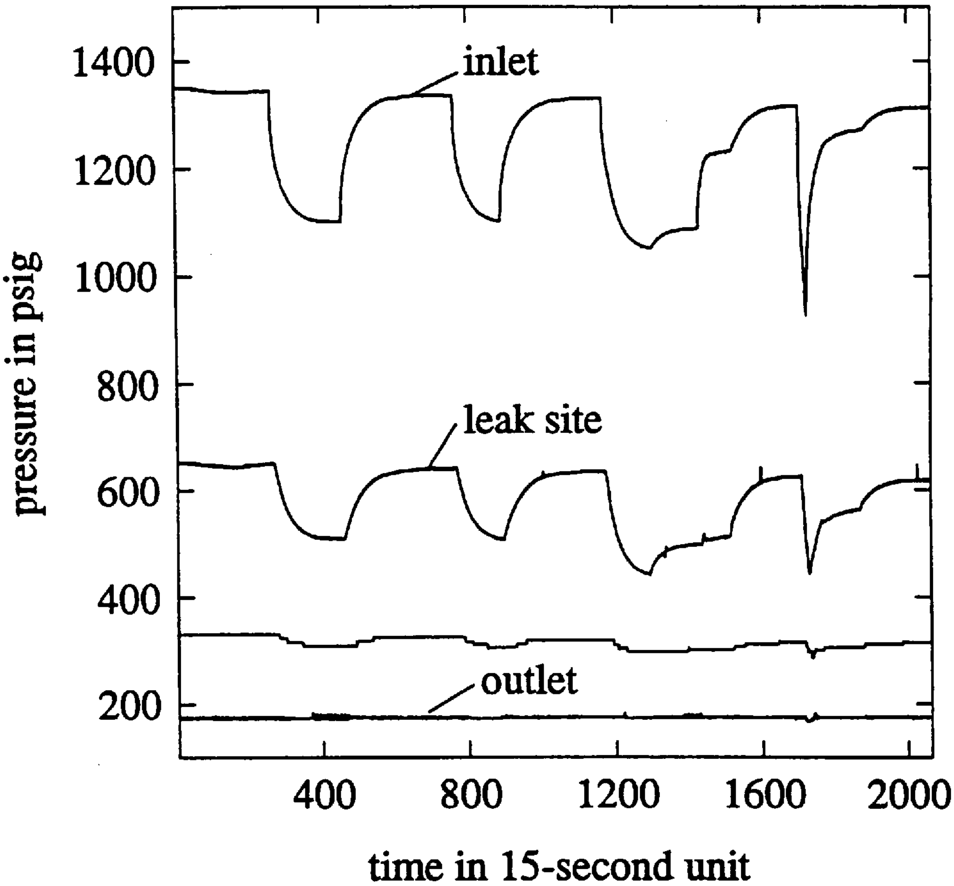

Fig. 11.1
Recorded pressure traces

The conditions imposed on the tests are summarized in Table 11.1.

Table 11.1 Summary of Tests

Test Case	Flow(bbl/hr) (pre-test)	Leak Size (% of flow)	state of flow and leak timing
D1	654	1.14	leak imposed during steady-state
E1	656	0.91	leak imposed 5 min after stopping pump 2
F1	510	1.05	leak imposed 5 min. after starting pump 2
G1	658	0.52	leak imposed during steady-state
H1	658	0.50	leak imposed 5 min. after stopping pump 2
I1	511	0.59	leak imposed 5 min. after starting pump 2
B2	660	16.0	leak imposed 3 min. after stopping pump 2
C1	520	28.0	leak imposed 3 min. after starting pump 2

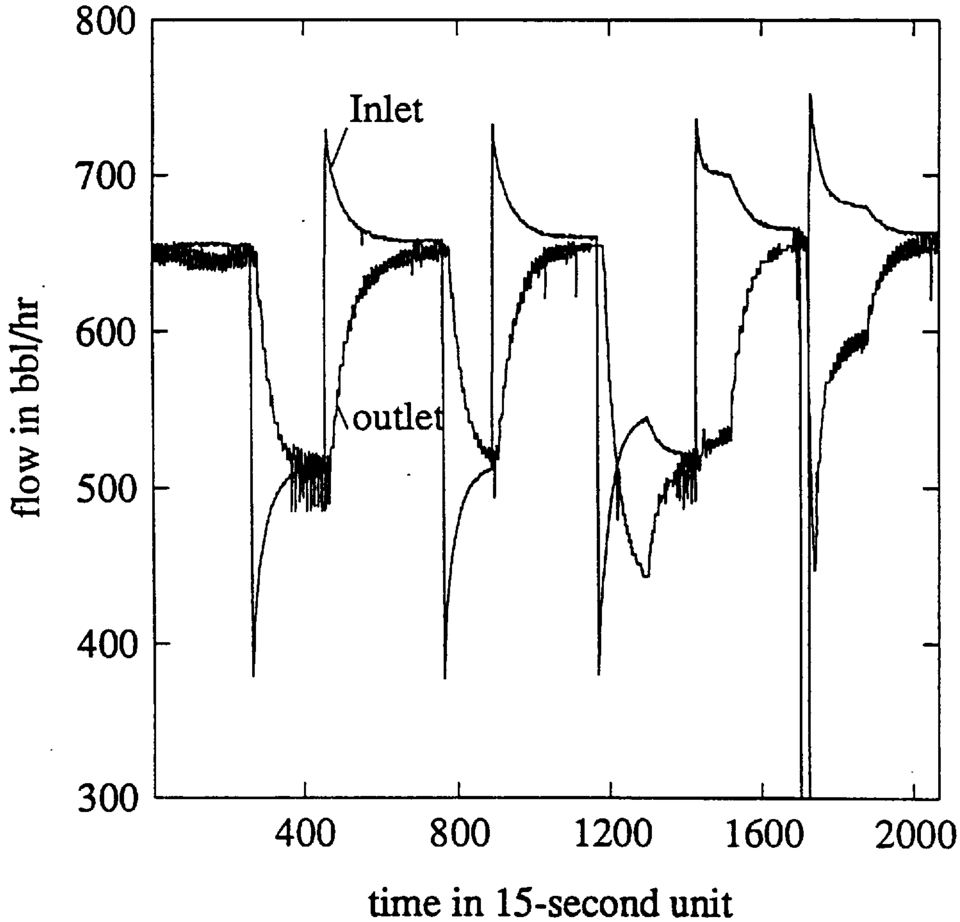

Fig. 11.2
Recorded flow traces

Five product batches existed in the pipeline during tests. Starting from the inlet, the product gravities in °API were 69.2, 58.2, 61.6, 40.9, and 34.9. The relative sizes in % volume, starting from the inlet, were 2.7, 12.7, 63.3, 12.7, and 8.7 at the beginning of the tests, and changed to 10.1, 12.5, 62.6, 12.5, and 2.3 toward the end of the tests.

11.2 GENERAL APPROACH

The pipeline has many diameter changes (see Fig. 6.1) and conveys five batches of liquids as noted above. Using mass-weighted averages, the prototype pipeline was modeled as a pipeline with a constant diameter carrying a single batch of liquid. Tuning of the model was accomplished by running the system model described in

Section 10.2. The inlet flow and the outlet head were used to drive the system model which included the imposed leak. The Darcy-Weisbach friction factor and the wave speed were varied and the computed inlet pressure and outlet flow were compared with the measured data. The friction factor and the wave speed that best matched the measured data were taken as the "correct" values.

Using the "correct" friction factor and the wave speed, the detector was then executed in the manner described in Section 10.2. The detector generated discrepancy traces of inlet head, inlet flow, outlet head, and outlet flow. These traces were then analyzed to see if a leak discrepancy pattern could be recognized.

In testing the field data, it was discovered that the similitude parameter R of the pipeline system being tested was high. The noise in the measured data masked the distinct features of the leak discrepancy such that condition number 4 (see Section 10.4) could not be satisfied even for large leaks. Consequently, a less stringent leak discrepancy pattern was tested for reliability and then used to detect and to locate the onset of the imposed leaks.

11.3 EFFECTS OF DATA NOISE ON LEAK DETECTABILITY

The term "noise" used in this study refers to that part of a signal which does not represent the quantity being measured. Fluctuations around a fixed or moving mean are considered noise. As seen previously in Figs. 6.3 and 6.6, noise typically exists in measured data.

Noise, when mistaken as part of the measured data, gets amplified in the detector described in Section 10.2. Fig. 10.1 is used to explain this noise amplification. Suppose that a perturbation occurs in the measured pressure at the pipe inlet at time t_4. The algorithm in the detector program views these perturbations as physical and proceeds to compute the pressure and the flow at the pipeline outlet at an earlier time t_3. Because the frictional flow resistance attenuates disturbances over time, the pressure and the flow perturbations at the outlet at t_3 must be greater in order to survive the attenuation and appear later at the inlet.

This amplification of perturbations back in time is physical and real if the perturbation is of physical origin. Problems arise when the perturbation is due to noise. The situation is worse when noise exists in both the pressure and the flow data. Noise makes the pressure and flow data inconsistent to each other, and causes immediate and non-physical changes in pressure and flow at the computational nodes adjacent to the pipe inlet. These changes are then amplified back in time and appear at the pipe outlet as described above.

Similar amplifications of noise contained in the pressure and flow data at the pipe outlet make the computed pressure and flow at the inlet fluctuate with large amplitude and in a chaotic fashion. Meanwhile, the measured pressure and flow data at the pipe ends remain at their original and physical magnitude. In forming the discrepancy traces, the measured data may be overshadowed by the computed data with amplified noise. When this occurs, the leak discrepancy patterns described in Section 10.4 may not be recognizable.

The detrimental effect of data noise depends on the level of noise itself and on the extent of attenuation in the pipeline. The latter can be characterized by the similitude parameter R and by the type of transients (i.e. flow increase versus flow decrease). To achieve the same leak detectability, noisier data demands a smaller R value, and thus limits the spacing between measurement stations.

11.4 FILTERING OF MEASURED DATA

A digital low-pass filter, described in Doebelin (1983), may be used to reject some of the noise contained in the measured data. The filter is expressed as

$$N_o[mT] = N_o[(m-1)T] + \frac{T}{\tau}(N_i[(m-1)T] - N_o[(m-1)T]) \qquad (11.1)$$

where T is data sampling interval, which is 15 seconds in this study. The integer m denotes the order of data points over time. The sequence of numbers $N_i[mT]$ is the original data, and the number sequence $N_o[mT]$ is the filtered data. τ is the time constant of the filter in seconds.

The filter was used only when the leak could not be detected using the original measured data. When used, the value of τ was increased gradually from 15 seconds until satisfactory results were obtained. All four measured data groups: inlet flow, inlet pressure, outlet flow, and outlet pressure were filtered using the same τ.

11.5 MODIFIED LEAK DISCREPANCY PATTERN WHEN R IS HIGH

The R parameter for the tests varied from 4.5 to 6.5, depending on the initial flow rate and frictional pressure drop. With this high R value and with noisy pressure and flow data (see Fig. 6.3), the fourth condition of Section 10.4 could not be satisfied even for large leaks (test C1). Consequently, the fourth condition was modified. The four conditions are restated below:

1. Immediate and simultaneous rise in the discrepancy (measured - calculated) of inlet head and inlet flow.

2. Immediate rise in the discrepancy of outlet head. Immediate and simultaneous fall in the discrepancy of outlet flow.

3. The difference in the timing of the sudden changes in discrepancy traces at the pipe ends must indicate the location of the leak, and

4. The appropriate rise and fall of all four discrepancy traces must persist for a number of consecutive time steps.

The first three conditions are the same as before. The last one is less stringent than condition 4 stated in Section 10.4. The number of consecutive time steps to be used is not known a priori. Condition four allows more than one discrepancy to qualify as a leak discrepancy pattern. However, reliability can be improved by using an increasingly larger number of consecutive steps. An example is presented later (see Table 11.2).

One consequence of relaxing the fourth condition of Section 10.4 is an increase in the response time needed to detect the occurrence of the leak. Another consequence is that the minimum detectable leak size gets smaller as the leak occurs closer to the pipe ends.

11.6 RESULTS

The discrepancy pattern for test B2 (see Table 11.1) is shown in Fig. 11.3. This case has an *R* value of 5.84. The transients for this test were created by stopping one of the three pumps. The transients caused a flow decrease and thus somewhat diminished the effect of the high *R* value. The 16 percent leak was detected and located without any data filtering.

A close examination of Fig. 11.3 reveals that there are many sets of discrepancy patterns that satisfy the four conditions. They occur at different times and indicate different leak locations. Which one is real? A procedure was devised to eliminate false alarms, if possible, so that a leak can be detected with certainty.

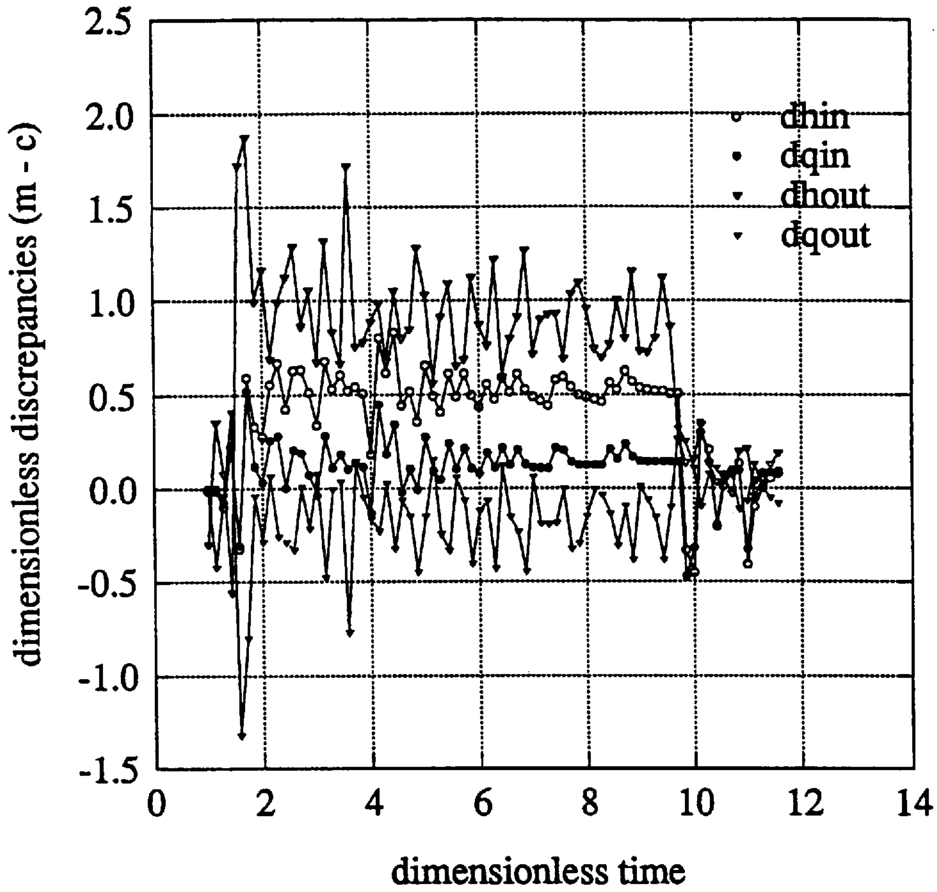

Fig. 11.3
Discrepancy traces indicating a 16.4 % leak during pump shut-down transients -test B2.

The real leak discrepancy pattern is separated from the false ones by increasing the number of consecutive time steps considered (see condition 4 of Section 11.4). Table 11.2 illustrates this process. The first column indicates the location of suspected leaks. Fourteen computational reaches and fifteen computational nodes were used in the detector. Besides the two boundary nodes, a leak can occur at any of the remaining thirteen nodes. The zero in column 1 indicates that a suspected leak (or leaks) occured at mid-length. The minus one indicates a leak (or leaks) occured at one computational reach upstream from the mid-length. The plus one indicates a leak (or leaks) occured at one computational reach downstream from the mid-length. The imposed leaks in the field test were positioned between location -1 and -2. The frequency columns indicate the number of qualified discrepancies at the locations specified in the first column. For each pattern, the sum of the absolute values of the four discrepancies (inlet head, inlet flow, outlet head, outlet flow) are computed. At each location, the number of such sums is shown under the frequency column. At each location, the maximum amongst the sums is shown under the "max" column. Many discrepancy patterns qualify if only one time step is required, and would result in many false leak alarms. The number of false alarms is reduced considerably if four consecutive time steps are required. The number of qualified patterns continue to decrease as more consecutive steps are used. Eventually, if the leak is detectable, only one pattern can qualify as the leak discrepancy pattern. For test B2, thirty one points were used to eliminate false alarms. The persisting pattern indicated the correct leak location and timing.

Table 11.2 Eliminating false patterns by increasing number of consecutive time steps (test B2, data not filtered)

Location indicator	1 Step		4 Steps		31 Steps	
	freq.	max	freq.	max	freq.	max
-6	11	2.24	3	1.28	0	0
-5	10	4.15	2	0.85	0	0
-4	15	4.51	2	1.30	0	0
-3	5	1.00	1	0.38	0	0
-2	13	1.69	1	1.00	0	0
-1	13	5.76	2	5.76	1	5.76
0	12	1.85	1	0.36	0	0
1	13	4.64	1	0.70	0	0
2	12	2.16	4	1.92	0	0
3	12	2.51	2	1.17	0	0
4	12	2.37	1	2.37	0	0
5	14	1.94	1	0.74	0	0
6	12	1.95	1	1.35	0	0

The effect of uncertainty in R for test B2 was investigated by recreating discrepancy traces using different R values in the detector. Variations with ±2.5 percent, ±5 percent, ±10 percent, and ±30 percent of the "correct" R value were used. In all cases, the leak was detected and located without resorting to data filtering.

Using the same process for test C1, the 28 percent leak imposed during a pump start-up transient was detected and located correctly. The R value for this test is 4.47, which is less then the 5.84 for test B2. However, the increasing velocity during transients made the noise amplification more significant. Consequently, data filtering was necessary.

Fig. 11.4 shows the discrepancy traces wothout(left) and with(right) data filtering. Both figures give an overall impression that definite patterns exist. However, the discrepancies without data filtering did not qualify. The leak was not detected because the discrepancy in the outlet flow did not stay consistently low. After filtering of the measured data, this problem was removed and the leak was detected and located correctly.

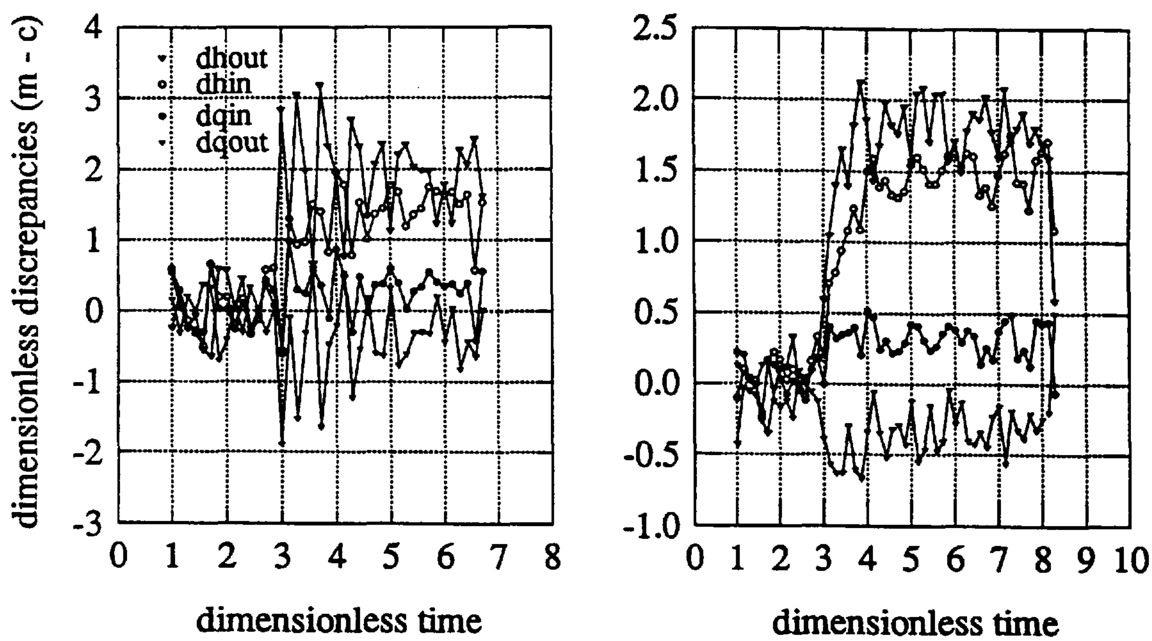

Fig. 11.4
Discrepancy traces indicating a 28% leak during a pump start-up transient - test B2.
left: without data filtering. right: data filtering with a time constant of 60 seconds

Fig. 11.5 shows the effect of uncertainty in *R*. The discrepancies in the left were obtained using the best estimation for *R*, and those in the right were obtained with an *R* value 10 percent larger. With data filtering, the leak was detected and located correctly.

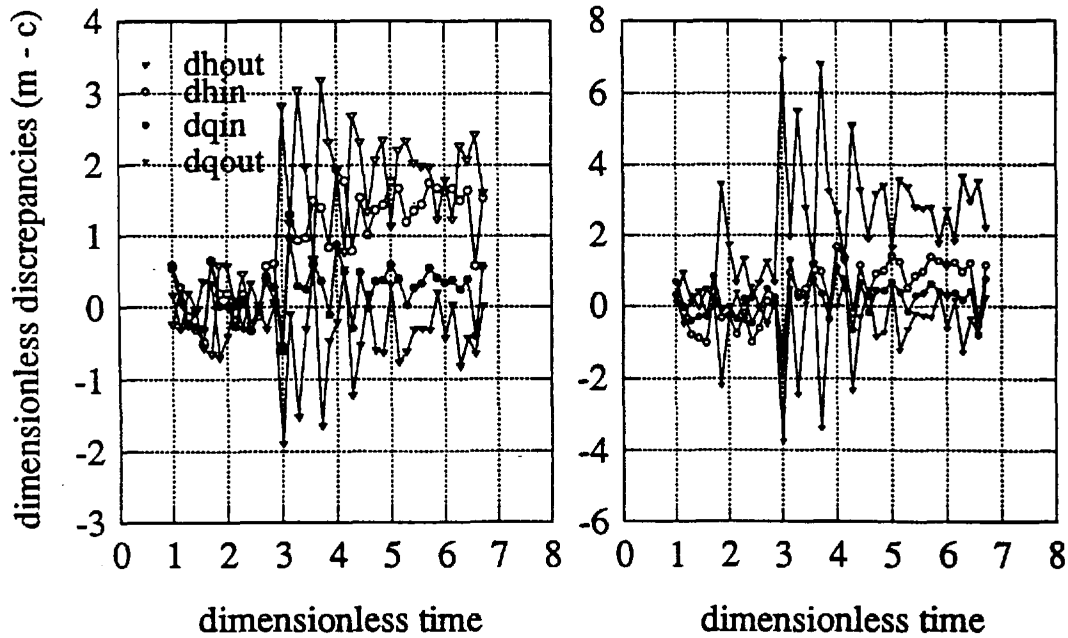

Fig. 11.5
Discrepancy traces indicating a 28% leak during a pump start-up transient - test B2. Left: best estimation for R used. Right: 10% increase in R

The same process was applied to test D1 where a 1.1 percent leak was imposed during a "steady-state" flow. This test has an R value of 6.5. A set of representative discrepancy traces using filtered data with $\tau = 60$ is shown in Fig. 11.6. Table 11.3 shows the process of eliminating the false patterns that satisfy the modified conditions. As the number of consecutive steps increases from 1 to 6, a large number of false patterns are eliminated. At 7 consecutive steps, only 2 patterns remain. At this point, the true leak pattern, the one that indicates a leak location of -1 or -2, has been eliminated! Only one pattern remains when the number of consecutive steps is increased to 11. The surviving pattern has a wrong location and can only be associated with noise.

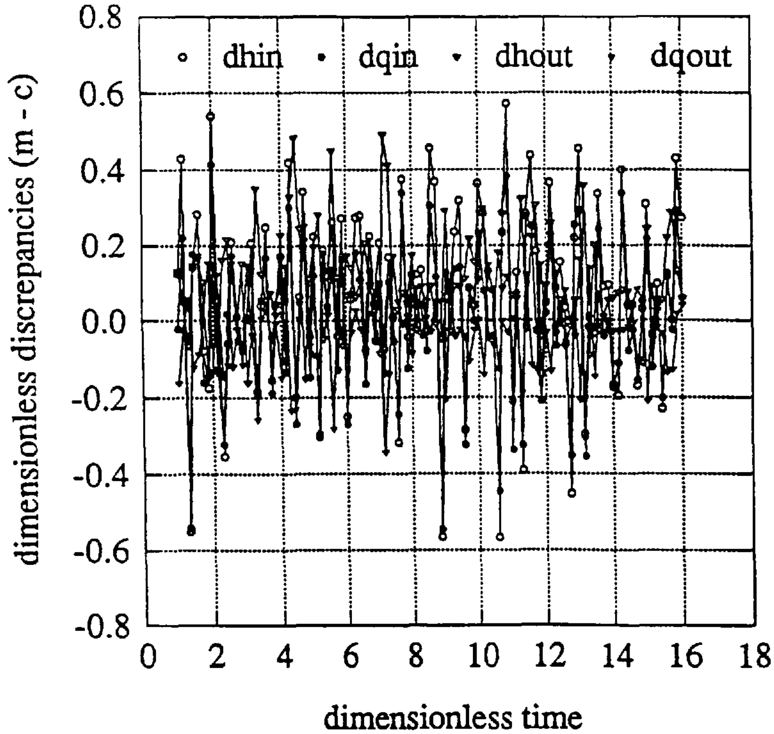

Fig. 11.6
Discrepancy traces that failed to indicate a 1.1% leak during steady-state flow

Table 11.3 Eliminating false patterns by increasing number of consecutive time steps (test D1, data filtered with $\tau = 60$ seconds)

Location indicator	1 Step		6 Steps		7 Steps		11 Steps	
	freq.	max	freq.	max	freq.	max	freq.	max
-6	5	1.72	0	0	0	0	0	0
-5	8	1.54	0	0	0	0	0	0
-4	2	2.30	0	1	0	0	0	0
-3	6	1.54	1	1.54	1	1.54	1	1.54
-2	8	1.40	1	0.81	0	0	0	0
-1	6	1.98	1	1.12	0	0	0	0
0	6	1.85	0	0	0	0	0	0
1	4	1.75	0	0	0	0	0	0
2	8	1.84	1	1.56	0	0	0	0
3	5	1.62	0	0	0	0	0	0
4	5	1.99	0	0	0	0	0	0
5	5	1.52	2	1.44	1	0.97	0	0
6	8	2.01	0	0	0	0	0	0

The conclusion drawn from Table 11.3 is that, because of data noise, the 1.1 percent leak in test D1 can not be detected with certainty. However, if one chooses to accept 5 candidates and tolerates false alarms, then there is a 20 percent chance of detecting the leak.

11.7 CONCLUSIONS ON FIELD TRIALS

The results of the field trials demonstrate that leak detectability based on transient flow simulation can tolerate a significant amount of uncertainty (up to ±30 percent tested) in the parameter R.

The four conditions, developed in Section 10.4 to identify leak discrepancy patterns, appear to be too stringent for the field trials. Noise in the measured data on a pipeline with a high R value, such as the one tested, reduces the definition of the true leak discrepancy pattern. Consequently, one of the four conditions is modified. With the modification, noise can be tolerated without sacrificing reliability for large leaks (approximately 15 percent of throughput and larger tested). However, smaller leaks (approximately 1 percent of throughput tested) can no longer be detected with certainty.

The four conditions prior to the modification result from the propagation nature of transients. Despite noise, they should identify true leak discrepancy patterns with certainty when R is low and when transients produce lower velocities.

11.8 GENERAL TRENDS OF VARIABLE RANKING

The infinite number of variations in transients makes it difficult to rank the variables systematically as previously done for the mass balance method in Chapter 7. Only the general trends can be indicated and related to the variables listed in Table 3.3.

1: The pipe length, diameter, initial velocity, friction factor, and acoustic wave speed are of equal importance to leak detectability. This is so because these five variables are components of the similitude parameter R, which alone characterizes pipeline systems.

The variables involved in determining the friction factor are pipe diameter, length, wall roughness, temperature, pressure, liquid density, and flow rate. The variables involved for wave speed determination are pipe diameter, wall thickness, Young's modulus, Poisson's ratio, pressure, temperature, liquid mass density, and bulk modulus.

2: The importance of data noise to leak detectability depends on the *R* value. A given level of noise may be tolerable in pipelines with small *R* but not in pipelines with large *R*.

The variables involved here are the uncertainties in pressure and flow measurements, the maximum span and spacing of these measurements, and SCADA poll time and time skew. Closer spacing of pressure and flow measurements is needed for noisy data. Better response can be achieved if *R* is kept below 2 approximately. This may be achieved by reducing the spacing between measurements and/or by lowering throughput.

3: The importance of data noise to leak detectability depends on the type of transients. It is more difficult to detect a leak with noisy measured data when transients produce higher flow as opposed to transients that produce lower flow.

4: Aside from noise generation, discontinuity in product gravity across interfaces, positions of the batch interfaces, and pipe diameter changes do not appear to be critical variables in detecting large leaks (10% to 20% of throughput approximately). This observation is supported by the fact that a pipeline model with a single fluid batch and with uniform properties, (see Section 11.2) has been used to detect large leaks successfully.

References

API, 1984, Manual of Petroleum Measurement Standards, Chapter 11.2.1M - Compressibility Factors for Hydrocarbons: 638 - 1074 Kilograms per Cubic Metre Range, American Petroleum Institute, Washington D. C.

ASTM, API, and IP, 1980, Petroleum Measurement Tables - Volume Correction Factors, Volume X - Background, Development, and Program Documentation, ASTM D1250, API Standard 2540, and IP 200, American Society for Testing and Materials, Philadelphia, Pennsylvania.

Doebelin, E. O., 1983, Measurement Systems - Application and Design, Third Edition, McGraw-Hill Book Company, New York, New York.

Jessup, R. S., 1930, "Compressibility and Thermal Expansion of Petroleum Oils in the Range of 0 to 300 °C," Bureau of Standards Journal of Research, Vol. 5, National Bureau of Standards, Gaithersburg, Maryland.

Liou, C. P., 1990, "Pipeline Leak Detection and Location," Proceedings of the International Conference on Pipeline Design and Installation, Pipeline Division, American Society of Civil Engineers, pp. 255-269, Las Vegas, Nevada.

Liou, C. P., 1991, "Leak Detection and Location by Transient Flow Simulations," Proceedings of the 1991 API Pipeline Conference, American Petroleum Institute, pp. 268-281, Dallas, Texas.

Liou, C. P., Brockway, C. G., and Miller, R. B., 1992, "Pipeline Variable Uncertainties and Their Effects on Leak Detectability," Proceedings of the 1992 API Pipeline Cybernetics Symposium, American Petroleum Institute, pp. 127-149, Houston, Texas.

Liou, C. P., 1993, "Mass Imbalance Error of Waterhammer Equations and Leak Detection," To be published in the December 1993 issue of the Journal of Fluids Engineering, Transactions of the American Society of Mechanical Engineers.

Mears M. N., 1993, "Real World Applications of Pipeline Leak Detection," Proceedings of the International Conference on Pipeline Infrastructure II, American Society of Civil Engineers, pp 189 - 209, San Antonio, Texas.

Oppenheim Research, 1991, "Analysis of a Software-Based Pipeline Leak Detection Systems Survey," Final Report Prepared for the American Petroleum Institute, Oppenheim Research, Tallahassee, Florida.

Scarborough, J. B., 1962, Numerical Mathematical Analysis, Fifth Edition, The Johns Hopkins Press, Baltimore, Maryland.

Wylie, E. B., and Streeter V. L., 1993, Fluid Transients in Systems, Prentice Hall, Inc.,Englewood Cliffs, New Jersey.

Order No. 831-11490

1-01400—12/93—3C (9C)

American Petroleum Institute
1220 L Street, Northwest
Washington, D.C. 20005